Shape Control of Au Nanoparticles Using Oxide Template with Ordered Tubular Mesopores and Their Photocatalytic Properties

（規則性細孔を有する酸化物鋳型を利用した金ナノ粒子の

形状制御と光触媒特性）

January, 2016

Doctor of Engineering

Teruhisa Okuno

奥野　照久

Toyohashi University of Technology

別紙４ （課程博士）

Department 電気・電子情報工学専攻	Student ID Number 学籍番号	第 093507 号	Supervisors 指導教員	松田　厚範
Applicant's name 氏名	奥野　照久			武藤　浩行

Abstract
論文内容の要旨　（博士）

Title of Thesis 博士学位論文名	Shape Control of Au Nanoparticles Using Oxide Template with Ordered Tubular Mesopores and Their Photocatalytic Properties (規則性細孔を有する酸化物鋳型を利用した金ナノ粒子の形状制御と光触媒特性)

(Approx. 800 words)

(要旨　1,200 字程度)

TiO_2 is generally known as a material that is nontoxic, inexpensive and able to decompose many kinds of organic compounds under sunlight. However, one drawback of photocatalysis by TiO_2 is that it can only be excited by ultraviolet (UV) radiation, which occupies only a small portion of solar radiation. Therefore, an extension of its absorption wavelength range to the visible (Vis) is an important issue to improve the photocatalytic performance of TiO_2. Combining plasmonic metal nanoparticles (NPs) such as Au with TiO_2 is an outstanding strategy to improve the photocatalytic efficiency of semiconductor due to the unique optical and electric properties of plasmonic metals. In particular, Au nanorods (NRs) with large aspect ratio can absorb the light in near-infrared (NIR) region by surface plasmon resonance (SPR). The use of NIR light for the photocatalysis is large advantage because the lights in NIR region (over 800 nm) were hardly used for the photocatalysis under sunlight due to low energy of NIR light.

In this thesis, Au NPs and Au NRs were deposited on the photoactive mesoporous SiO_2-TiO_2 template and the photocatalysis using SPR of Au NPs and Au NRs deposited in the template was investigated. The effects of TiO_2-Au interface, surface modification of the template and SPR wavelength of Au NPs and Au NRs on the photocatalysis under Vis and NIR light irradiation were discussed.

In the first study, TiO_2 nanocrystal-containing mesoporous SiO_2 template were fabricated by sol-gel method and Au NPs or Au NRs were deposited in the as-formed tubular mesopores by thermal reduction method. A morphology change of the Au NPs was investigated when the content of TiO_2 in the template was varied. Au NRs with a length of 10 to 400 nm were obtained in the template containing 20 mol% TiO_2 and the length of Au NRs was shortened with increasing in TiO_2 content because thermoexcited conduction electrons are generated from TiO_2 and these generated electrons transfer to the Au ions to accelerate their reduction. Also Au NPs in the template containing 20 mol% TiO_2 were deposited by UV radiation to the sample during heat treatment. UV radiation during Au deposition in the template produced electrons photocatalytically and accelerated the Au deposition rate, leading to the dominant formation of Au NPs. The rate constants per unit area for photobleaching of MB upon UV radiation by SiO_2-TiO_2, Au NPs and Au NRs/SiO_2-TiO_2 containing 20 mol% TiO_2 were evaluated. Bare SiO_2-TiO_2 showed 3.24×10^{-2} $min^{-1}m^{-2}$ of rate constant per unit area, the Au NPs- and Au NRs-deposited SiO_2-TiO_2 possessed rate constants that were two and three times larger than that of the bare template. Vis irradiation of the prepared samples had no significant effect on their photocatalytic properties because the electronic contact between TiO_2 and Au was not

formed by thermal reduction method.

In the second study, Au NPs and Au NRs were deposited in SiO_2-TiO_2 by photodeposition method with/without surface modification of the template by 3-aminopropyltriethoxysilane (APTES) and Vis light-induced photocatalysis of prepared samples was investigated. Without APTES, spherical Au NPs with a diameter of < 15 nm formed dominantly at the outside of the mesoporous structure and showed the extinction at 542 nm. The surface modification of the template with APTES prior to the deposition of Au resulted in the formation of Au NRs with a diameter of ca. 5 nm and a length of 10−15 nm in the tubular mesopores of the template and this sample showed two extinction peaks at 528 and 700 nm. Au NPs-deposited sample worked well as a photocatalyst to bleach MB under Vis light irradiation. Au NRs-deposited sample showed weak and abnormal photocatalytic activity, showing nonexponential curve in the photobleaching dynamics of MB because APTES being on the surface of the template suppressed the adsorption of MB onto the sample. Heat treatment to remove APTES from the sample led to the amelioration of the photocatalytic activity. The formation of good electronic contact between Au NPs and TiO_2 was found to be essential to the high Vis light-induced photocatalytic performance.

Finally, comparison of the photocatalytic activities of Au NPs/SiO_2-TiO_2 with different amounts of Au (0.3, 0.6, 1.2 and 1.8 mol% Au) and Au NRs/SiO_2-TiO_2 was carried out under UV, Vis and NIR light irradiation. Au NPs/SiO_2-TiO_2 with an amount of 0.6 mol% Au showed the highest photocatalytic activity among the samples with different amount of Au under both UV and Vis light irradiation. The specific surface area of Au/SiO_2–TiO_2 decreased with increasing the amount of Au, resulting in the decrease of the photocatalytic activity of 1.2 and 1.8Au/SiO_2-TiO_2. Au NRs/SiO_2–TiO_2 showed higher photocatalytic activity than Au NPs/SiO_2-TiO_2 under both UV and Vis light irradiation. The reasons of the high photocatalytic activity of Au/SiO_2–TiO_2 were investigated by measuring the action spectra and were considered to be the high specific surface area (353.2 m^2g^{-1}), the formation of Schottky barrier between Au NPs and TiO_2, the wider light absorption by SPR of Au NRs.

Contents

Chapter 1 General Introduction

1.1 Photocatalyst

Semiconductor photocatalysis has received much attention during last three decades as a promising solution for both energy generation and environmental problems. Since the discovering of Honda-Fujishima effect [1] that water can be photo-electrochemically decomposed into hydrogen and oxygen using a semiconductor (TiO_2) electrode under ultraviolet [UV] radiation, extensive works have been carried out to produce hydrogen from water splitting using a variety of semiconductor photocatalysts. In recent years, scientific and engineering interest in heterogeneous photocatalysis has been also focused on environmental applications such as water treatment and air purification. Many review papers on semiconductor photocatalysis can be found in literature [2-6]. Nowadays, the mechanism of the illuminated catalyst, the surface phenomena, and the generated species has been elucidated [6-8]. Also, the parameters that affect the photocatalytic process and consequently the reaction rate have been studied. Several articles already were published where a detailed explanation about the influence of solution pH, catalyst dosage, substrate concentration, temperature, photonic flux etc [7-9].

It has been well established that the photocatalytic process begins when photons of energy higher or equal to the band gap energy are absorbed by a semiconductor particle and an electron (e^-) from the valence band [VB] is transferred to the conduction band [CB] generating a hole (h^+) in the VB. The absorption of these photons creates within the bulk electron-hole pairs, which dissociate into free photoelectrons in the CB and photoholes in the VB. The e^- and h^+ can recombine on the surface or in the bulk of the particle releasing the energy as heat or migrate to the surface where they can react

with adsorbed molecules on the surface of the particle as illustrated in Fig. 1.1.

In a fluid medium, the flat band potential, V_{fb}, of the semiconductor locates the energy of both charge carriers at the semiconductor-electrolyte interface and depends on the nature of the material and the system equilibria. Adsorbed species can be reduced by CB electrons if they have redox potentials more positive than the V_{fb} of the CB and can be oxidized by hole if they have redox potentials more negative than the V_{fb} of the VB. In presence of adsorbed water, electrons transfer from water molecule to the positive holes to produce ·OH radicals which are powerful oxidants and react with organic and toxic compounds. ·OH radicals play an important role in initiating oxidation reactions, especially for substances that adsorb weakly on the TiO_2 surface. This oxidation pathway is known as indirect oxidation to differentiate it from the direct oxidation by holes. However, the role of the ·OH radicals is probably overestimated, and some controversial aspects have been reported regarding the origin of photogenerated free ·OH radicals [10,11].

Among various materials, TiO_2 is the most widely used photocatalyst that is nontoxic, chemically stable, inexpensive, and able to decompose many kinds of organic compounds under sunlight as mentioned above. However, a major drawback of TiO_2 photocatalysis is the large band gap. TiO_2 can only be activated upon irradiation with a photon of light < 390 nm, limiting its use under solar irradiation [12-14]. UV light makes up 3–5 % of the solar spectrum, whereas the spectrum consists of ~ 40 % visible [Vis] light. Therefore, in order to utilize TiO_2 to its full potential it is necessary to decrease the band gap size facilitating Vis light absorption.
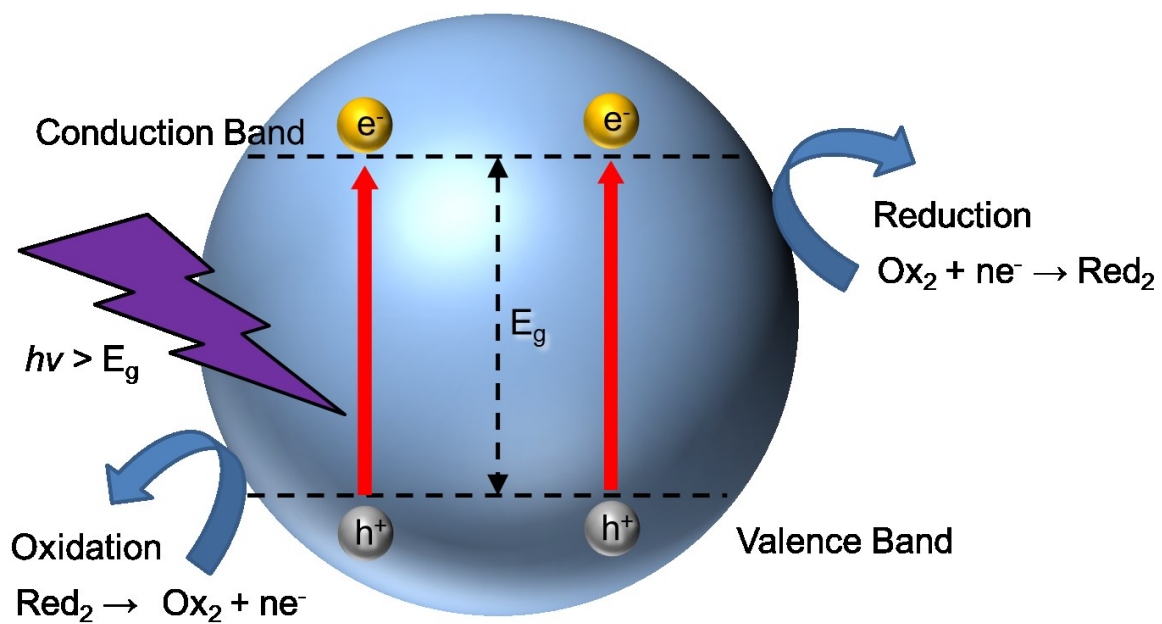
Fig. 1.1. Schematic representation of the photocatalysis on TiO_2 particle.

1.2 Improving photocatalytic materials

1.2.1 Ion doping to TiO$_2$

Non-metal doping has shown great promise in achieving Vis light activated photocatalysis, with nitrogen being the most effective dopant. Asahi et al. were the first to show Vis light absorption through N doping. They reported nitrogen doped TiO$_2$ promoted photocatalytic activity up to λ = 520 nm [15]. The nitrogen substitutional doping of TiO$_2$ was early claimed as a method for narrowing the band gap by exclusively changing the valence band structure; fine electronic details of this are however under discussion. Asahi et al. claimed that the presence of nitrogen narrows the band gap of TiO$_2$ thus making it capable of performing Vis light driven photocatalysis [15]. However, Ihara et al. suggested that it is the oxygen vacancies that contributed to the Vis light activity, and the doped nitrogen only enhanced the stabilization of these oxygen vacancies [16]. They also confirmed this role of oxygen vacancies in plasma-treated TiO$_2$ photocatalysts [16]. In addition the structural oxygen vacancy caused Vis light photocatalytic activity was also reported by Martyanov et al. [17]. Currently there appears to be some agreement on the mechanism of nitrogen doped Vis light absorption explained by Irie and Nakamura [18,19]. They explained that TiO$_2$ oxygen lattice sites substituted by nitrogen atoms form an occupied midgap (N-2p) level above the (O-2p) valence band (Fig. 1.2). Irradiation with UV light excites electrons in both the valence band and the narrow (N-2p) band, but irradiating with Vis light only excites electrons in the narrow (N-2p) band [18,19].

Carbon, phosphorous and sulfur have also shown positive results for Vis light responsive TiO$_2$ [20,21]. The non-metal dopants effectively narrow the band gap of TiO$_2$ (<3.2 eV) [22-24]. Change of the lattice parameters and the presence of trap states

within the conduction and valence bands from electronic perturbations give rise to band gap narrowing [12]. Not only does this allow for Vis light absorption but the presence of trap sites within the TiO_2 bands increases the lifetime of photoinduced charge carriers. Doping of TiO_2 with transition metals such as Cr, Co, V and Fe has extended the spectral response of TiO_2 well into the Vis region also improving photocatalytic activity [12,25-28]. However, transition metals may also act as recombination sites for the photo induced charge carriers, thus, lowering the quantum efficiency. Transition metals have also been found to cause thermal instability to the TiO_2 nanomaterials [29]. Kang argues that despite the fact that a decrease in band gap energy has been achieved by many groups through metal doping, photocatalytic activity has not been remarkably enhanced because the metals introduced were not incorporated into the TiO_2 framework. In addition, metals remaining on the TiO_2 surface cover photo reaction sites [30].
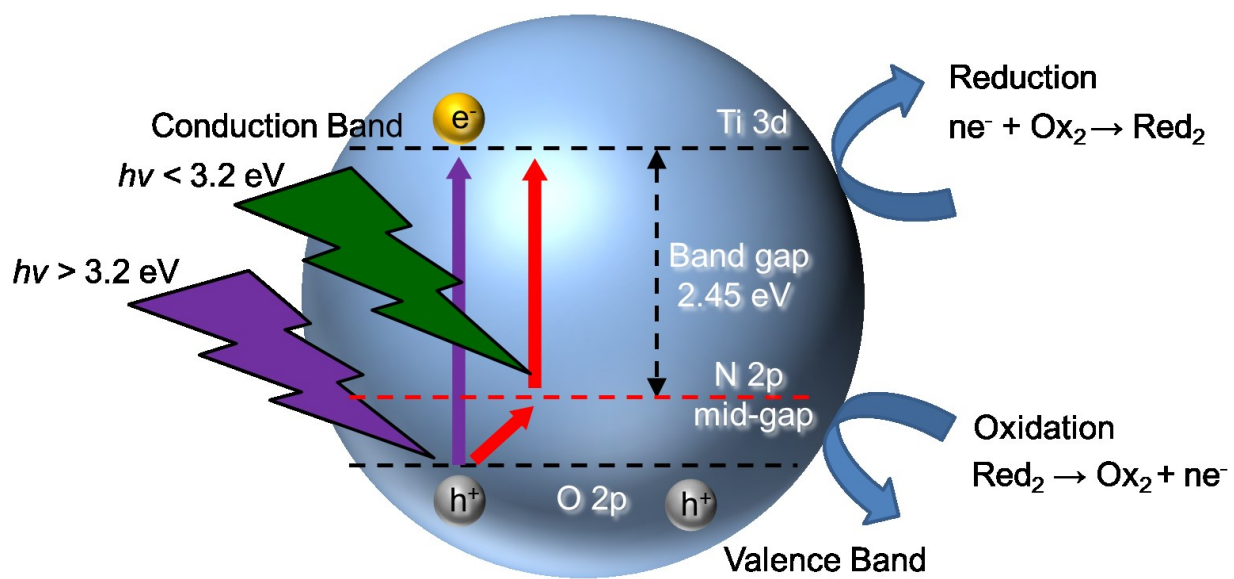
Fig. 1.2. Schematic of N-doped TiO_2 photocatalysis.

1.2.2 Surface modification of TiO$_2$ with plasmonic metal nanoparticles

Combining plasmonic metal nanoparticles [NPs] with semiconductors is an outstanding strategy to improve the photocatalytic efficiency of semiconductor due to the unique optical and electric properties of plasmonic metals [31–33]. Au NPs deposited on TiO$_2$ supports have been reported that have activities for oxidation of alcohol under Vis light [34-36]. When the size of metal NPs is much smaller than the wavelength of light, coherent oscillation of the conduction band electrons is induced by interaction with an electromagnetic field and this is called localized surface plasmon resonance [LSPR] [37-39]. The LSPR is a collective oscillation of electrons in NPs when they resonate with the electromagnetic field of the incident light with certain natural frequency [40]. This process can help the NPs' conduction electrons to gain energy from certain wavelength of irradiation and result in high energy electrons at the surface, which are capable of activating molecules on the NPs for chemical reactions. The advantage of this principle is that the gained energy from light irradiation is at the surface of the NPs and can interact with reactant molecules efficiently and avoid energy loss caused by the electron transmitting or transferring. Applying this effect, the reaction can be designed to use light instead of heat to proceed at high efficiency and at moderate temperature [41-43]. Furthermore, these NPs can also absorb UV light due to inter-band electron transitions (from 5d to 6sp) [44,45] and provide extra energy for the reactions.

1.3 Noble metal photocatalysts

1.3.1 Plasmon absorption of noble metal nanoparticles

The LSPR is a collective oscillation of electrons in NPs when they resonate with the electromagnetic field of the incident light with certain natural frequency [40] as shown in Figure 1.3 [46]. Mie was the first to explain the different colors of Au NPs solutions through Maxwell's equation at year 1908. In Mie's theory, when the nanoparticles are much smaller than the wavelength of incident light, only electric dipole term is significant [47,48]:

$$\sigma_{ext}(\omega) = 9\frac{\omega}{c}\varepsilon_m^{3/2}V\frac{\varepsilon_2(\omega)}{[\varepsilon_{1(\omega)}+2\varepsilon_m]^2+\varepsilon_2(\omega)^2} \qquad (1)$$

Where V is the particle volume, ω is the angular frequency of the exciting light, c is the speed of light, ε_m and $\varepsilon(\omega) = \varepsilon_1(\omega) + i\varepsilon_2(\omega)$ are the dielectric functions of the surrounding medium and the material itself respectively. When condition $\varepsilon_1(\omega) = -2\varepsilon_m$ is fulfilled, the energy from irradiation absorption by the bulk metal is condensed into a single, surface plasmon band. For a metal nanosphere with a radius that is much smaller than the wavelength of light, the metal polarizability can also be given by the following equation, edited from [37]:

$$\alpha = (a/r)g_d^3 \qquad (2)$$

$$\text{With } g_d = (\varepsilon_1-\varepsilon_0)/(\varepsilon_1+2\varepsilon_0) \qquad (3)$$

Where α is the radius, r is the distance between molecular and the center of nanosphere,

ε_i is dielectric constant of the metal nanoparticles and ε_0 is the dielectric constant of the surrounding medium. A strong resonance occurs when $\varepsilon_i = -2\varepsilon_0$. Noble metals such as gold and silver can fit this equation.
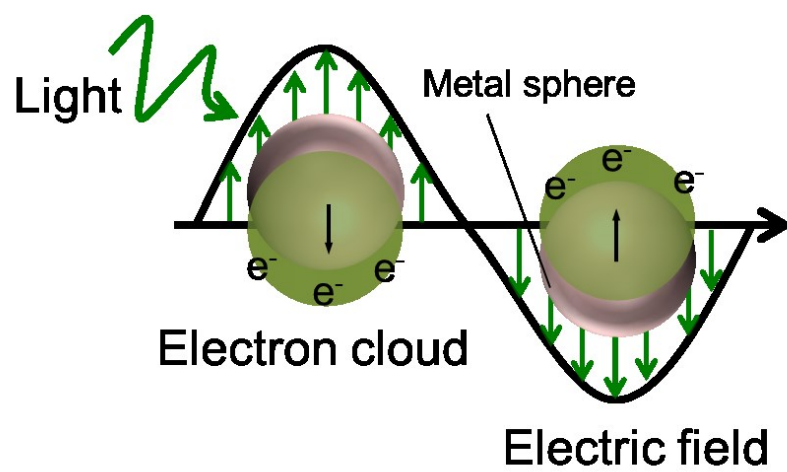
Fig. 1.3. The Localized Surface Plasmon Resonance (LSPR) effect.

1.3.2 Light absorption of different nanostructures

The LSPR strength may be influenced by the dielectric constants of both the metal and the surrounding material, the particle size and particle shape of the metal and the surrounding environment. The point effect is well known in macroscopic system, which is also applied to the nanoscale. Noble metal nanomaterials with thorny structures, edges and concave curvatures, such as nanowires, cubes, triangular plates and N-P junctions, have different absorption spectra from each other [49]. When the shape of the NPs changes, electric field density appears on the NP surface will shift and change the oscillation frequency of the electrons which may cause enhancement of the local electromagnetic fields [37,50,51].

The LSPR effect also strongly depends on the diameter of the particles [44]. Take Au NPs for example: in the particles diameter range between 5 nm and 10 nm, the strength of surface plasmon drops with the decrease of the particle diameter which is due to the increase of the frequency of electron scattering at a particle boundary in the electronic excited state. When the particle diameter is smaller than 3 nm, the surface plasmon peak nearly disappears. This may be caused by the number of the conduction electrons that reduces a result of the quantum-size effects. As the particles grow bigger, the absorption band broadens and covers the Vis range [52,53].

1.4 Fabrication of Au nanorods

To obtain metal NPs exhibiting effective surface plasmon resonance [SPR] that strongly absorbs light of aimed wavelength, the morphology and assembly must be precisely controlled. [54-56]. Several methods for synthesizing Au NPs including Au nanorods [NRs] have been reported. These methods include photochemical and

electrochemical deposition [57,58] and seeding growth methods [59,60]. In these methods, however, the Au NPs are suspended in a solvent. Therefore, the Au NPs are required to be immobilized in a designed fashion in/on a solid matrix for various kinds of practical applications. The immobilization process for Au NPs still requires further development [61,62]. Also, electron beam lithography [63,64] and electron beam induced deposition [65,66] can meet the requirement, but cannot be used for the deposition of metal NPs on powder/porous TiO_2 effectively. A large variety of liquid phase syntheses for morphology-controlled metal NPs have also been reported.[54,67] However, the immobilization process of metal NPs on TiO_2 is normally too complicating to be applied to practical applications [62,68].

On the other hand, the use of hard templates such as anodic alumina and mesoporous silica for the synthesis of Au NRs makes the complicated immobilization processes redundant, and several related studies have been reported [69,70]. Those methods using hard templates are also advantageous to control the diameter and dispersion state of Au NRs because they depend on the pore structure. Furthermore, the mesoporous template can also act as a functional matrix for the deposited metal nanoparticles. For instance, the high specific surface area of the matrix can be advantageous for catalysis. Thus, photocatalytic activity of TiO_2 can be further improved by the deposition of TiO_2 onto a mesoporous SiO_2.

1.5 Mesoporous material

Mesoporous materials are materials with pores in the range of 2–50 nm according to the IUPAC classification in which

micropores have a diameter < 2 nm,

mesopores have a diameter between 2 and 50 nm and

macropores have a diameter > 50 nm [71].

The pores can have different shapes such as spherical or cylindrical and be arranged in varying structures. Some structures have pores that are larger than 50 nm in one dimension, see e.g. the two first structures, but there the width of the pore is in the mesorange and the material is still considered to be mesoporous.

Mesoporous materials can have a wide range of compositions but mainly consist of oxides such as SiO_2, TiO_2, ZnO_2, Fe_2O_3 or combinations of metal oxides, but also mesoporous carbon can be synthesized [72-76]. The mesoporous materials are generally prepared by growing these oxide walls around the micelles. Both organic metal precursors such as alkoxides [77-79] as well as inorganic salts such as metal chloride salts [73] can be used. Alternatively a mesoporous template can be used to grow another type of mesoporous material inside it. This is often used for synthesizing e.g. mesoporous carbon [76,80,81].

1.5.1 Mesoporous silica

In 1992 a new family of ordered mesoporous materials was reported [72,77] and this became the starting point of a new research field. These materials are named MCM-X (Mobil Crystalline of Materials) and were synthesized by Mobile Corporation laboratories. Mesoporous silica with different pore structures was synthesized e.g. MCM-41 with hexagonally ordered cylindrical pores and MCM-48 with a cubic pore structure. These materials are synthesized with cationic surfactants under basic conditions.

This was though not the first attempt of synthesizing mesoporous silica. There is a

patent from 1971 regarding synthesis of low-density silica where cationic surfactants were used [82]. In this patent there is no report concerning porosity, only the low bulk density was of importance. Later this material has been synthesized, characterized and compared to MCM-41[83]. It is clear that this material is a predecessor to the mesoporous silica that is synthesized today, even though the importance of this type of material was not recognized then.

The first mesoporous silica synthesized with non-ionic triblock polymers were reported in 1998 by Zhao et al. [78,84]. These materials are named SBA-X (Santa Barbara Amorphous) where X is a number corresponding to a specific pore structure and surfactant, e.g. SBA-15 has hexagonally ordered cylindrical pores synthesized with P123 as surfactant while SBA-16 has spherical pores arranged in a body centered cubic structure and is synthesized with F127. SBA-15 is the most extensively studied mesoporous silica and also the subject of attention in this thesis.

1.5.2 Synthesis of mesoporous silica

Mesoporous silica is mainly prepared by sol-gel synthesis. The solution (sol) is the colloidal system where micelles are formed by surfactants and are dispersed in an aqueous solution. When the silica precursor is added to the sol it hydrolyses and a silica network is formed in which the liquid is enclosed, a gel. The transition between sol and gel is gradual and the sol becomes a gel when it can support a stress elastically. Finally the gel is heated (calcined) whereby the surfactants decompose and evaporate. Left is now the porous silica network.

Surfactants (surface active agents) are amphiphilic molecules, i.e. they are composed of a hydrophilic (water-loving), and a hydrophobic (water-hating), part.

Surfactants are classified by their head group: anionic, cationic, zwitterionic and non-ionic. The lipophilic part is often a hydrocarbon chain. Due to their amphiphilicity, the surfactants form micelles in oil or aqueous solutions to lower the free energy in the system. If the solvent has two immiscible phases the surfactants are located in the oil/water interface with the hydrophilic part towards the water and the lipophilic part in the oil.

When the concentration of surfactants is low in an aqueous solution, the surfactants are located as separate molecules in the air/water interface. This reduces the surface tension since it is larger for water than for the hydrocarbons. Increasing the surfactant concentration in the solution further reduces the surface energy until a critical value. At this point, the critical micelle concentration [CMC] is reached and aggregates of surfactants (micelles) are formed. The CMC is determined by two competing factors; bringing the nonpolar chains out of the water phase into the oil phase (hydrophobic effect) and repulsion between the polar head groups which opposes the formation of micelles [85]. The CMC and shape of the micelles are determined by the nature of the surfactant and conditions in the solution such as temperature or salt additions.

The aggregate structure of the amphiphilic molecules is determined by the critical packing parameter [CPP]

$$CPP = \frac{v}{l \cdot a} \qquad (1)$$

where v is the volume of the hydrophobic chain [nm^3], a is the area of the hydrophilic part [nm^2] and l [nm] the length of the hydrophobic chain. The volume v and length l can be expressed by

$$\nu = 0.027(n_c + n_{Me}) \qquad (2)$$

$$l = 0.15 + 0.27n_c \qquad (3)$$

where n_c is the number of carbon atoms and n_{Me} the number of methyl groups.

When mesoporous silica is synthesized, several types of surfactant can be used e.g. cationic hexadecyl trimethyl ammonium bromide [72,77], non-ionic poly(ethylene oxide) [PEO] surfactants [86] or Pluronics [78]. In this work Pluronic P123, a non-ionic amphiphilic triblock copolymer has been used as surfactant. There are several non-ionic triblock copolymers under the trademark Pluronics. These polymers were patented in 1973 and are also called Poloxamers. They all consist of hydrophilic polyethylene oxide chains and hydrophobic polypropylene oxide chains [PPO]. There are several different Pluronics with varying molecular weights and PEO/PPO ratios (EOxPOyEOx). The notation for a Pluronic triblock copolymer starts with a letter followed by two or three numbers. The letter describes the appearance of the polymer: F (flake), P (paste) or L (liquid). The first one or two numbers multiplied with 300 indicates the molecular weight of the PPO block and the last number gives the PEO weight fraction. Hence, P123 is a paste with ~3600 g/mol PPO and 30 wt% PEO while F127 is solid flakes with the same weight of PPO but 70 wt% PEO. These differences give rise to the variation of pore structures observed in the mesoporous materials, e.g. F127 is used for synthesizing spherical pores in a body centered cubic structure while P123 is used for hexagonally ordered cylindrical pores [78].

1.5.3 SBA-15

SBA-15 is a mesoporous silica (SiO_2) which has cylindrical pores arranged in a hexagonal order synthesized with the Pluronic triblock-copolymer P123. For this material, the pore size refers to the width of the cylindrical pores which can be tuned between 4-26 nm [78,84,87,88] even though pore sizes above 12 nm are rare. The length of the pores varies from ~200 nm [89,90] to several microns.

Around each mesopore is a microporous network called the corona [91,92]. This network interconnects the mesopores with each other and is responsible for the high surface area of SBA-15. The microporous network was first shown by platinum replicas [92] where the nanorods from filled mesopores were interconnected by the network which makes the nanorods remain in the hexagonal structure even after removal of the silica.

The corona is mainly supposed to originate from trapped hydrophilic chains of the surfactants [93-95]. An additional explanation for the corona is stressinduced defects where the micropore fraction increases with the effective pore wall thickness to average pore diameter ratio [96]. It is stable up to 1173 K, but above this temperature the network disappears and the material has similar structure to MCM-41 [92]. The corona plays a crucial role when using SBA-15 as a template for other materials. Replicas can be synthesized in two variants, one rod-like and one straw-like. Due to that the micropores also will be filled with the replica material the mesopore replicas will be fixed in the hexagonal structure and the particle morphology will be retained.

1.6 Overview of thesis

The main purpose of this research work in my thesis is the fabrication of

multi-wavelength light responsive photocatalyst by the shape control of Au NPs with photoactive mesoporous SiO_2-TiO_2 template. As described in section 1.2.2, plasmonic metal NPs such as Au are well known to enhance the photocatalytic activity under Vis by deposition to the surface of the photocatalysts. However, the photocatalysis with Au NPs under NIR light has seldom been reported although Au NRs with large aspect ratio can absorb the light in NIR region. In this thesis, I focused on the Au NRs. Au NRs with a certain length can absorb NIR light, and this Au NRs-deposited TiO_2 photocatalyst promises to occur the photocatalysis under NIR light irradiation. If photocatalysis under NIR light occurs, higher photocatalytic activities are provided under sunlight because the spectrum consists of ~46 % NIR light. In order to deposit Au NRs, photoactive mesoporous SiO_2-TiO_2 was used as a template. The shape of Au NPs was controlled in the template with the photocatalysis of TiO_2, and discussed the photocatalytic activities of prepared samples under UV, Vis and NIR light.

This doctoral thesis consists of 4 chapters indicated below:

Chapter 1

This chapter shows the background, the objectives and the contents of this thesis.

Chapter 2

In this chapter, shape control of Au NPs was carried out with photoactive mesoporous SiO_2-TiO_2 template by thermal reduction of Au ions. The shape control of Au NPs was achieved by the different composition of TiO_2 in the template or UV radiation during thermal reduction of Au ions. As a result from the investigation of photocatalytic activity, the enhancement of the photocatalytic activity of the template was investigated under UV, but photocatalysis under Vis light was not confirmed. It was because the effective formation of crystalline TiO_2/Au interface for photocatalysis by

Vis irradiation was not achieved.

Chapter 3

In this chapter, Au NPs and NRs were deposited in the template by photodeposition method to form the contact between TiO_2 and Au. Both Au NPs- and NRs-deposited sample showed the photocatalysis under Vis light irradiation. However, organic being on the surface of the template, which is used to anchor Au ions on the template, suppressed the adsorption of reactant onto the sample by electrostatic force, which caused a significant decrease in the photocatalytic activity. Therefore, it was needed to deposit Au NPs in the template without surface modification of the template with organic being to achieve high photocatalytic acitivty.

Chapter 4

In this chapter, detailed investigation of the photocatalytic activities of Au NPs- and Au NRs-deposited sample prepared by photodeposition method without organic being was carried out. Au NRs-deposited sample showed the photocatalysis under the wavelength of 500-1000 nm light by SPR of Au NRs, whereas Au NPs-deposited sample showed the photocatalysis under the wavelength of 500-700 nm light. Furthermore, the photocatalytic activity of Au deposited-sample was clearly improved by simultaneous Vis light irradiation with UV radiation.

General conclusions

The conclusions of this thesis are described in this chapter.

References

[1] A. Fujishima and K. Honda, "Electrochemical Photolysis of Water at a Semiconductor Electrode", *Nature*, **238**, 37 (1972).

[2] M. R. Hoffmann, S. T. Martin, W. Y. Choi and D. W. Bahnemann, "Environmental Applications of Semiconductor Photocatalysis", *Chem. Rev.,* **95**, 69 (1995).

[3] A. L. Linsebigler, G. Q. Lu and J. T. Yates, "Photocatalysis on TiO_2 Surfaces: Principles, Mechanisms, and Selected Results", *Chem. Rev.*, **95**, 735 (1995).

[4] A. Mills and S. Le Hunte, "An overview of semiconductor photocatalysis", *J. Photochem. Photobiol. A,* **108**, 1 (1997).

[5] J. Zhao and X. D. Yang, "Photocatalytic oxidation for indoor air purification a literature review", *Build. Environ*, **38**, 645 (2003).

[6] D. Bahnemann, "Photocatalytic water treatment: solar energy applications", *Sol. Energ.*, **77**, 445 (2004).

[7] P. Pichat and M.A. Tarr, "Chemical Degradation methods for wastes and pollutants: Environmental and industrial applications", *Marcel Dekker Inc. New York*, Basel pp. 77-119 (2013).

[8] D. Friedmann, C. Mendive and D. Bahnemann, "TiO_2 for water treatment: Parameters affecting the kinetics and mechanisms of photocatalysis", *Appl. Catal. B Environ.*, **99**, 398 (2010).

[9] S. Ahmed, M. G. Rasul, R. Brown and M. A. Hashib, "Influence of parameters on the heterogeneous photocatalytic degradation of pesticides and phenolic contaminants in wastewater: A short review", *J. Environ. Manage*, **92**, 311 (2011).

[10] P. Salavador, "On the Nature of Photogenerated Radical Species Active in the Oxidative Degradation of Dissolved Pollutants with TiO_2 Aqueous Suspensions: A Revision in the Light of the Electronic Structure of Adsorbed Water", *J. Phys. Chem. C*, **111**, 17038 (2007).

[11] A. Fujishima, X. Zhang and D. Tryk, "TiO_2 photocatalysis and related surface

phenomena", *Surf. Sci. Rep.*, **63**, 515 (2008).

[12] D. B. Hamal and K. J. Klabunde, "Synthesis, characterization, and visible light activity of new nanoparticle photocatalysts based on silver, carbon, and sulfur-doped TiO_2", *J. Colloid Interface Sci.*, **311**, 514 (2007).

[13] Y.-L. Kuo, H.-W. Chen and Y. Ku, "Analysis of silver particles incorporated on TiO_2 coatings for the photodecomposition of o-cresol", *Thin Solid Films*, **515**, 3461 (2007).

[14] H. Luo, T. Takata, Y. Lee, J. Zhao, K. Domen and Y. Yan, "Photocatalytic Activity Enhancing for Titanium Dioxide by Co-doping with Bromine and Chlorine", *Chem. Mater.*, **16**, 846 (2004).

[15] R. Asahi, T. Morikawa, K. Oikawa, K. Aoki and Y. Taga, "Visible-light photocatalysis in nitrogen-doped titanium oxides" *Science*, **293**, 269 (2001).

[16] T. Ihara, M. Miyoshi, Y. Iriyama, O. Matsumoto and S. Sugihara, "Visible-light-active titanium oxide photocatalyst realized by an oxygen-deficient structure and by nitrogen doping", *Appl. Catal., B,* **42**, 403 (2003).

[17] I. N. Martyanov, S. Uma, S. Rodrigues and K. Klabunde, "Structural defects cause TiO_2-based photocatalysts to be active in visible light", *Chem. Commun.*, **7**, 2476 (2004).

[18] H. Irie, Y. Watanabe and K. Hashimoto, "Nitrogen-Concentration Dependence on Photocatalytic Activity of $TiO_{2-x}N_x$ Powders", *J. Phys. Chem. B,* **107**, 5483 (2003).

[19] R. Nakamura, T. Tanaka and Y. Nakoto, "Mechanism for Visible Light Responses in Anodic Photocurrents at N-Doped TiO_2 Film Electrodes", *J. Phys. Chem. B*, **108**, 10617 (2004).

[20] T. Ohno, T. Mitsui and M. Matumura, "Photocatalytic Activity of S-doped TiO_2

Photocatalyst under Visible Light", *Chem. Lett.*, **32**, 364 (2003).

[21] S. Sakthivel and H. Kisch, "Daylight photocatalysis by carbon-modified titanium dioxide", *Angew. Chem. Int. Ed. Engl.*, **42**, 4908 (2003).

[22] T. Morikawa, R. Asahi, T. Ohwaki, K. Aoki, and Y. Taga, "Band-gap narrowing of titanium dioxide by nitrogen doping", *Jpn. J. Appl. Phys. 2*, **40**, L561 (2001).

[23] K. Nagaveni, M. S. Hedge, N. Ravishankar, G. N. Subbanna, and G. Madras, "Synthesis and Structure of Nanocrystalline TiO_2 with Lower Band Gap Showing High Photocatalytic Activity", *Langmuir*, **20**, 2900 (2004).

[24] T. Umebayashi,T. Yamaki, H. Itoh and K. Asai, "Band gap narrowing of titanium dioxide by sulfur doping", *Appl. Phys. Lett.*, **81**, 454 (2002).

[25] E. Borgarello, J. Kiwi, M. Grätzel, E. Pelizzetti and M. Visca, "Visible light induced water cleavage in colloidal solutions of chromium-doped titanium dioxide particles", *J. Am. Chem. Soc.*, **104**, 2996 (1982).

[26] M. Iwasaki, M. Hara, H. Kawada, H. Tada and S. Ito, "Cobalt Ion-Doped TiO(2) Photocatalyst Response to Visible Light.", *J. Colloid Interface Sci.*, **224**, 202 (2000).

[27] S. Klosek and D. Raftery, "Visible Light Driven V-Doped TiO_2 Photocatalyst and Its Photooxidation of Ethanol", *J. Phys. Chem. B*, **105**, 2815 (2001).

[28] J. Zhu, F. Chen, J. Zhang, H. Chen and M. Anpo, "Fe^{3+}-TiO_2 photocatalysts prepared by combining sol–gel method with hydrothermal treatment and their characterization", *J. Photochem. Photobiol. A*, **180**, 196 (2006).

[29] W. Choi,A. Termin and M. R. Hoffmann, "The Role of Metal Ion Dopants in Quantum-Sized TiO_2: Correlation between Photoreactivity and Charge Carrier Recombination Dynamics", *J. Phys. Chem. B*, **98**. 13669 (1994).

[30] M. Kang, "The superhydrophilicity of Al–TiO2 nanometer sized material

synthesized using a solvothermal method", *Mat. Lett.*, **59**, 3122 (2005).

[31] T. Hirakawa and P. V. Kamat, "Charge separation and catalytic activity of Ag@TiO$_2$ core-shell composite clusters under UV-irradiation", *J. Am. Chem. Soc.*, **127**, 3928 (2005).

[32] N. Zhou, L. Polavarapu, N. Gao, Y. Pan, P. Yuan, Q. Wang and Q. H. Xu, "TiO$_2$ coated Au/Ag nanorods with enhanced photocatalytic activity under visible light irradiation", *Nanoscale*, **5**, 4236 (2013).

[33] Y. Pan, S. Deng, L. Polavarapu, N. Gao, P. Yuan, C. H. Sow and Q.-H. Xu, "Plasmon-enhanced photocatalytic properties of Cu$_2$O nanowire–Au nanoparticle assemblies", *Langmuir*, **28**, 12304 (2012).

[34] E. Kowalska, R. Abe and B. Ohtani, "Visible light-induced photocatalytic reaction of gold-modified titanium(IV) oxide particles: action spectrum analysis", *Chem. Commun.*, **2**, 241 (2009).

[35] S. Naya, A. Inoue and H. Tada, "Self-Assembled Heterosupramolecular Visible Light Photocatalyst Consisting of Gold Nanoparticle-Loaded Titanium(IV) Dioxide and Surfactant", *J. Am. Chem. Soc.*, **132**, 6292 (2010).

[36] D. Tsukamoto, Y. Shiraishi, Y. Sunagano, S. Ichikawa, S. Tanaka and T. Hirai, "Gold nanoparticles located at the interface of anatase/rutile TiO$_2$ particles as active plasmonic photocatalysts for aerobic oxidation", *J. Am. Chem. Soc.*, **134**, 6309 (2012).

[37] K. L. Kelly, E. Coronado, L. L. Zhao and G. C. Schatz, "The Optical Properties of Metal Nanoparticles: The Influence of Size, Shape, and Dielectric Environment", *J. Phys. Chem. B*, **107**, 668 (2003).

[38] M. Rycenga, C. M. Cobley, J. Zeng, W. Li, C. H. Moran, Q. Zhang, D. Qin and Y. Xia, "Controlling the synthesis and assembly of silver nanostructures for plasmonic

applications", *Chem. Rev.*, **111**, 3669 (2011).

[39] C.-H. Chou and F.-C. Chen, "Plasmonic nanostructures for light trapping in organic photovoltaic devices", *Nanoscale*, **6**, 8444 (2014).

[40] S. Zeng, K.-T. Yong, I. Roy, X.-Q. Dinh, X. Yu and F. Luan, "A review on functionalized gold nanoparticles for biosensing applications", *Plasmonics*, **6**, 491 (2011).

[41] X. Chen, H. Y. Zhu, J. C. Zhao, Z. T. Zheng and X. P. Gao, "Visible-Light-Driven Oxidation of Organic Contaminants in Air with Gold Nanoparticle Catalysts on Oxide Supports", *Angew. Chem. Int. Edit.*, **47**, 5353 (2008).

[42] H. Y. Zhu, X. Chen, Z. F. Zheng, X. B. Ke, E. Jaatinen, J. C. Zhao, C. Guo, T. F. Xie and D. J. Wang, "Mechanism of supported gold nanoparticles as photocatalysts under ultraviolet and visible light irradiation", *Chem. Commun.*, 7524 (2009).

[43] H. Y. Zhu, X. B. Ke, X. Z. Yang, S. Sarina and H. W. Liu, "Reduction of nitroaromatic compounds on supported gold nanoparticles by visible and ultraviolet light", *Angew. Chem. Int. Edit.*, **49**, 9657 (2010).

[44] C. Voisin, N. Del Fatti, D. Christofilos and F. Vallée, "Ultrafast Electron Dynamics and Optical Nonlinearities in Metal Nanoparticles", *J. Phys. Chem. B*, **105**, 2264 (2001).

[45] K. Yamada, K. Miyajima and F. Mafuné, "Thermionic emission of electrons from gold nanoparticles by nanosecond pulse-laser excitation of interband", *J. Phys. Chem. C*, **111**, 11246 (2007).

[46] K. A. Willets and R. P. Van Duyne, "Localized surface plasmon resonance spectroscopy and sensing", *Annu. Rev. Phys. Chem.*, **58**, 267 (2007).

[47] S. Link and M. A. El-Sayed, "Shape and size dependence of radiative, non-radiative and photothermal properties of gold nanocrystals", *Inter. Rev. Phys.*

Chem., **19**, 409 (2000).

[48] P. Mulvaney, "Surface Plasmon Spectroscopy of Nanosized Metal Particles", *Langmuir*, **12**, 788 (1996).

[49] A. Henglein and D. Meisel, *Langmuir*, **14**, 7392 (1998).

[50] K. L. Kelly and K. Yamashita, "Nanostructure of Silver Metal Produced Photocatalytically in TiO₂ Films and the Mechanism of the Resulting Photochromic Behavior", *J. Phys. Chem. B*, **110**, 7743 (2006).

[51] S. Eustis and M. A. El-Sayed, "Why gold nanoparticles are more precious than pretty gold: Noble metal surface plasmon resonance and its enhancement of the radiative and nonradiative properties of nanocrystals of different shapes", *Chem. Soc. Rev.*, **35**, 209 (2006).

[52] M. M. Alvarez, J. T. Khoury, T. G. Schaaff, M. N. Shafigullin, I. Vezmar and R. L. Whetten, "Optical absorption spectra of nanocrystal gold molecules", *J. Phys. Chem. B*, **101**, 3706 (1997).

[53] R. Jin, Y. Cao, C. A. Mirkin, K. L. Kelly, G. C. Schatz and J. G. Zheng, "Photoinduced conversion of silver nanospheres to nanoprisms", *Science*, **294**, 1901 (2001).

[54] T. Hyeon, "Chemical synthesis of magnetic nanoparticles", *Chem. Commun.*, 927 (2003).

[55] G. Kawamura, Y. Yang and M. Nogami, "End-to-end assembly of CTAB-stabilized gold nanorods by citrate anions", *J. Phys. Chem. C*, **112**, 10632 (2008).

[56] G. Kawamura, Y. Yang, K. Fukuda and M. Nogami, "Shape control synthesis of multi-branched gold nanoparticles", *Mater. Chem. Phys.*, **115**, 229 (2009).

[57] K. Esumi, K. Matsuhisa and K. Torigoe, "Preparation of rodlike gold particles by

UV irradiation using cationic micelles as a template", *Langmuir*, **11**, 3285 (1995).

[58] Y. Y. Yu, S. S. Chang, C. L. Lee and C. R. C. Wang, "Gold nanorods: electrochemical synthesis and optical properties", *J. Phys. Chem. B*, **101**, 6661 (1997).

[59] N. R. Jana, L. Gearheart and C. J. Murphy, "Seed-Mediated Growth Approach for Shape-Controlled Synthesis of Spheroidal and Rod-like Gold Nanoparticles Using a Surfactant Template", *Adv. Mater.*, **13**, 1389 (2001).

[60] G. Kawamura and M. Nogami, "Application of a conproportionation reaction to a synthesis of shape-controlled gold nanoparticles", *J. Cryst. Growth*, **311**, 4462 (2009).

[61] C. J. Murphy and C. J. Orendorff, "Alignment of Gold Nanorods in Polymer Composites and on Polymer Surfaces", *Adv. Mater.*, **17**, 2173 (2005).

[62] A. Gole, C. J. Orendorff and C. J. Murphy, "Immobilization of Gold Nanorods onto Acid-Terminated Self-Assembled Monolayers via Electrostatic Interactions", *Langmuir*, **20**, 7117 (2004).

[63] H. Wang, G. M. Laws, S. Milicic, P. Boland, A. Handugan, M. Pratt, T. Eschrich, S. Myhajlenko, J. A. Allgair and B. Bunday, "Low temperature ZEP-520A development process for enhanced critical dimension realization in reactive ion etch etched polysilicon", *J. Vac. Sci. Technol. B*, **25**, 102 (2007).

[64] Y. Lin, Y. Zou, Y. Mo, J. Guo and R. G. Lindquist, "E-beam patterned gold nanodot arrays on optical fiber tips for localized surface plasmon resonance biochemical sensing", *Sensors*, **10**, 9397 (2010).

[65] S. J. Randolph, J. D. Fowlkes, and P. D. Rack, "Focused, nanoscale electron-beam-induced deposition and etching", *Crit. Rev. Solid State Mater. Sci.*, **31**, 55 (2006).

[66] S. Graells, R. Alcubila, G. Badenes and R. Quidant, "Growth of plasmonic gold

nanostructures by electron beam induced deposition", *Appl. Phys. Lett.*, **91**, 121112 (2007).

[67] M. C. Daniel and D. Astruc, "Gold nanoparticles: assembly, supramolecular chemistry, quantum-size-related properties, and applications toward biology, catalysis, and nanotechnology", *Chem. Rev.,* **104**, 293 (2004).

[68] H. Nakashima, K. Furukawa, Y. Kashimura and K. Torimitsu, "Self-Assembly of Gold Nanorods Induced by Intermolecular Interactions of Surface-Anchored Lipids", *Langmuir*, **24**, 5654 (2008).

[69] T. Sawitowski, Y. Miquel, A. Heilmann and G. Schmid, "Optical Properties of Quasi One-Dimensional Chains of Gold Nanoparticles", *Adv. Funct. Mater.*, **11**, 435 (2001).

[70] Z. Li, C. Kubel, VI. Parvulescu and R. Richards, "Size tunable gold nanorods evenly distributed in the channels of mesoporous silica", *ACS Nano*, **2**, 1205 (2008).

[71] K. S. W. Sing, D. H. Everett, R. A. W. Haul, L. Moscou, R. A. Pierotti, J. Rouquérol and T. Siemieniewska, "REPORTING PHYSISORPTION DATA FOR GAS/SOLID SYSTEMS with Special Reference to the Determination of Surface Area and Porosity", *Pure & Appl. Chem.*, **57**, 603 (1985).

[72] C. T. Kresge, M. E. Leonowicz, W. J. Roth, J. C. Vartuli and J. S. Beck, "Ordered mesoporous molecular sieves synthesized by a liquid-crystal template mechanism", *Nature*, **359**, 710 (1992).

[73] P. Yang, D. Zhao, D. I. Margolese, B. F. Chmelka and G. D. Stucky, "Generalized syntheses of large-pore mesoporous metal oxides with semicrystalline frameworks", *Nature*, **396**, 152 (1998).

[74] F. Jiao and P. G. Bruce, "Two- and three-dimensional mesoporous iron oxides with

microporous walls". *Angew. Chem. Int. Ed. Engl.*, **43**, 5958 (2004).

[75] S. Jun, S. H. Joo, R. Ryoo, M. Kruk, M. Jaroniec, Z. Liu, T. Ohsuna and O. Terasaki, "Synthesis of New, Nanoporous Carbon with Hexagonally Ordered Mesostructure", *J. Am. Chem. Soc.*, **122**, 10712 (2000).

[76] R. Ryoo, S. H. Joo, M. Kruk and M. Jaroniec, "Ordered Mesoporous Carbons", *Adv. Mater.*, **13**, 677 (2001).

[77] J. S. Beck, J. C. Vartuli, W. J. Roth, M. E. Leonowicz, C. T. Kresge, K. D. Schmitt, C. T. Chu, D. H. Olson, E. W. Sheppard, C. T. McCullen, J. B. Higgins and J. L. Schlenker, "A New Family of Mesoporous Molecular Sieves Prepared with Liquid Crystal Templates", *J. Am. Chem. Soc.*, **114**, 10834 (1992).

[78] D. Zhao, Q. Huo, J. Feng, B. F. Chmelka and G. D. Stucky, "Nonionic Triblock and Star Diblock Copolymer and Oligomeric Surfactant Syntheses of Highly Ordered, Hydrothermally Stable, Mesoporous Silica Structures", *J. Am. Chem. Soc.*, **120**, 6024 (1998).

[79] I. Kartini, P. Meredith, J. C. Diniz da Costa, J. D. Riches and G. Q. M. Lu, "Formation of mesostructured titania thin films using isopropoxide precursors", *Curr. Appl. Phys.*, **4**, 160 (2004).

[80] S. H. Joo, S. J. Choi, I. Oh, J. Kwak, Z. Liu, O. Terasaki and R. Ryoo, "Ordered nanoporous arrays of carbon supporting high dispersions of platinum nanoparticles", *Nature*, **412**, 169 (2001).

[81] M. Kruk, M. Jaroniec, T. Kim and R. Ryoo, "Synthesis and characterization of hexagonally ordered carbon nanopipes", *Chem. Mater.*, **15**, 2815 (2003).

[82] V. Chiola, J. E. Ritsko, C. D. Vanderpool, US patent No. 3556725 (1971).

[83] F. Di Renzo, H. Cambon and R. Dutartre, "A 28-year-old synthesis of

micelle-templated mesoporous silica", *Microporous Mater.*, **10**, 283 (1997).

[84] D. Zhao, J. Feng, Q. Huo, N. Melosh, G. H. Fredrickson, B. F. Chmelka and G. D. Stucky, "Triblock copolymer syntheses of mesoporous silica with periodic 50 to 300 angstrom pores", *Science*, **279**, 548 (1998).

[85] D. F. Evans and H. Wennerström, *The Colloidal Domain: Where Physics, Chemistry, Biology and Technology Meet, 2nd ed.*, Wiley-VCH, New York, 1999.

[86] S. A. Bagshaw, E. Prouzet and T. J. Pinnavaia, "Templating of mesoporous molecular sieves by nonionic polyethylene oxide surfactants", *Science*. **269,** 1242 (1995).

[87] L. Cao, T. Man and M. Kruk, "Synthesis of Ultra-Large-Pore SBA-15 Silica with Two-Dimensional Hexagonal Structure Using Triisopropylbenzene As Micelle Expander", *Chem. Mater.*, **21**, 1144 (2009).

[88] L. Cao and M. Kruk, "Synthesis of large-pore SBA-15 silica from tetramethyl orthosilicate using triisopropylbenzene as micelle expander", *Colloids Surf. Physicochem. Eng. Aspects*, **357**, 91 (2010).

[89] H. Zhang, J. Sun, D. Ma, X. Bao, A. Klein-Hoffman, G. Weinberg, D. Su and R. Schlogl, "Unusual Mesoporous SBA-15 with Parallel Channels Running along the Short Axis", *J. Am. Chem. Soc.*, **126**, 7440 (2004).

[90] J. Sun, H. Zhang, R. Tian, M. Ding, X. Bao, D. S. Su and H. Zou, "Ultrafast enzyme immobilization over large-pore nanoscale mesoporous silica particles", *Chem. Comm.*, 1322 (2006).

[91] M. Impéror-Clerc, P. Davidson and A. Davidson, "Existence of a Microporous Corona around the Mesopores of Silica-Based SBA-15 Materials Templated by Triblock Copolymers", *J. Am. Chem. Soc.*, **122**, 11925 (2000).

[92] R. Ryoo, C.H. Ko, M. Kruk, V. Antochshuk and M. Jaroniec, "Block-Copolymer-Templated Ordered Mesoporous Silica: Array of Uniform Mesopores or Mesopore−Micropore Network?", *J. Phys. Chem. B*., **104**, 11465 (2000).

[93] M. Kruk, M. Jaroniec, C.H. Ko and R. Ryoo, "Characterization of the Porous Structure of SBA-15", *Chem. Mater.*, **12**, 1961 (2000).

[94] S. Ruthstein, V. Frydman, S. Kababya, M. Landau and D. Goldfarb, "Study of the Formation of the Mesoporous Material SBA-15 by EPR Spectroscopy", *J. Phys. Chem. B.*, **107**, 1739 (2003).

[95] C. Göltner-Spickermann, "Non-ionic templating of silica: formation mechanism and structure", *Curr. Opin. Colloid Interface Sci.*, **7**, 173 (2002).

[96] L. Vradman, L. Titelman and M. Herskowitz, "Size effect on SBA-15 microporosity", *Microporous Mesoporous Mater.*, **93**, 313 (2006).

Chapter 2 Shape control of Au NPs in oxide template using photocatalysis of TiO$_2$ and the photocatalytic activity

2.1 Introduction

Au nanostructures have been attracting much attention because of the high chemical stability coincident with their unique optoelectronic properties, which are dependent on the morphology of the Au nanostructures [1-4]. SPR is one of the most interesting properties of Au NRs [2-5]. The wavelength of SPR is affected by the length, diameter, and aspect ratio of the Au NRs [6,7]. Aligned Au NRs perform polarization of light [8-10]. Such multi functionality of the Au NRs opens up new application fields such as wavelength-sensitive nonlinear optical devices and polarization filters [8,9,11]. Several methods for synthesizing Au nanostructures including Au NRs have been reported. These methods include photochemical and electrochemical deposition [12,13] and seeding growth methods [14,15]. In these methods, however, the Au nanostructures are suspended in a solvent. Therefore, the Au nanostructures are required to be immobilized in a designed fashion in/on a solid matrix for various kinds of practical applications. The immobilization process for Au nanostructures still requires further development [3,10,16].

Those methods using hard templates are also advantageous to control the diameter and dispersion state of Au NRs as discussed in previous chapter. However, methods that control the morphology of the Au NRs have several problems. For example, the elongation of the Au NRs requires more Au to be deposited in the template. This obstructs, for example, the investigation of the shape-dependent properties of the Au nanostructures. The Au NPs, a novel method to control the morphology of the Au

NRs in hard templates without changing the gold amount is eagerly demanded.

In this work, nanocrystallized SiO_2-TiO_2 with tubular mesopores was prepared and used as an active template. The shape control of Au NPs and Au NRs was carried out by photocatalysis of TiO_2 in the tubular mesopores. The shape of the Au NPs and Au NRs was observed, and the SPR characteristics and photocatalytic activities of prepared samples were measured.

2.2 Experimental

2.2.1 Materials

Pluronic P123 (($EO)_{20}(PO)_{70}(EO)_{20}$, poly(ethylene oxide), and poly(propylene oxide)) was purchased from Sigma-Aldrich (St. Louis, MO, USA). Tetraethoxysilane [TEOS] and 3-aminopropyltriethoxysilane [APTES] were obtained from Shin-Etsu Chemical Co., Ltd. (Tokyo, Japan). Titanium tetra-n-butoxide [TTB] and $HAuCl_4$ were acquired from Wako Pure Chemical Industries, Ltd. (Osaka, Japan) and Kishida (Osaka, Japan), respectively. Methylene blue [MB] was purchased from Wako (Tokyo, Japan).

2.2.2 Synthesis of mesoporous template

The preparation procedure of $80SiO_2 \cdot 20TiO_2$ (mol%) [20Ti] is described as a typical example. A mixture of P123 (1.74 g), NaCl (2.92 g), and 1 mM HCl (100 mM) was added to TEOS (4.18 g) and stirred at 35°C for 24 h. TTB (1.70 g) was then added to the solution and stirred further for 6 h. For the preparation of $(100-x)SiO_2 \cdot xTiO_2$, only the ratio of TEOS to TTB was varied (x = 20, 30, 40 and 50 mol%). The stirred solution was transferred into an autoclave vessel and kept at 100°C for 4 h. The precipitated powder was collected by suction filtration, then washed with ion-exchanged

water [IEW] and ethanol, and dried in an ambient environment. The obtained powder was calcined at 550°C for 5 h to remove the surfactant from the mesopore. Fig. 2.1 shows the schematic diagram of the template fabrication experimental procedures.

2.2.3 Loading of Au

The obtained powder was immersed in the 1 wt% APTES solution (in ethanol) and stirred at 25°C for 3 h. The powder was then filtered with suction, washed with ethanol, and dried at 60°C in air. The amino-functionalized powder was mixed into a 1 mM $HAuCl_4$ aqueous solution and stirred at 25°C for 2 h. After the suction filtration, the product was washed with IEW and dried in an ambient environment. The product was then calcined at 350°C for 3 h (at a heating rate of 1°C/min) with or without UV radiation (USHIO SP-7, 230-440 nm, 2.5 mW cm^{-2} at 365 nm). Fig. 2.2 shows the schematic diagram of the Au deposition experimental procedure and Fig. 2.3 shows the schematic diagram of UV radiation method during calcination.

2.2.4 Characterization

X-ray diffraction [XRD] measurements were performed using a Rigaku RINT 2000 diffractometer (Rigaku Corporation, Tokyo, Japan) with CuKα radiation (λ = 1.5406 Å). Transmission electron microscopy [TEM] images and energy dispersive spectroscopy [EDS] were taken using an H-800 transmission electron microscope (Hitachi Corporation, Tokyo, Japan) and a JEOL JEM-2100F (JEOL, Ltd., Tokyo, Japan) transmission electron microscope operating at 200 kV. UV/visible-near infrared diffuse reflectance [Vis-NIR DR] spectra were measured using a JASCO V-670 UV-Vis-NIR spectroscope (JASCO Corporation, Tokyo, Japan). Surface areas were

determined by N_2 adsorption isotherms with the Brunauere EmmetteTeller [BET] method by using a Micromeritics TriStar II 3020 adsorption analyzer (USA). The samples were degassed at 150℃ for 2 h in a vacuum before the measurement.

2.2.5 Photocatalytic measurement of prepared powders

The photocatalytic activity of the prepared powders was evaluated by measuring the rate of MB bleaching in aqueous solution. The prepared composite (10 mg) was stirred in an aqueous solution of MB (1.88×10^{-5} mol L^{-1}, 20 mL) in the dark for 10 min to allow the complete adsorption of MB on the surface of the powder. The suspended powder was then irradiated with UV (230-440 nm, 1.0 mW cm^{-2} at 365 nm) and/or Vis light (490-550 nm or 570-690 nm, 8.5 mW cm^{-2}) under magnetic stirring. A small portion of the solution was withdrawn after light irradiation for certain periods (1, 2, 3, 5, 7, 10 and 15 min) and centrifuged at 5000 r min^{-1} for 5 min to remove the powder. The concentration of MB in this solution was evaluated by recording the absorbance of MB in solution at 664 nm with a UV-Vis spectrophotometer (JASCO, V-560, Japan).
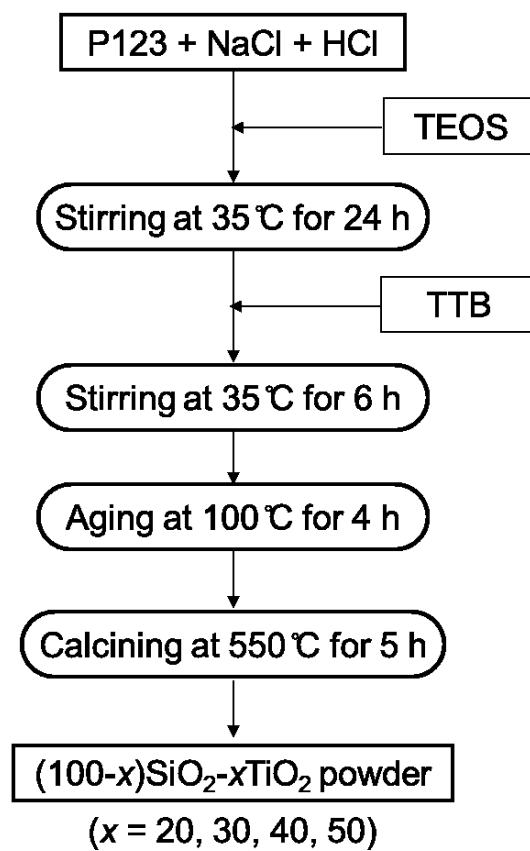
```
                    ┌─────────────────────────┐
                    │   P123 + NaCl + HCl     │
                    └─────────────────────────┘
                                 │        ┌──────────────┐
                                 │◄───────│     TEOS     │
                                 ▼        └──────────────┘
                    ╭─────────────────────────╮
                    │ Stirring at 35℃ for 24 h │
                    ╰─────────────────────────╯
                                 │        ┌──────────────┐
                                 │◄───────│     TTB      │
                                 ▼        └──────────────┘
                    ╭─────────────────────────╮
                    │ Stirring at 35℃ for 6 h  │
                    ╰─────────────────────────╯
                                 │
                                 ▼
                    ╭─────────────────────────╮
                    │  Aging at 100℃ for 4 h   │
                    ╰─────────────────────────╯
                                 │
                                 ▼
                    ╭─────────────────────────╮
                    │ Calcining at 550℃ for 5 h│
                    ╰─────────────────────────╯
                                 │
                                 ▼
                    ┌──────────────────────────────┐
                    │ (100-x)SiO₂-xTiO₂ powder     │
                    └──────────────────────────────┘
                         (x = 20, 30, 40, 50)
```

Fig. 2.1. Schematic diagram of the $(100\text{-}x)\mathrm{SiO_2}\text{-}x\mathrm{TiO_2}$ template fabrication procedures.

```
┌─────────────────────────┐
│      APTES + EtOH       │
└─────────────────────────┘
            │
            │         ┌──────────────────────────────┐
            │◀────────│ (100-x)SiO₂-xTiO₂ powder     │
            │         └──────────────────────────────┘
            ▼
   ╭─────────────────────────╮
   │  Stirring at 25 ℃ for 3 h │
   ╰─────────────────────────╯
            │
            ▼
   ╭─────────────────────────╮
   │  Filtration and washing  │
   ╰─────────────────────────╯
            │
            ▼
┌──────────────────────────────┐   ┌──────────────────────────────┐
│ Amino-functionalized powder  │   │  HAuCl₄·4H₂O + H₂O           │
└──────────────────────────────┘   └──────────────────────────────┘
              │                              │
              └──────────────┬───────────────┘
                             ▼
              ╭─────────────────────────────╮
              │  Stirrinng at 25 ℃ for 2 h   │
              ╰─────────────────────────────╯
                             │
                             ▼
   ╭──────────────────────────────────────────────────────────╮
   │ Calcining at 350 ℃ for 3 h with/without UV radiation      │
   ╰──────────────────────────────────────────────────────────╯
                             │
                             ▼
            ┌──────────────────────────────────────┐
            │  Au/(100-x)SiO₂-xTiO₂ powder         │
            └──────────────────────────────────────┘
```
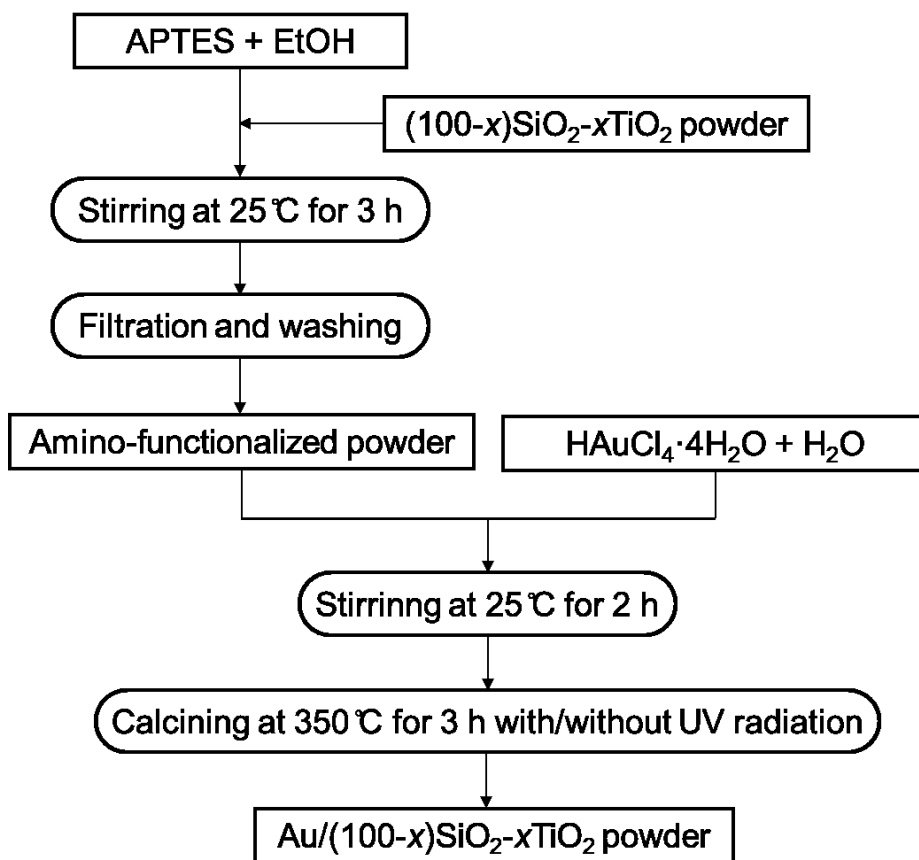
Fig. 2.2. Schematic diagram of the Au deposition procedures.
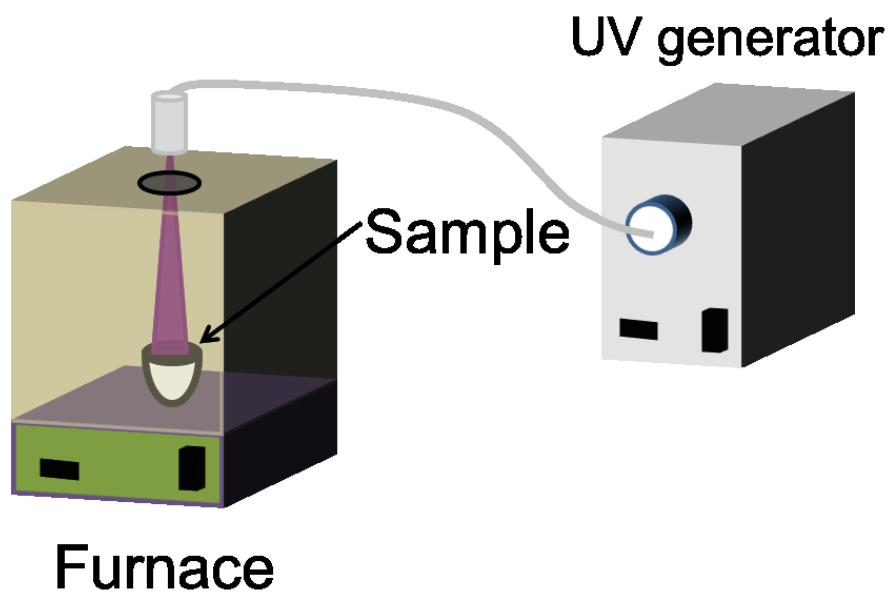
Fig. 2.3. Schematic diagram of UV radiation method during calcination.

2.3 Results and discussion

2.3.1 Characterization of mesoporous SiO$_2$ or SiO$_2$-TiO$_2$ template

Fig. 2.4 shows the XRD patterns of the mesoporous 100SiO$_2$ template [0Ti], 80SiO$_2$·20TiO$_2$ [20Ti] and 50SiO$_2$·50TiO$_2$ [50Ti]. In the XRD pattern of the mesoporous 100SiO$_2$ template, amorphous SiO$_2$ was observed as a halo at ca. 23°. On the other hand, the 80SiO$_2$·20TiO$_2$ template showed anatase and rutile TiO$_2$ peaks in addition to an amorphous halo of SiO$_2$. The peaks of the TiO$_2$ crystals appeared stronger in the pattern of the 50SiO$_2$·50TiO$_2$ template in comparison with those of 20Ti.

Fig. 2.5 shows the TEM images of prepared templates (0Ti, 20Ti and 50Ti). A TEM observation of these templates revealed that all of them possessed a 2-D hexagonal mesoporous structure with the same caliber of ca. 7 nm (Fig. 2.5 (a), (b) and (c)). The high-resolution TEM images of 20Ti and 50Ti showed ca. 4 nm crystals with a fringe spacing of 3.52 Å, which were well dispersed in the samples (insets of Fig.2.5(b) and (c)). The fringe spacing is consistent with the d value of {011} planes of anatase TiO$_2$. This proves that the templates consist of pure amorphous SiO$_2$, or SiO$_2$ and well-dispersed TiO$_2$ nanocrystals, forming a 2-D hexagonal mesoporous structure.

Particles without mesopores were rarely observed in the TEM images of 20Ti and 50Ti prepared by aging in water at 100°C for 4 h. On the other hand, 20Ti (and 50Ti) aged for 24 h in water at 100°C showed the formation of large nonporous particles outside the mesoporous structure as shown in Fig. 2.6(a). The components of the nonporous particles and mesoporous region were solely attributed to TiO$_2$ and SiO$_2$, respectively (Fig. 2.6(b)). Thus, the TiO$_2$ crystal formation in our samples should be based on the dissolution and deposition of the TiO$_2$ component by aging in hot water at 100°C where the TiO$_2$ component in the SiO$_2$-TiO$_2$ gel system is dissolved into water

and then reprecipitated as crystalline TiO_2 [17,18]. The short aging time in hot water resulted in the suppression of large TiO_2 particle formation and the sufficient deposition of TiO_2 nanocrystals with a highly dispersed state on/in the mesoporous matrix. In this work, therefore, the aging time of 4 h at 100°C was employed to prepare the templates, which possess almost the same pore size and structure regardless of the TiO_2 content. The molar ratio of SiO_2 to TiO_2 in the mesoporous region was checked by EDS, and it was found to be comparable to the nominal molar ratio. By using the templates, the effect of the TiO_2 nanocrystals on the shape of the Au NRs can be investigated due to the sufficient formation of interfaces between the deposited Au and TiO_2 nanocrystals.
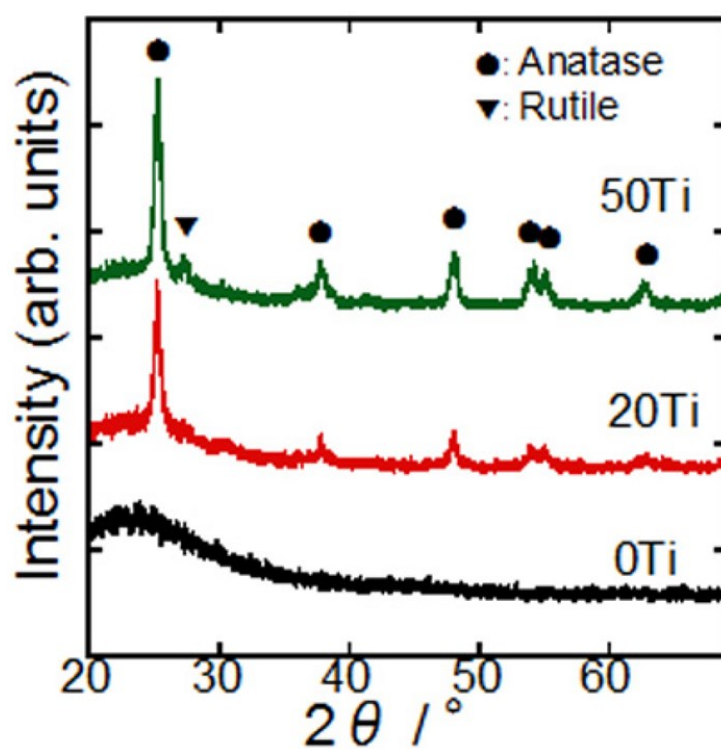
Fig. 2.4. XRD patterns of 0Ti, 20Ti and 50Ti.
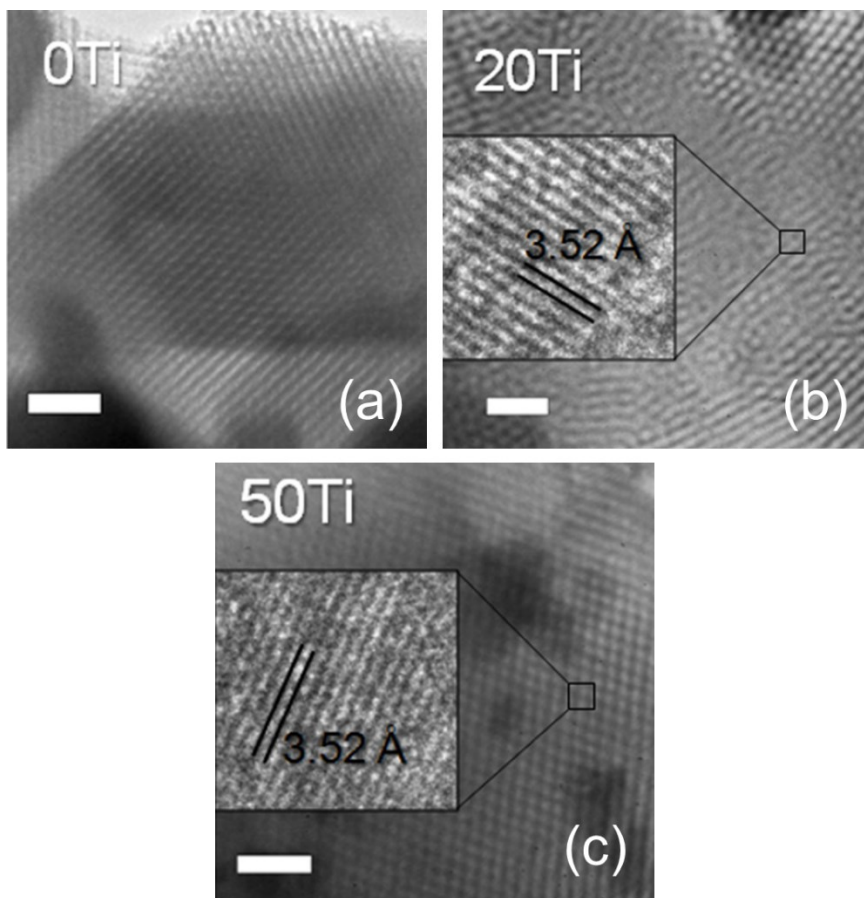
Fig. 2.5. TEM images of (a) 0Ti, (b) 20Ti and (c) 50Ti (scale bars, 50 nm). The insets in (b) and (c) are HR TEM images of the squared region.
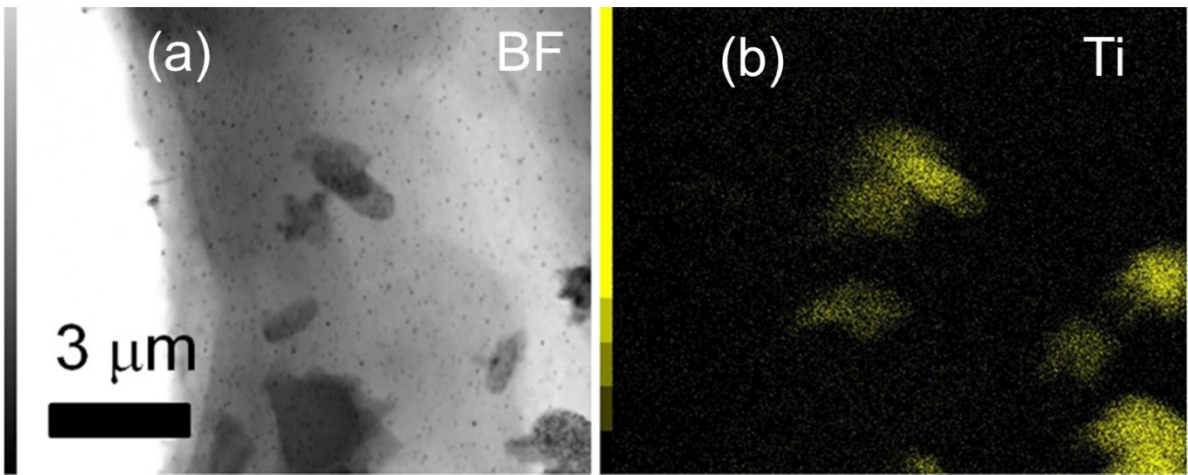
Fig. 2.6. TEM image and Ti elemental mapping of 20Ti. (a) Bright field TEM image

and (b) Ti elemental mapping of 20Ti treated in water at 100°C for 24 h.

2.3.2 Shape control of Au NPs by different compositions of template

Fig. 2.7 shows the TEM images of prepared templates after Au deposition. Long Au NRs were formed in 0Ti after Au loading. Fig. 2.8 shows the schematic diagram of the formation of Au NRs in mesopores with SiO_2 template. At the beginning of the Au loading, the Au^{3+} ions adsorb to the amino groups on the wall of the mesopores. Heat treatment of the resultant powder causes decomposition of the amino group-containing organic matter. The Au^{3+} ions are released and partly reduced to Au^+ ions and Au atoms by electrons provided from the decomposed organic matter. The Au atoms agglomerate and form Au nanoclusters, and then the Au ions released from the amino groups are reduced on the Au nanoclusters by autocatalysis of Au [19, 20], causing the Au metal to grow. Since the growth of Au occurs in the tubular mesopores, the final shape of the Au should be nanorod or nanoparticle. A morphology change of the Au NPs was then investigated when the content of TiO_2 in the template was varied. The length of the Au NRs formed in 20Ti (Fig. 2.7(b)) was shorter than that deposited in 0Ti, whereas Au NPs were predominantly obtained in 50Ti (Fig. 2.7(c)). These results indicate that an increase in TiO_2 content leads to a shortening of the Au NRs. This is presumably because thermoexcited conduction electrons are generated from TiO_2, and these generated electrons transfer to the Au ions to accelerate their reduction [21]. Fig. 2.9 shows the schematic diagram of the formation of Au NPs and NRs in mesopores with SiO_2-TiO_2 template. TiO_2 heated at 350°C generates approximately 8.8×10^{13} times as many thermoexcited electrons as TiO_2 does at room temperature [22]. Therefore, the amount of electrons supplied to the Au ions increases as the TiO_2 content increases. As a result, Au metal is rapidly deposited prior to its migration for the formation of long Au NRs and Au NPs were predominantly formed in the tubular mesopores by using

templates containing more than 50 mol% TiO_2.

Fig. 2.10 shows the diffuse reflectance [DR] spectra of prepared templates after Au deposition. Au NRs deposited in 0Ti showed two extinction peaks in the DR spectrum: a sharp extinction peak at 500 nm and a broad extinction peak spreading over the whole region of the NIR region. The shorter- and longer-wavelength extinctions are attributed to the transverse mode of SPR and the light scattering by fairly long Au NRs [23], respectively. The length of the Au NRs was shortened when 20Ti was used. An extinction peak appeared at around 600 nm, and the extinction intensity at wavelengths longer than 1,200 nm increased. This is presumably due to the shortening of the Au NRs, which leads to a decrease in the light scattering intensity of the long Au NRs (appearing over the whole NIR region) and an increase in the LSPR mode caused by the short Au NRs (appearing at the NIR region toward the shorter wavelength side, e.g. 600 nm and approximately 2,000 nm in this case). With 30Ti, the LSPR peaks blue-shifted and appeared at 580 and approximately 900 nm. When 50Ti was used, only Au NPs were deposited accompanied by a 520-nm peak, which is attributed to the SPR of the Au nanorparticles. By the use of a mesoporous SiO_2 template containing less than 30 mol% TiO_2, Au NPs exhibiting LSPR, which is excited by NIR light, are deposited regardless of the presence of TiO_2 nanocrystallites in the template.
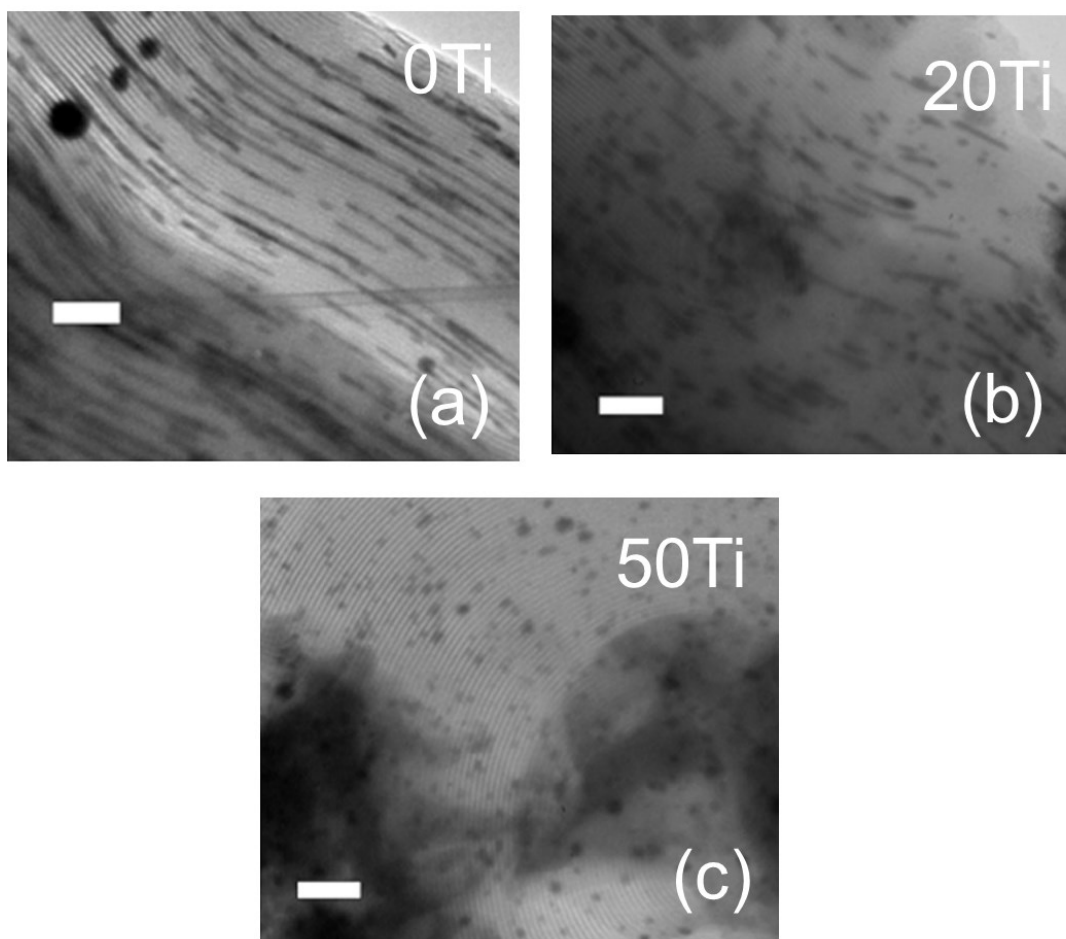
Fig. 2.7. TEM images of prepared templates after Au deposition. TEM images of (a) 0Ti,

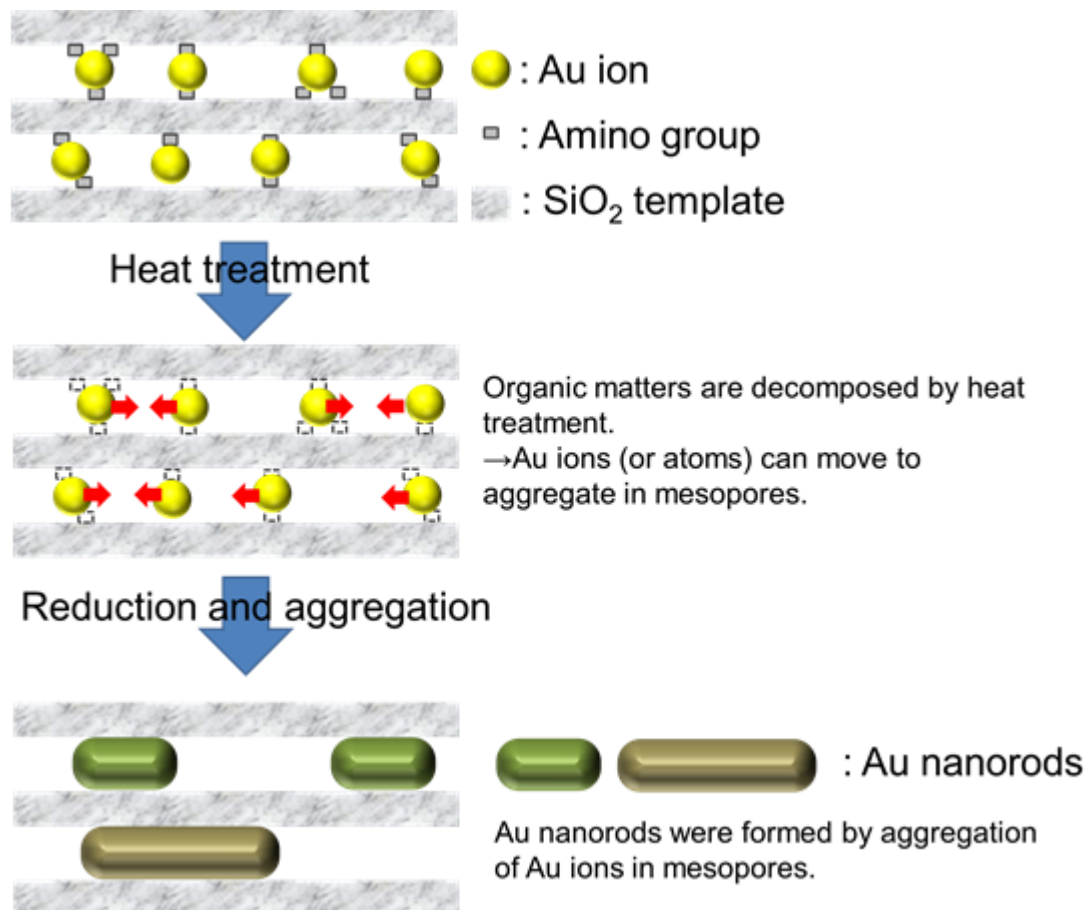(b) 20Ti and (c) 50Ti after Au deposition (scale bar, 100 nm).

Fig. 2.8. Schematic diagram of the formation of Au NRs in mesoporous SiO_2-TIO_2.
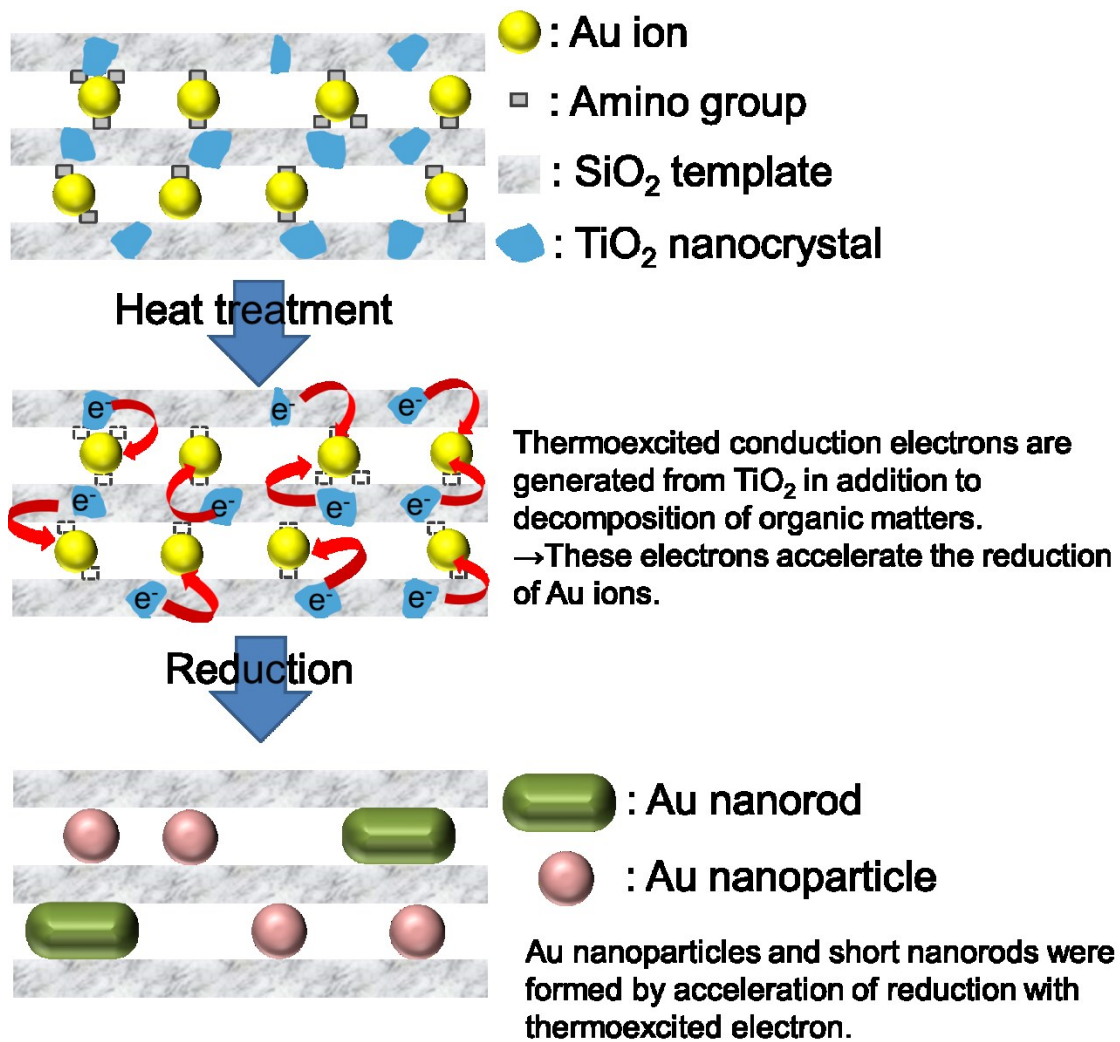
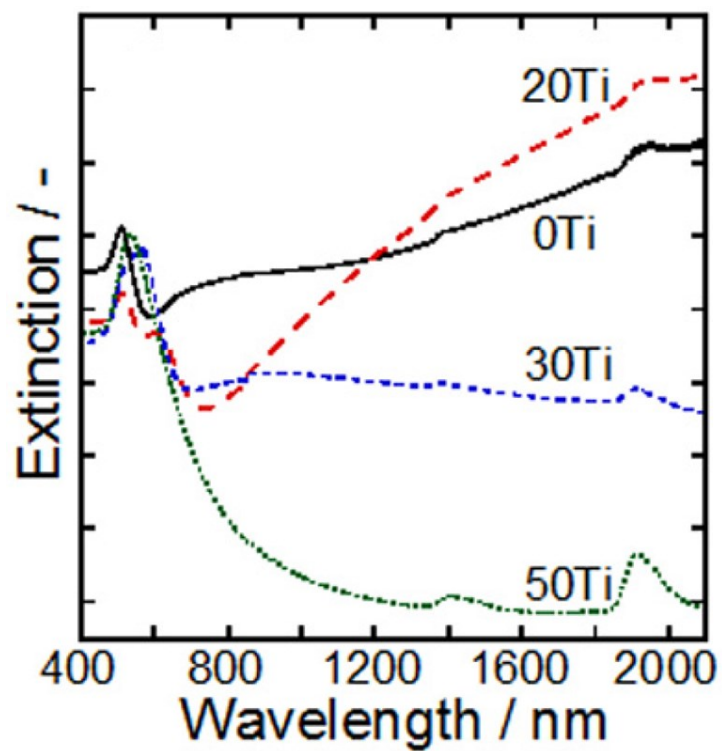Fig. 2.9. Schematic diagram of the formation of Au NPs and NRs in mesoporous SiO₂-TIO₂.

Fig. 2.10. DR spectra of 0Ti, 20Ti, 30Ti and 50Ti after Au deposition.

2.3.3 Shape control of Au nanoparticle by UV radiation

Since TiO_2 is known as a photocatalyst that generates electrons and holes by UV radiation, the effects of UV radiation during Au loading on the shape of the Au NPs were investigated. As for the TiO_2 crystalline phases, anatase TiO_2 was widely recognized as the most suitable phase for photocatalysis [24,25]; but recent reports suggest that mixed rather than single phases can be even more active [26,27]. Also, since the TiO_2 nanocrystals in our samples possess diameters of a few nanometers, which are almost the optimum size for photocatalysis [24], UV radiation of the templates should generate charges and influence the shape of the Au NRs. Fig. 2.11 shows the TEM images of 0Ti after thermal Au deposition with/without simultaneous UV radiation. In the case where 0Ti was used, Au NRs with a length of 10 to 100 nm were deposited regardless of the UV radiation. It is worth mentioning that the Au NRs in 0Ti were fabricated with a short length by shortening the calcination time in order to discuss the shift of the resonant wavelength in the measurable NIR region. In the DR spectra, the LSPR wavelengths of the samples prepared with and without UV radiation were 930 and 990 nm, respectively. The wavelengths were slightly shifted, and the LSPR extinction intensity decreased slightly upon UV radiation (Fig. 2.12). The results reveal that UV radiation has only a minor effect on the shape of the deposited Au NRs when 0Ti is used. On the other hand, although Au NRs with a length of 10 to 400 nm were obtained in 20Ti without UV radiation (Fig. 2.13(a)), Au NPs were predominantly deposited when UV radiation was carried out (Fig. 2.13(b)). The extinction peaks in the NIR region almost disappeared when the sample was exposed to UV radiation as shown in Fig. 2.14. These results clearly show that UV radiation during Au loading in 20Ti influences the shape of the Au NPs. Furthermore, since the Au NPs are insensitive

toward UV light, it is evident that the photocatalytic activity of TiO_2 is affected by the shape of the Au NPs in the template.

Two mechanisms were considered for the preferential formation of Au NPs by UV radiation: acceleration of the Au-ion reduction rate by the generated electrons or oxidation of deposited Au metal by the generated holes. In the case where UV radiation at room temperature was carried out on the Au ion-adsorbed 20Ti, an increase in extinction intensity was observed from the Vis to the NIR region (Fig. 2.15(a)). The increased extinction was attributed to the formation of Au NRs of various lengths because of the wide wavelength region of SPR. On the other hand, UV radiation of 0Ti resulted in a slight increase in extinction intensity over a similarly wide wavelength region (Fig, 2.15(a)). This is probably due to the marginal deposition of Au NPs by UV radiation, which partly decomposes the organic matter adsorbed on the mesoporous wall, and thus, a small number of electrons are generated that reduce Au ions. This would explain the spectral change in Fig. 2.12, where the thermal and photo decomposition of the organic matter occurs simultaneously at the beginning of the Au loading process; thus, the Au reduction rate is slightly increased. Furthermore, since the variation of the extinction intensity in 20Ti is much larger than that in 0Ti, it is clear that UV radiation accelerates the reduction of Au ions as a result of the electrons generated from TiO_2. On the other hand, UV radiation after the thermal deposition of Au NRs in 20Ti led to little change in the DR spectra (Fig. 2.15(b)). This indicates that the holes, which are expected to oxidize the deposited Au NRs to Au ions, have negligible effect on the shape change in the Au NPs. Thus, it is concluded that the photocatalysis of TiO_2 causes the reduction of the gold ions rather than oxidation of the Au metal. The generated holes may be consumed to decompose organic matter adsorbed on the wall of the template. In

addition, UV radiation of the Au NRs deposited in 0Ti also resulted in no change in the DR spectra.

The results obtained suggest the probable mechanism of Au deposition by the simultaneous heat treatment and UV radiation, where the predominant formation of Au NPs was observed (Fig. 2.13(b)). The heat treatment causes the decomposition of organic matter adsorbed on the wall of the template. These results in the partial reduction of Au^{3+} ions, followed by the formation of scattered Au nanoclusters. The partially reduced Au ions are released from their electrostatic adsorption to the amino groups and associated with the oxygen atoms on the wall surface of the matrix, enabling mobility of the Au ions [28]. The Au ions, therefore, can reach the neighboring Au nanoclusters and are reduced on the surface of the nanoclusters by autocatalysis of Au [19,20], resulting in the formation of Au NRs because the growth of Au occurs in the tubular mesopores. Thermally excited electrons of TiO_2 accelerate the reduction rate of the Au ions; thus, a large content of TiO_2 in the template leads to the preferential formation of Au NPs. Furthermore, UV radiation also accelerates the reduction rate of the Au ions. Therefore, the combination of heat treatment and UV radiation leads to a fast rate of Au deposition. The time taken for the movement of the Au ions is shortened, and the formation of Au NPs instead of Au NRs becomes dominant. By optimizing the heating and UV radiation condition of our method, Au NRs and NPs are selectively deposited regardless of the composition of the template, where the amount of deposited Au atoms is constant but the shape of the Au NPs is different.
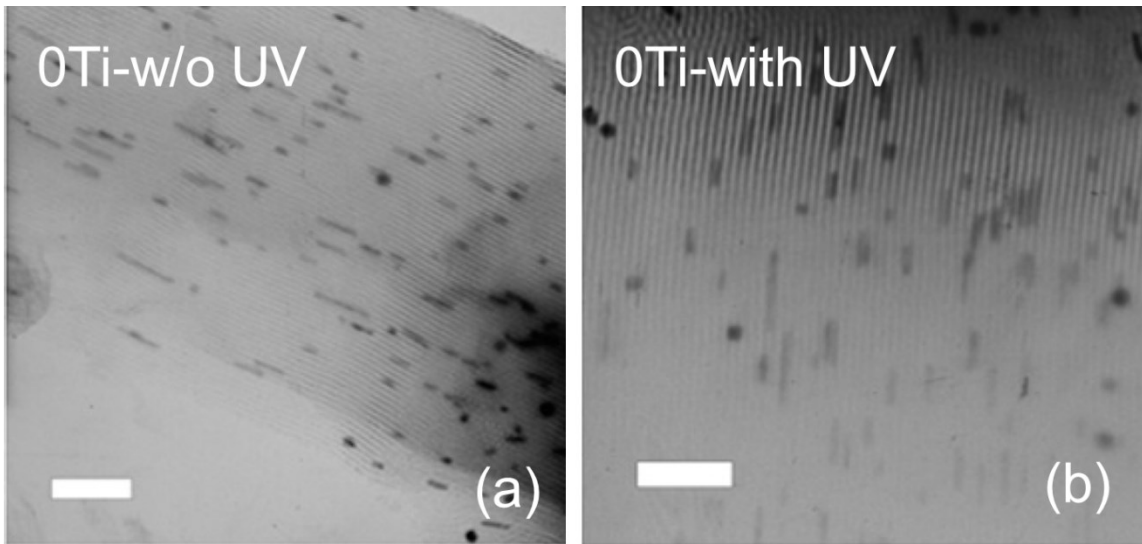
Fig. 2.11. TEM images of 0Ti after thermal Au deposition (a) without or (b) with simultaneous UV radiation (scale bars, 100 nm).
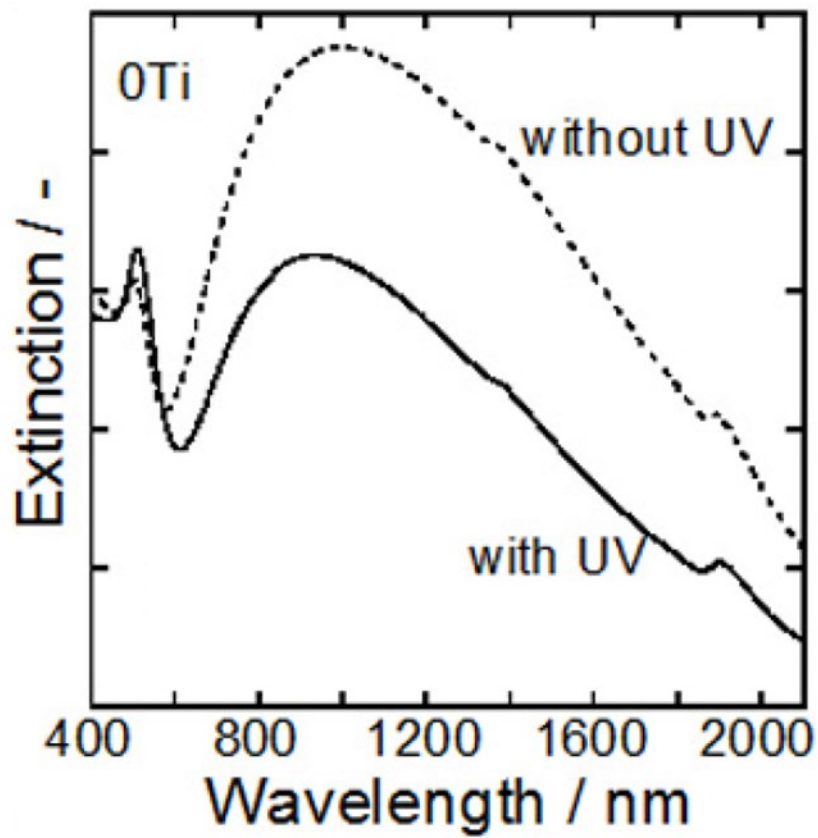
Fig. 2.12. DR spectra of 0Ti after thermal Au deposition without/with simultaneous UV radiation.
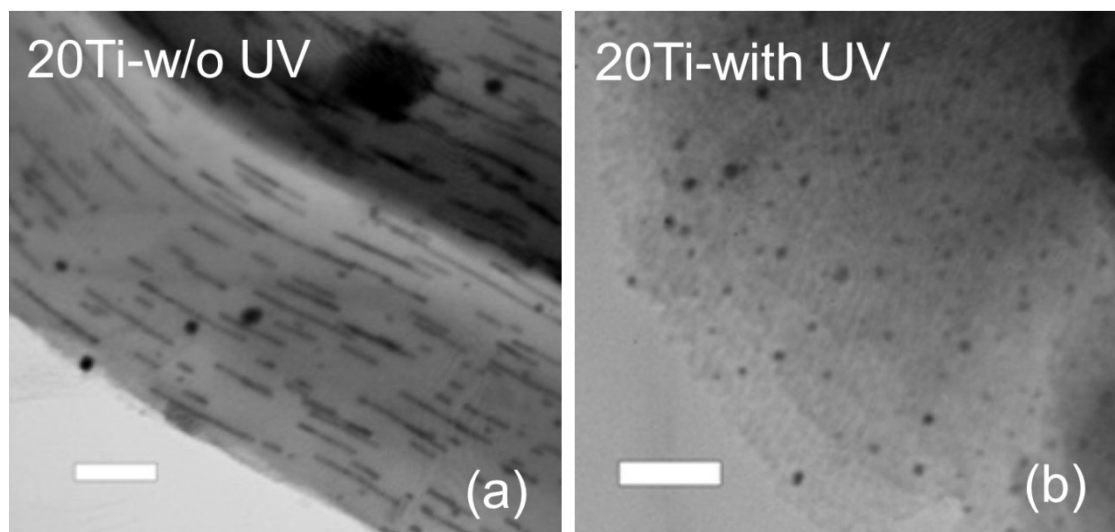
Fig. 2.13. TEM images of 20Ti after thermal Au deposition (a) without or (b) with simultaneous UV radiation (scale bars, 100 nm).
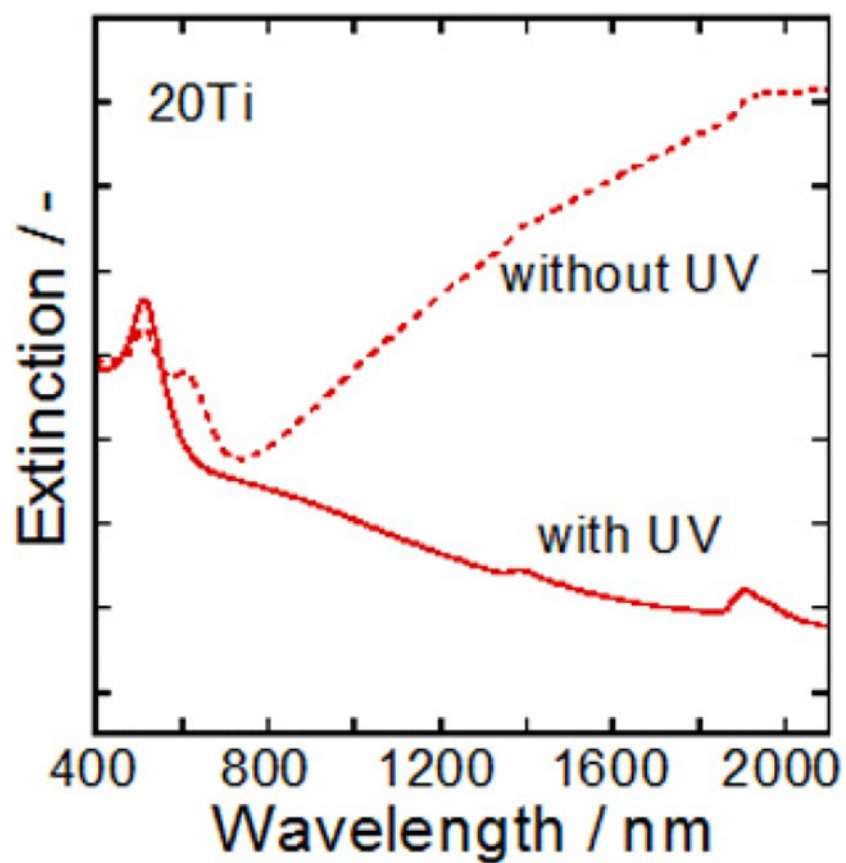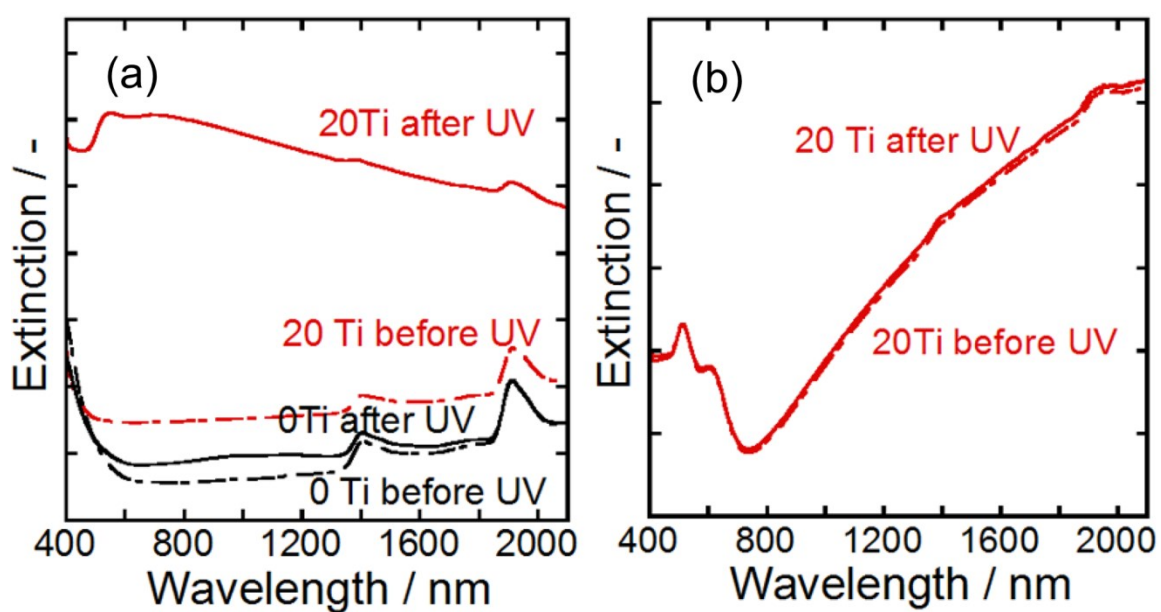
Fig. 2.14. DR spectra of 20Ti after thermal Au deposition without/with simultaneous
UV radiation.

Fig. 2.15. DR spectra of (a) Au^{3+} ion-adsorbed 20Ti and 0Ti before and after UV radiation (no heat treatment) and (b) of the Au NRs thermally pre-deposited in 20Ti before and after UV radiation.

2.3.4 Photocatalytic activity under UV radiation

In order to investigate the effect of the shape of Au NPs on the photocatalytic activity, the photocatalytic activities of 20Ti and 20Ti deposited with Au NPs or Au NRs were measured. The time dependence of MB bleaching by the 20Ti templates with and without Au NPs under UV radiation is shown in Fig. 2.16. The concentration of MB maintains its initial value when the MB solution is irradiated with UV light for 15 min without the composite, revealing that UV irradiation itself has no direct influence on the bleaching of MB. On the other hand, MB in a solution containing 20Ti template without Au is photo-bleached upon UV radiation. The concentration of MB decreases by 75% after UV irradiation for 15 min. Au deposition enhances the photocatalytic activity of 20Ti template. The 20Ti with Au NPs and NRs bleach about 85% and 95% of the MB, respectively, after UV radiation for 15 min. For comparing, the photocatalytic activity of Degussa P25 is evaluated in the same way. The concentration of MB decreases by 53% after UV radiation for 15 min. Because the specific surface area of catalysts strongly affects their photocatalytic activity, the surface area of each sample was measured. The surface area of the prepared powders are 518.5 m^2 g^{-1} (20Ti), 312.3 m^2 g^{-1} (Au NPs-deposited) and 388.6 $m^2 g^{-1}$ (Au NRs-deposited), respectively, as shown in Table 2.1. The surface area of 20Ti with Au NPs is smaller than that of the samples with Au NRs. This is because Au NPs are well dispersed in the mesopores compared with Au NRs, resulting in blocking of the more mesopores more frequently. The reaction rate constants (k) were also calculated using the equation,

$$k = \ln(I_0/I_x)/t \qquad (1)$$

where I_0 is the initial concentration of MB (1.88×10^{-5} mol L^{-1}), and I_x is the concentration of MB after irradiation with UV for a certain time t. These results are shown in Table 2.1, and demonstrated that deposition of Au, regardless of its shape, enhanced the photocatalytic activity of the 20Ti template even though the specific surface area decreased. The 20Ti templates with Au NPs and NRs possess k per unit area (k/A) which is two and three times larger, respectively, than that of the bare 20Ti template. This means that Au NRs improve the photocatalytic activity of the 20Ti template to a greater extent than Au NPs, and the prepared 20Ti template with Au NRs shows the higher photocatalytic activity than that of Degussa P25.

The enhanced photocatalytic activity achieved by the presence of Au NPs is presumably due to the fact that the Au NPs are effective traps for electrons generated by TiO$_2$ due to the formation of a Schottky barrier at the Au-TiO$_2$ interface. The effective electron trapping allows more efficient charge separation of the electron-hole pairs, increasing their lifetimes [29,30]. Furthermore, it has been reported that the photoactivity of Au nanoparticle-coated TiO$_2$ under UV radiation is enhanced when the particle size of Au increases. This is because the efficiency of charge separation between TiO$_2$ and Au NPs improves as the particle size increases [31]. In our case, Au NRs have the same diameter as Au NPs (-7 nm), but they are much longer than the NPs. Thus the deposition of Au NRs on 20Ti template effectively increases the lifetimes of holes and electrons generated in TiO$_2$, leading to a larger k per unit area for photobleaching of MB. Au NPs in both samples were totally well dispersed judging from their TEM images, thus the dispersion state had no effect on the photocatalytic activity. This enhancement exceeded the attenuation effect of decreased surface area by Au deposition on the photocatalytic activity, therefore, k/A of Au NR sample was even higher than P25.
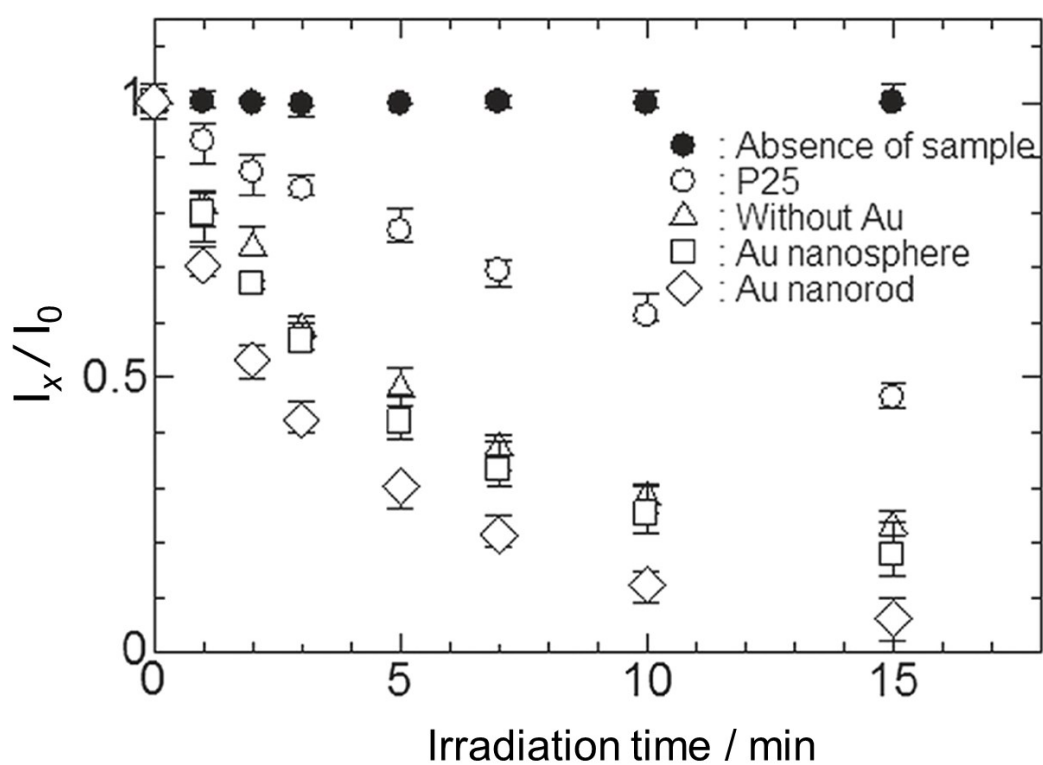
58

Fig. 2.16. Time dependence of the bleaching of MB through photocatalysis by the mesoporous SiO_2-TiO_2 samples with and without Au NPs under UV radiation. (I_0: initial absorbance of MB solution, I_x: absorbance of MB solution after certain time).

Table 2.1. Specific surface area, rate constant of MB bleaching, and rate constant per unit area of mesoporous SiO_2-TiO_2 samples with/without Au and P25

Sample	Specific surface area [m^2g^{-1}]	k [min^{-1}]	k/A [min^{-1} m^{-2}]
Bare 20Ti	518.5	0.168	3.24×10^{-2}
20Ti with Au NPs	312.3	0.209	7.04×10^{-2}
20Ti with Au NRs	388.6	0.375	1.01×10^{-1}
P25	46.5	0.051	9.75×10^{-2}

2.3.5 Photocatalytic activity under UV and Vis irradiation

The time dependence of bleaching of MB through photocatalysis by the Au-deposited samples under UV and/or Vis irradiation is presented in Fig. 2.17 and Fig. 2.18. The wavelengths of Vis light were selected to effectively excite the SPR of deposited Au NPs in the samples; 490-550 nm and 570-690 nm for the Au NP- and Au NR-deposited samples, respectively. Irradiation of the Au-deposited samples with UV light cause bleaching of MB through the improved photocatalysis of TiO_2, as shown in Fig. 2.16. However, Vis irradiation of 490-550 nm associated with/without UV radiation has almost no influence on the photocatalytic behavior of the samples. There is also no difference when 570-690 nm light is used instead of 490-550 nm light. In this study, the bleaching reaction of MB or any effect on the reaction upon UV radiation by Vis irradiation was not observed. According to the recent reports, TiO_2 crystals modified with Au nanoparticles oxidize organic compounds such as 2-propanol upon irradiation with Vis light [32,33]. This reaction is caused by electron transfer from the Au NPs, which are SPR active under Vis light, to the conduction band of TiO_2. The electron-deficient Au oxidizes the organic compounds to return to its metallic state [34]. However, according to Shibata et al. [35], this electron transfer can occur between specific crystal interfaces of TiO_2 and Au. Our method of depositing Au presumably leads to the formation of various interfaces that even involve Au with amorphous phases of TiO_2 and SiO_2. As a result, Vis irradiation of our samples had little effect on photocatalysis because the effective formation of crystalline TiO_2/Au interface, so-called electronic contact between TiO_2 and Au for photocatalysis by Vis irradiation was not achieved.
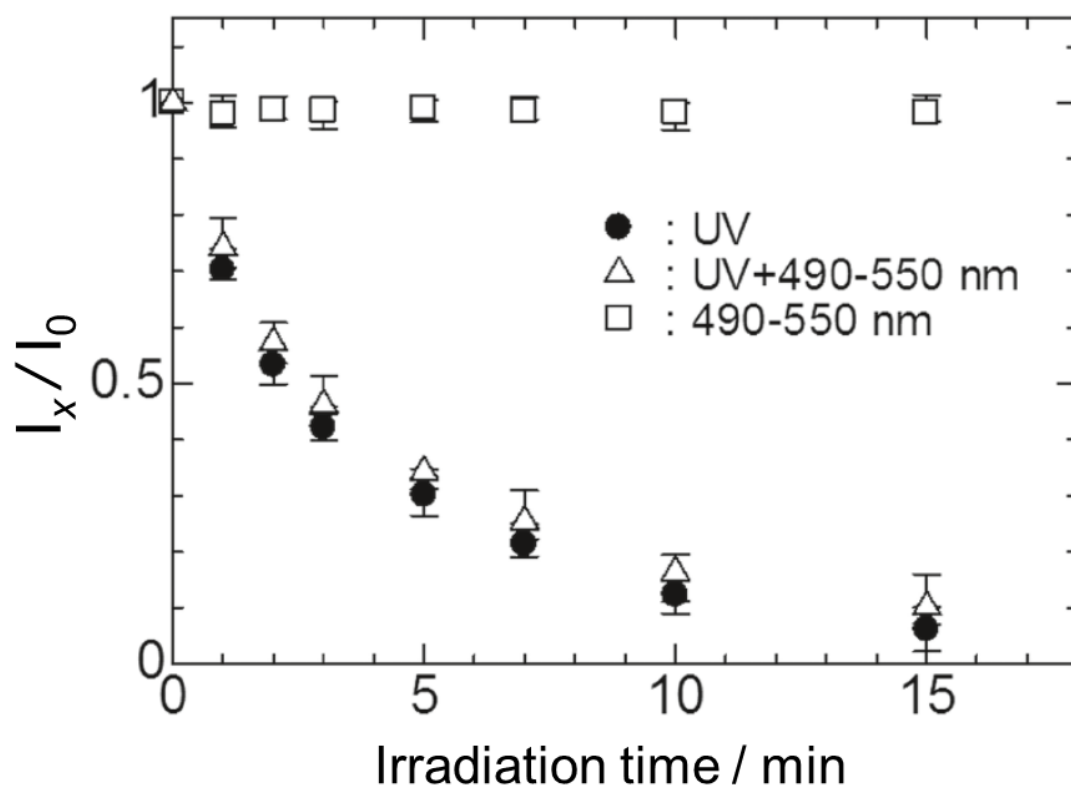
Fig. 2.17. Time dependence of the bleaching of MB through photocatalysis by Au NR-deposited 20Ti sample under UV and/or Vis irradiation (490-550 nm).
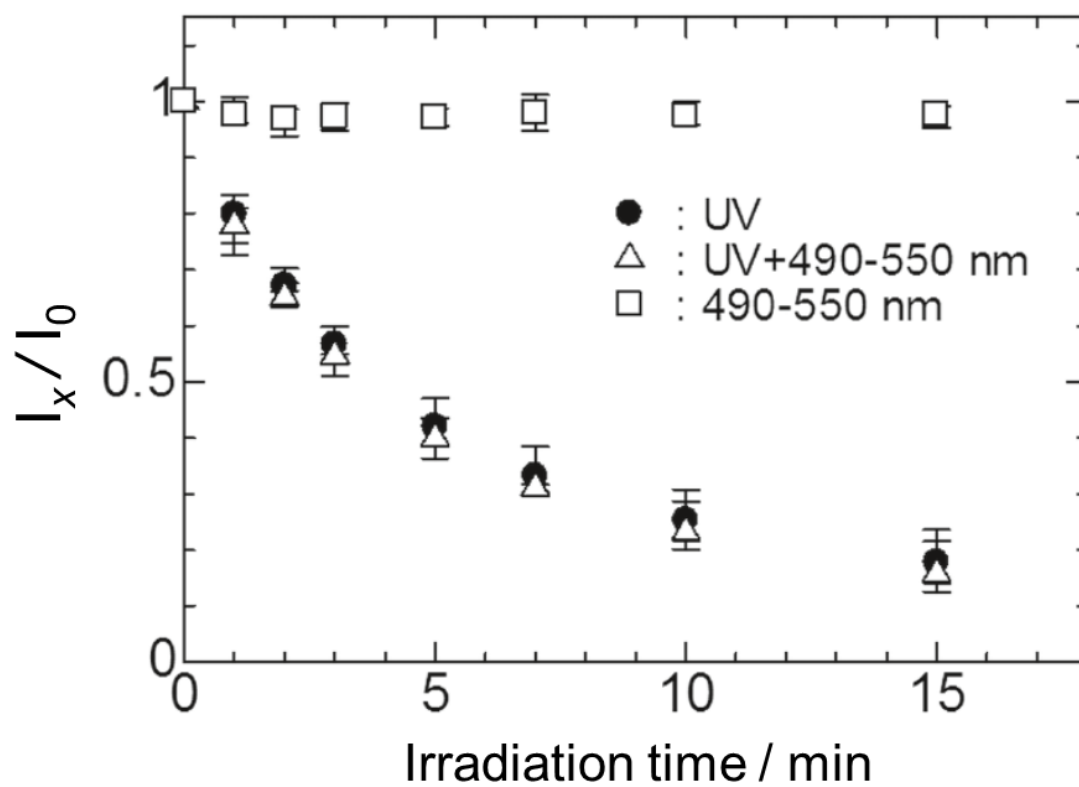
Fig. 2.18. Time dependence of the bleaching of MB through photocatalysis by Au NP-deposited 20Ti sample under UV and/or Vis irradiation (490-550 nm).

2.4 Conclusion

TiO$_2$ nanocrystal-containing mesoporous templates were fabricated and Au NRs or Au NPs were deposited in the as-formed tubular mesopores Since the provision of thermally generated electrons from TiO$_2$ increased when a template contained a large amount of TiO$_2$, Au ions were rapidly reduced and deposited as shorter Au NRs or Au NPs. Similarly, UV radiation during Au deposition in the TiO$_2$-containing template produced electrons photocatalytically and accelerated the Au deposition rate, leading to the dominant formation of Au NPs. The rate constant per unit area for photobleaching of MB upon UV radiation by the samples was evaluated. The Au NPs- and Au NRs-deposited SiO$_2$-TiO$_2$ composites possessed rate constants that were two and three times larger than that of the bare template. Vis irradiation of the prepared samples had no significant effect on their photocatalytic properties. This is presumably because the electronic contact between TiO$_2$ and Au was not formed by our sample preparation procedure. Thus, it was found that the electronic contact is needed for the photocatalysis by Vis irradiation, but not necessary for the enhancement of TiO$_2$ photocatalysis upon UV irradiation by Au deposition.

References

[1] M. C. Daniel and D. Astruc, "Gold nanoparticles: assembly, supramolecular chemistry, quantum-size-related properties, and applications toward biology, catalysis, and nanotechnology.", *Chem. Rev.,* **104**, 293 (2004).

[2] J. Perez-Juste, I. Pastoriza-Santos, L. M. Liz-Marzan and P. Mulvaney, "Gold nanorods: synthesis, characterization and applications", *Chem. Rev.*, **249**,1870 (2005).

[3].G. Kawamura, Y. Yong and M. Nogami, "Facile assembling of gold nanorods with

large aspect ratio and their surface-enhanced Raman scattering properties", *Appl. Phys. Lett.*, **90**, 261908 (2007).

[4] G. Kawamura, Y. Yang and M. Nogami, "End-to-end assembly of CTAB-stabilized gold nanorods by citrate anions", *J. Phys. Chem. C*, **112**, 10632 (2008).

[5] P. Mulvaney, J. Perez-Juste, M. Giersig, L. M. Liz-Marzan and C. Pecharroman, "Drastic surface plasmon mode shifts in gold nanorods due to electron charging", *Plasmonics*, **1**, 61 (2006).

[6] A. Brioude, X. C. Jiang and M. P. Pileni, "Optical Properties of Gold Nanorods: DDA Simulations Supported by Experiments", *J. Phys. Chem. B*, **109**,13138 (2005).

[7] X.Huang, S. Neretina and M. A. El-Sayed, "Gold Nanorods: From Synthesis and Properties to Biological and Biomedical Applications", *Adv. Mater.*, **21**, 4880 (2009).

[8] O. Wilson, G. J. Wilson and P. Mulvaney, *Adv. Mater.*, **14**,1000 (2002).

[9] J. Perez-Juste, B. Rodriguez-Gonzalez, P. Mulvaney and L. M. Liz-Marzan, *Adv. Funct. Mater.*, **15**,1065 (2005).

[10] C. J. Murphy and C. J. Orendorff, "Alignment of Gold Nanorods in Polymer Composites and on Polymer Surfaces", *Adv. Mater.*, **17**, 2173 (2005).

[11] Y. Tsutsui, T. Hayakawa, G. Kawamura and M. Nogami, "Tuned longitudinal surface plasmon resonance and third-order nonlinear optical properties of gold nanorods", *Nanotechnology*, **22**, 275203 (2011).

[12] K. Esumi, K. Matsuhisa and K. Torigoe, "Preparation of rodlike gold particles by UV irradiation using cationic micelles as a template", *Langmuir*, **11**, 3285 (1995).

[13] Y. Y. Yu, S. S. Chang, C. L. Lee and C. R. C. Wang, "Gold nanorods: electrochemical synthesis and optical properties", *J. Phys. Chem. B*, **101**, 6661 (1997).

[14] N. R. Jana, L. Gearheart and C. J. Murphy, "Seed-Mediated Growth Approach for

Shape-Controlled Synthesis of Spheroidal and Rod-like Gold Nanoparticles Using a Surfactant Template", *Adv. Mater.*, **13**, 1389 (2001).

[15] G. Kawamura and M. Nogami, "Application of a conproportionation reaction to a synthesis of shape-controlled gold nanoparticles", *J. Cryst. Growth*, **311**, 4462 (2009).

[16] A. Gole, C. J. Orendorff and C. J. Murphy, "Immobilization of Gold Nanorods onto Acid-Terminated Self-Assembled Monolayers via Electrostatic Interactions", *Langmuir*, **20**, 7117 (2004).

[17] A. Matsuda, Y. Kotani, K. Kogure, M. Tatsumisago and T. Minami, "Transparent Anatase Nanocomposite Films by the Sol-Gel Process at Low Temperatures", *J. Am. Ceram. Soc.*, **83**, 229 (2000).

[18] Y. Kotani, A. Matsuda, M. Tatsumisago, T. Minami, T. Umezawa and T. Kogure, "Formation of anatase nanocrystals in sol-gel derived TiO_2-SiO_2 thin films with hot water treatment", *J. Sol-Gel. Sci. Tech.*, **19**, 585 (2000).

[19] L. Rodriguez-Sanchez, M. C. Blanco and M. A. Lopez-Quintela, "Electrochemical Synthesis of Silver Nanoparticles", *J. Phys. Chem. B*, **104**, 9683 (2000).

[20] N. R. Jana, L. Gearheart and C. J. Murphy, "Evidence for Seed-Mediated Nucleation in the Formation of Gold Nanoparticles from Gold Salts", *Chem. Mater.*, **13**, 2313 (2001).

[21] J.Mizuguchi, "Titanium Dioxide as a Combustion-Assisting Agent", *J. Electrochem. Soc.*, **148**, J55 (2001).

[22] J. Mizuguchi and Y. Shinbara, "Disposal of used optical disks utilizing thermally-excited holes in titanium dioxide at high temperatures: A complete decomposition of polycarbonate", *J. Appl. Phys.*, **96**, 3514 (2004).

[23] L. M. Liz-Marzan, "Tailoring surface plasmons through the morphology and

assembly of metal nanoparticles", *Langmuir*, **22**, 32 (2006).

[24] M. A. Carreon, S. Y. Choi, M. Mamak, N. Chopra and G. A. Ozin, *J. Mater. Chem.*, "Pore architecture affects photocatalytic activity of periodic mesoporous nanocrystalline anatase thin films", **17**, 82 (2007).

[25] C. Aprile, A. Corma and H. Garcia, "Enhancement of the photocatalytic activity of TiO_2 through spatial structuring and particle size control: from subnanometric to submillimetric length scale", *Phys. Chem. Chem. Phys.*, **10**, 769 (2008).

[26] J. M. Wu and B. Qi, "Low-Temperature Growth of a Nitrogen-Doped Titania Nanoflower Film and Its Ability To Assist Photodegradation of Rhodamine B in Water", *J. Phys. Chem. C*, **111**, 666 (2007).

[27] J. M. We, A. Antonietti, S. Gross, M. Bauer and B. M. Smarsly, "Ordered mesoporous thin films of rutile TiO_2 nanocrystals mixed with amorphous Ta_2O_5", *Chem. Phys. Chem.*, **9**, 748 (2008).

[28] K. Matsubara and T. Tatsuma, "Morphological Changes and Multicolor Photochromism of Ag Nanoparticles Deposited on Single-crystalline TiO_2 Surfaces", *Adv. Mater.*, **19**, 2802 (2007).

[29] K. Yu, Y. Tian and T. Tatsuma, "Size Effects of Gold Nanaoparticles on Plasmon-Induced Photocurrents of Gold-TiO_2 Nanocomposites", *Phys. Chem. Chem. Phys.,* **8**, 5417 (2006).

[30] S. Sakthivel, M. V. Shankar, M. Palanichamy, B. Arabindoo, D. W. Bahnemann and V. Murugesan, "Enhancement of photocatalytic activity by metal deposition: characterisation and photonic efficiency of Pt, Au and Pd deposited on TiO_2 catalyst.", *Water. Res.*, **38**, 3001 (2004).

[31] T. Kiyonaga, M. Fujii, T. Akita, H. Kobayashi, H. Tada, "Size-dependence of Fermi

energy of gold nanoparticles loaded on titanium(iv) dioxide at photostationary state", *Phys. Chem. Chem. Phys.*, **10**, 6553 (2008).

[32] E. Kowalska, O. O. P. Mahaney, R. Abe, B. Ohtani, "Visible-light-induced photocatalysis through surface plasmon excitation of gold on titania surfaces", *Phys. Chem. Chem. Phys.*, **12**, 2344 (2010).

[33] A. Orlov, D. A. Jefferson, M. Tikhov and R.M. Lambert, "Enhancement of MTBE photocatalytic degradation by modification of TiO_2", *Catal. Commun.*, **8**, 821 (2007).

[34] M. Haruta, N. Yamada, Y. Kobayashi, S. Iijima, "Gold catalysts prepared by coprecipitation for low-temperature oxidation of hydrogen and of carbon monoxide", *J. Catal.,* **115**, 301 (1989).

[35] N. Shibata, A. Goto, K. Matsunaga, T. Mizoguchi, S.D. Findlay, T. Yamamoto and Y. Ikuhara, "Interface Structures of Gold Nanoparticles on TiO_2 (110)", *Phys. Rev. Lett.*, **102**, 136105 (2009).

Chapter 3 Fabrication of Au/SiO$_2$-TiO$_2$ by photodeposition method with/without surface modification

3.1 Introduction

In the previous chapter, shape control of Au NPs in the mesoporous SiO$_2$-TiO$_2$ template was achieved by changing the composition of TiO$_2$ in the template and UV radiation to the sample during heat treatment. However, photocatalysis of prepared samples under Vis light irradiation was not observed although the improvement of photocatalytic activities under UV radiation was observed. This cause is because the effective formation of crystalline TiO$_2$/Au interface for photocatalysis by Vis irradiation was not achieved. This reaction is caused by electron transfer from the Au NPs, which are SPR active under Vis light, to the conduction band of TiO$_2$. The electron-deficient Au oxidizes the organic compounds to return to its metallic state [1]. Shibata et al. have reported that electron transfer can occur between specific crystal interfaces of TiO$_2$ and Au [2]. However, our method of depositing Au presumably leads to the formation of various interfaces that even involve Au with amorphous phases of TiO$_2$ and SiO$_2$, therefore the effective formation of crystalline TiO$_2$/Au interface TiO$_2$ and Au, for photocatalysis by Vis irradiation was not achieved.

In this chapter, Au/SiO$_2$-TiO$_2$ was prepared by photodeposition method with/without surface modification of the template to investigate the effect of TiO$_2$/Au interface on the photocatalysis under Vis light. Photodeposition method is a technique to deposit metal NPs on TiO$_2$ by photocatalysis of TiO$_2$ under UV [3,4], Metal ions are reduced by excited electrons in TiO$_2$ and become to metal NPs. Therefore a good interface is formed between TiO$_2$ and metal NPs. The Vis light-driven photobleaching of

methylene blue [MB] is employed to evaluate the photocatalytic activity of the samples. The effects of interface and surface conditions of TiO_2 and Au NPs on the photocatalytic performance are discussed in relation to the electrostatic repulsion of MB and interfacial electron transfer from Au NPs to TiO_2.

3.2 Experimental

3.2.1 Preparation of $80SiO_2 \cdot 20TiO_2$ mesoporous template via a sol–gel route

SiO_2-TiO_2 template (SiO_2:TiO_2 = 4:1) was synthesized with similar method as chapter 2. For a typical synthesis, 1.74 g of Pluronic P123, 2.92 g of NaCl and 100 ml of 1 mM hydrochloric acid were added to 4.17 g of tetraethoxysilane and stirred at 35°C for 24 h. 1.70 g of titanium tetra-n-butoxide was then added to the solution and stirred for further 6 h. The solution was transferred into an autoclave vessel and kept at 100°C for 4 h. The precipitated powder was collected by suction filtration, then washed with ion-exchanged water [IEW] and ethanol [EtOH], and dried in an ambient environment. The obtained powder was calcined at 550°C for 5 h to remove the residual P123 from the mesopore.

3.2.2 Deposition of Au NPs by UV radiation

Prior to the deposition of Au NPs, some of the prepared template powders were dispersed in 1 wt% 3-aminopropyltriethoxysilane [APTES] solution (in EtOH) at 25°C for 3 h in order to modify the surface of mesoporous powder with amino groups for facilitating the insertion of Au^{3+} ions into the mesopores. The powder was then filtered with suction, washed with EtOH, and dried at 60°C in air. The untreated and amino-functionalized templates were dispersed into a mixture of 5.41 g of 1 mM

HAuCl$_4$ aqueous solution, 11.9 g of IEW and 11.34 g of methanol, and stirred at 25°C for 1.5 min under UV radiation (USHIO SP-7, 230–440 nm, 93 mW cm^{-2} at 365 nm). After the suction filtration and washing with IEW, the powder was dried in an ambient environment. Fig. 3.1 shows the schematic diagram of the Au deposition experimental procedures.

3.2.3 Characterization of prepared samples

Transmission electron microscope [TEM] images were observed by a JEOL JEM-2100F operating at 200 kV. X-ray diffraction [XRD] measurements were carried out using a Rigaku Ultima IV diffractometer with CuKα radiation (λ = 1.5406 Å). Diffuse reflectance [DR] spectra were measured with a JASCO V-670 UV-Vis-NIR spectroscope. The evaluation of photocatalytic activity was performed by measuring absorption spectra of MB aqueous solution as a function of the adsorption and Vis light irradiation time. The absorption spectra were measured with a JASCO V-560 UV-Vis spectroscope. The Vis light of aimed wavelengths was generated by an Asahi MAX-303 (Xe lamp, 300 W) equipped with an Asahi CMS-100 (monochromator, resolution: ca. 40 nm). Surface areas were estimated according to the Brunauer–Emmett–Teller [BET] method with a Micromeritics TriStar II 3020 adsorption analyzer.
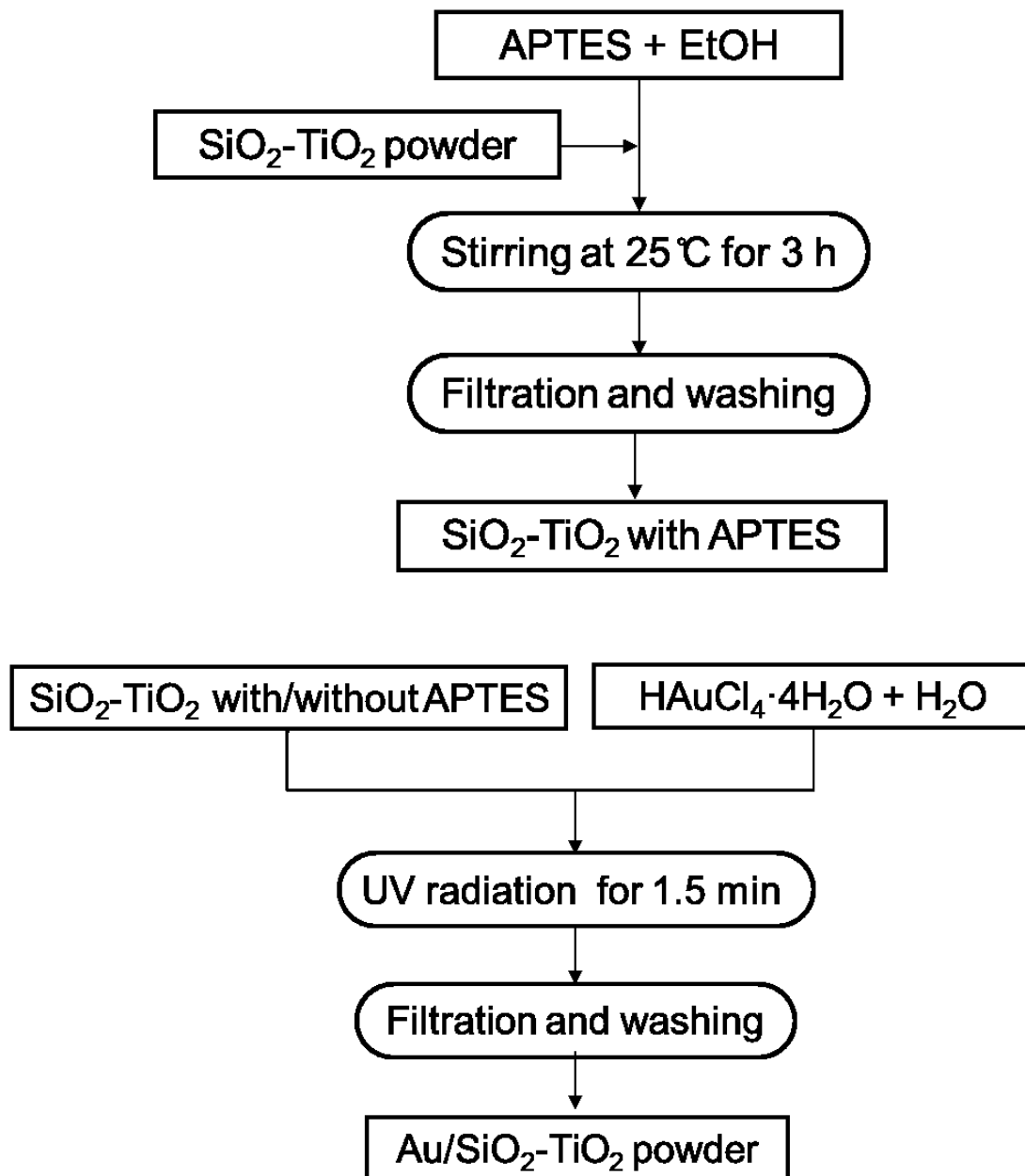
Fig.3.1. Schematic diagram of the Au deposition procedures.

3.3 Results and discussions

3.3.1 Characterization of SiO$_2$-TiO$_2$ and Au/SiO$_2$-TiO$_2$

The prepared $80SiO_2 \cdot 20TiO_2$ template with 2-D Hex mesoporous structure was observed with TEM (Fig. 3.2(a)), from which the caliber and wall thickness were estimated to be ca. 5 and 4 nm, respectively. The framework was composed of amorphous SiO$_2$ and ca. 3 nm-sized crystals, which were defined as anatase TiO$_2$ with high-resolution TEM image and XRD pattern shown in the inset of Fig. 3.2(a) and (b), respectively.

Figures 3.3(a) and (b) show the Au NP-deposited templates modified with/without APTES. Without APTES, spherical Au NPs with a diameter of < 15 nm formed dominantly at the outside of the mesoporous structure. The surface modification of the template with APTES prior to the deposition of Au resulted in the formation of Au NRs with a diameter of ca. 5 nm and a length of 10–15 nm in the tubular mesopores of the template, while small amount of spherical Au NPs with a diameter of ca. 10 nm were also deposited at the outside of the mesopores. These results indicated that Au^{3+} ions supplied from HAuCl$_4$ could only penetrate into tubular mesopores when the template was modified with APTES. The penetration presumably occurs because the Au^{3+} ions can be anchored by the amino groups of APTES on the inner wall of the mesopores [5]. The anchored Au^{3+} ions are reduced by electrons generated from anatase nanocrystals in the mesoporous framework by UV radiation, thus Au NPs/NRs are formed. The DR spectra shown in Fig. 3.4(a) well reflected the morphologies of Au NPs deposited on these templates modified with/without ATPES [6]. Namely, the sample prepared without APTES showed a relatively large extinction at 542 nm, which was attributed to the SPR of dominantly deposited spherical Au NPs. The half-width of the

extinction peak at 542 nm was unusually broad (128 nm). This is probably due to the formation of dimer of Au NPs (see the circled regions in Fig. 3.3(a)) and the coupling of their SPR [7], which occurs because Au NPs are deposited only on the limited space of anatase particles located outside of the mesoporous template, leading to gathering and aggregating of Au NPs. On the other hand, two extinction peaks at 528 and 700 nm were observed from the sample prepared with APTES. This was well consistent with the formation of Au NRs and a small fraction of spherical Au NPs on the template [8]. The XRD patterns shown in Fig. 3.4(b), however, presented no obvious difference between the samples. This revealed that the crystalline sizes calculated to be 13.5 and 13.4 nm using Scherrer's equation with Scherrer constant of 0.9 for the samples prepared with and without APTES, respectively, and the quantity of the deposited Au NPs were almost the same between the samples, though the morphology of Au NPs and their depositing location were different.
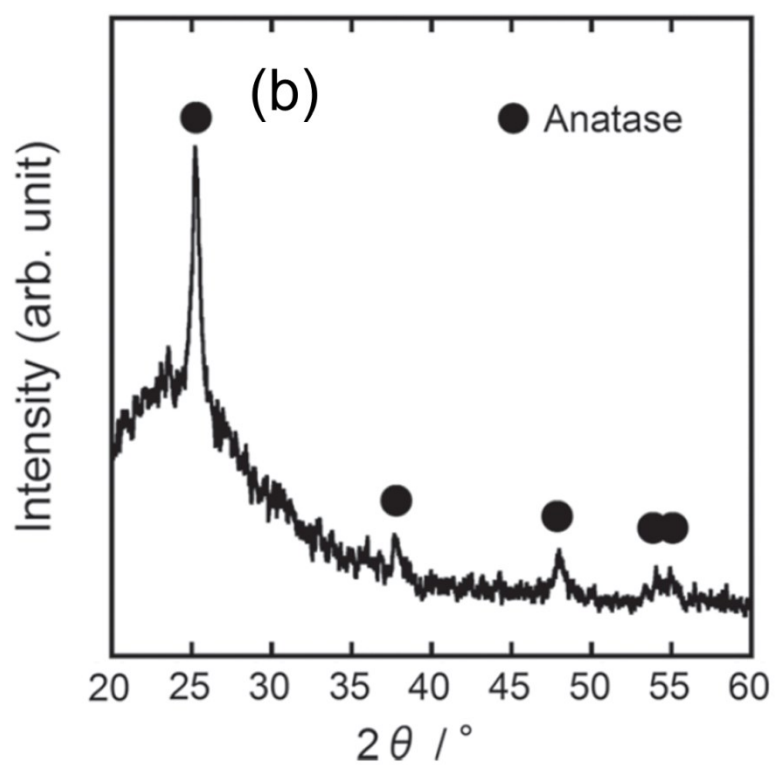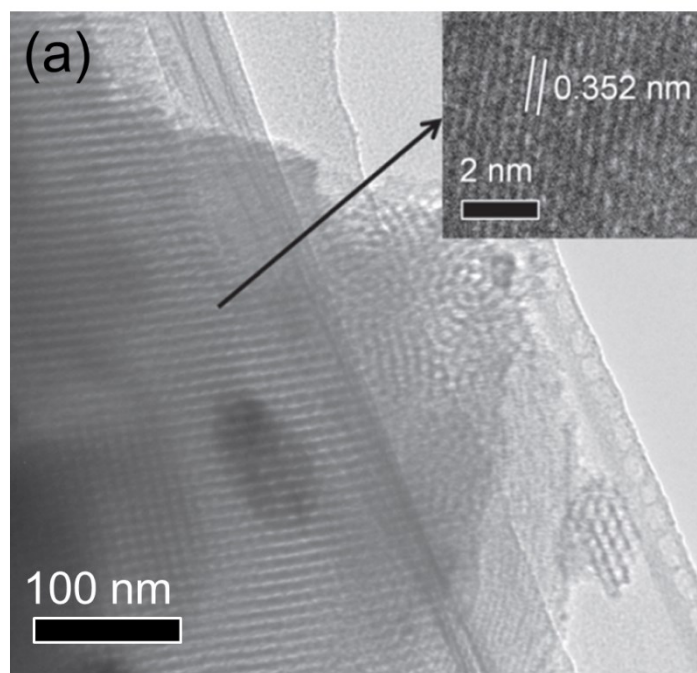
Fig. 3.2. (a) TEM image and (b) XRD pattern of a mesoporous $80SiO_2 \cdot 20TiO_2$ template.

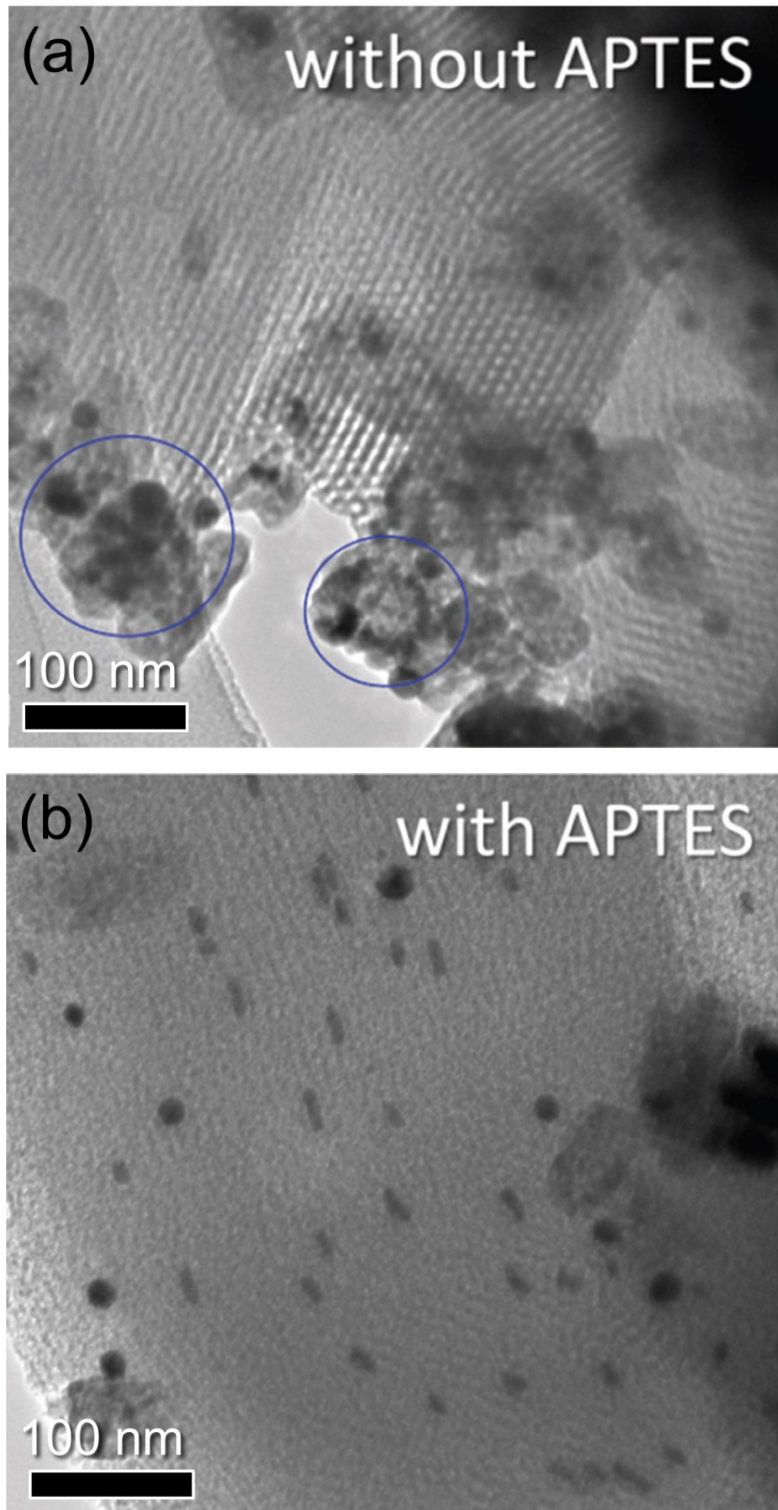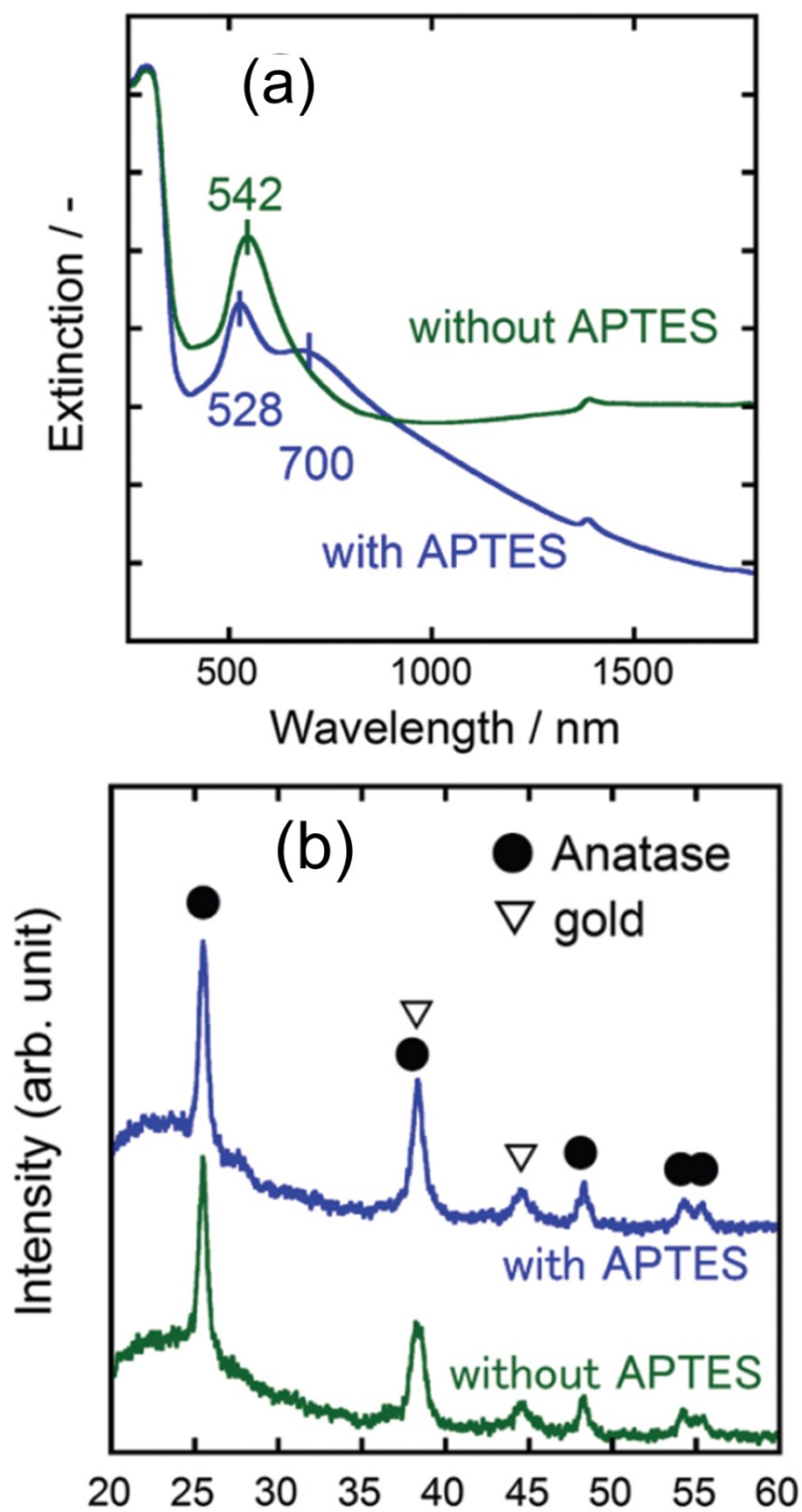Fig. 3.3. TEM images of Au-deposited mesoporous $80SiO_2 \cdot 20TiO_2$ sample prepared (a) with and (b) without APTES.

Fig. 3.4. (a) DR spectra and (b) XRD patterns of Au-deposited mesoporous $80SiO_2 \cdot 20TiO_2$ sample prepared with and without APTES.

3.3.2 Photocatalytic property of prepared samples under Vis light

The photocatalytic performance of the prepared samples under UV radiation was confirmed with the photobleaching of MB (data not shown). This bleaching occurs because of the UV absorption of anatase TiO_2 seen in Fig. 3.4(a) showing a strong extinction at the wavelength region shorter than 380 nm. In addition to the photocatalysis upon UV radiation, Vis light-induced photocatalysis should occur with these samples because of their Vis light absorption originated from SPR. Although the mechanism of photocatalysis caused by SPR of metal NPs on TiO_2 crystal is still controversial, a transfer of excited electrons of metal NPs to TiO_2 is most widely recognized as the leading cause of the photocatalysis, because the electron transfer generates active electrons and holes with long lifetime on TiO_2 and Au NPs, respectively [9-12]. First, the photocatalytic property of large Au/TiO_2 deposited on the surface of particles as shown in Fig. 3.3(a) was evaluated to compare the advantage of mesoporous structure. For that purpose, non-porous Au/SiO_2-TiO_2 was prepared by the similar method without P123. Fig. 3.5 shows the Vis-light-induced photobleaching dynamics of MB solution with samples prepared with/without P123. The wavelengths of irradiated light were set to 542 nm. Adsorption of MB on the samples was saturated by stirring for 10 min before Vis light irradiation. The y axis denoted the absorbance of MB solution after certain time (I_x) divided by the initial absorbance of MB solution (I_0). The sample prepared without P123 showed the adsorption of MB and decreased I_x/I_0 by 0.1 after stirring for 10 min before light irradiation. A further decrease in I_x/I_0 by 0.1 was caused by the subsequent Vis irradiation for 15 min. On the other hand, Au/SiO_2-TiO_2 prepared with P123 showed MB and decreased I_x/I_0 by 0.65 after stirring for 10 min before light irradiation. This improvement of the amount of adsorption is due to the

formation of mesoporous structure. Furthermore, the decrease in I_x/I_0 by 0.2 was caused by Vis irradiation. Rate constants of the photobleaching (first-order reaction) were calculated to be 0.474 and 3.78 h^{-1} for the samples prepared without and with P123, respectively. The rate constant of non-porous sample was around 15% of the rate constant of mesoporous sample, which is presumably attributed to Au/TiO_2 deposited on the surface of the template. Second, the effects of surface modification of powders were investigated with the samples prepared with/without APTES. Fig. 3.6(a) shows the Vis light-induced photobleaching dynamics of MB solution with samples prepared with/without APTES. The wavelengths of irradiated light were set to 528 and 542 nm, which were the SPR extinction peak wavelengths of the corresponding samples. The result of the sample prepared without APTES is same as the result of the sample prepared with P123 shown in Fig. 3.5. Normally, photobleaching occurs to decrease I_x/I_0 exponentially as a function of the reaction time as seen in the sample prepared without APTES. However, the sample prepared with APTES showed a nonexponential decrease in I_x/I_0 after starting Vis light irradiation. Fig. 3.6(b) shows the Vis light-induced photobleaching dynamics of MB solution with the sample prepared with APTES. The irradiation time was longer than the data shown in Fig. 3.6(a), and two different wavelengths of Vis light were employed to excite SPR of the sample effectively. With light of 528 nm, a decrease of I_x/I_0 by 0.45 occurred by the irradiation for 24 min. Irradiation of light of 700 nm that caused no obvious bleaching of MB within 15 min decreased I_x/I_0 by 0.20 for 24 min. In contrast, Vis light irradiation of another wavelength for 24 min caused no change in I_x/I_0. Since no adsorption of MB on the sample prepared with APTES occurred, the obtained results of Vis light-induced photobleaching of MB by the sample were discussed as follows. Because the hydroxy

groups appear on the surface of $80SiO_2 \cdot 20TiO_2$ template without modification of APTES, the template possesses negative charges and thus attracts MB that has positively charged sulfur by an electrostatic force. In contrast, the APTES-modified template possesses positive charges because amino groups appear on the surface, resulting in the repulsion of MB from the sample. But when the sample prepared with APTES is irradiated with Vis light, the generated holes would gradually decompose the adsorbed APTES, and thus MB becomes to be accessible to the bared sample surface. MB accessed to the sample surface should be bleached by the generated holes with continuous Vis light irradiation. This multi-step process of photobleaching of MB on the sample prepared with APTES would lead to the nonexponential curves seen in Fig. 3.6(b). The schematic illustration of the phenomenon is shown in Fig. 3.7.
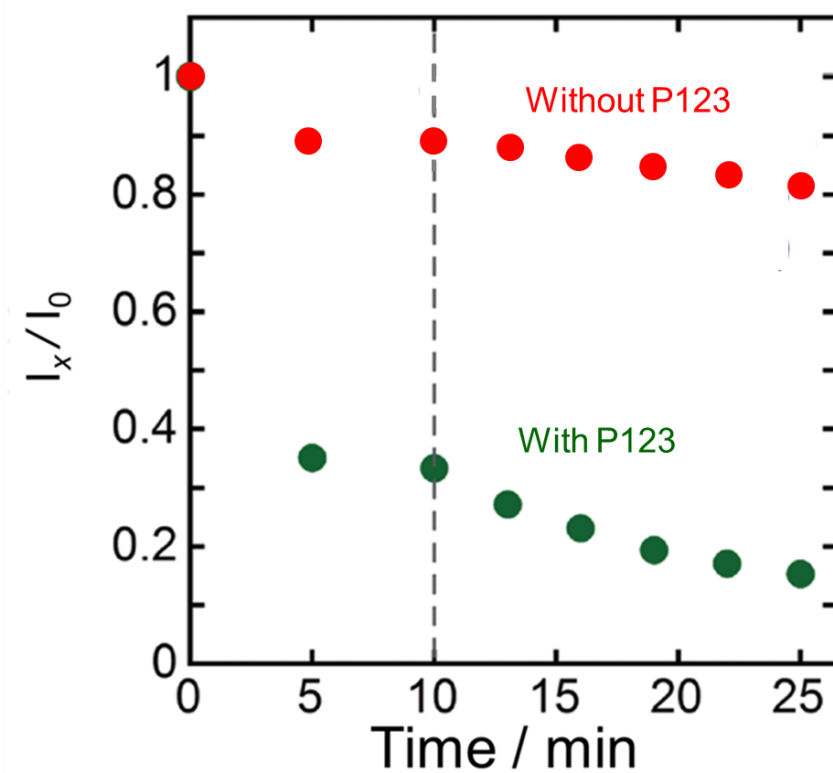
Fig. 3.5. Photobleaching dynamics of MB solution with Au-deposited $80SiO_2 \cdot 20TiO_2$ samples prepared with and without P123 under 542 nm light irradiation

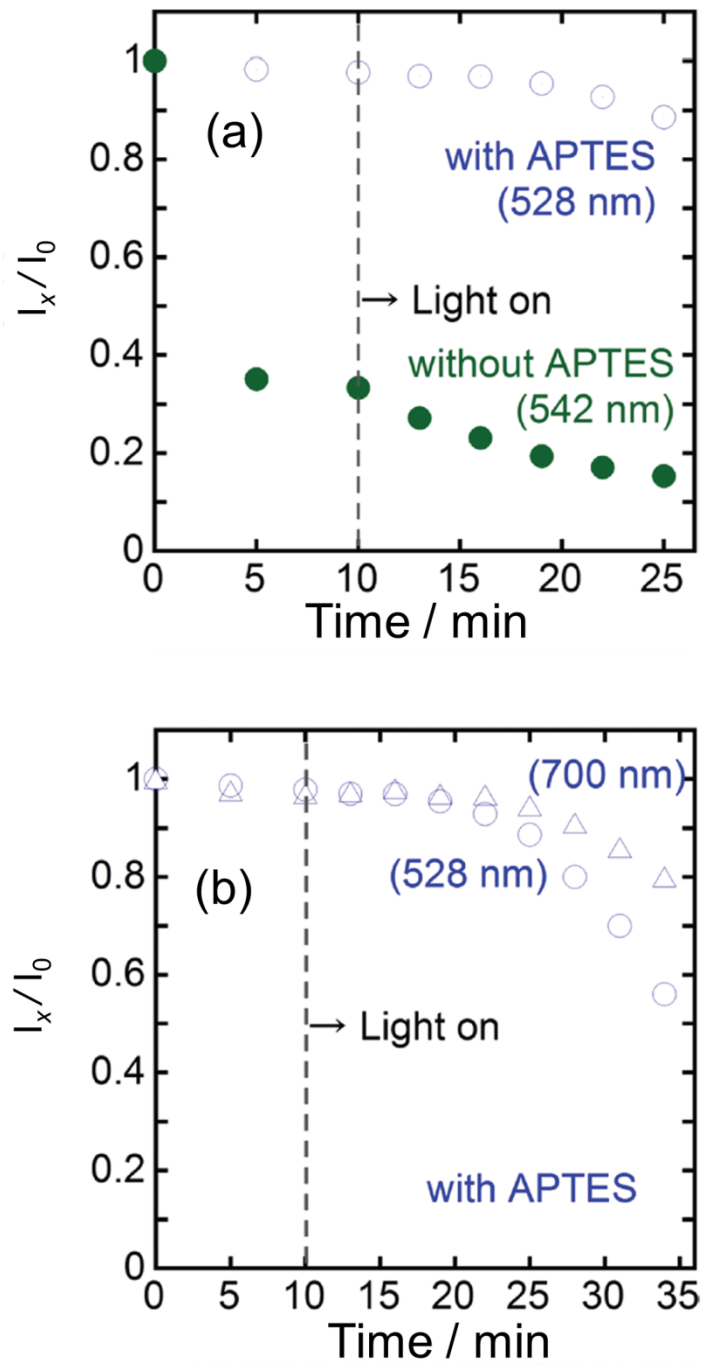Fig. 3.6. Photobleaching dynamics of MB solution with Au-deposited mesoporous $80SiO_2 \cdot 20TiO_2$ samples prepared (a) with and without APTES under 528 and 542 nm light irradiation, (b) with APTES under 528 and 700 nm light irradiation.
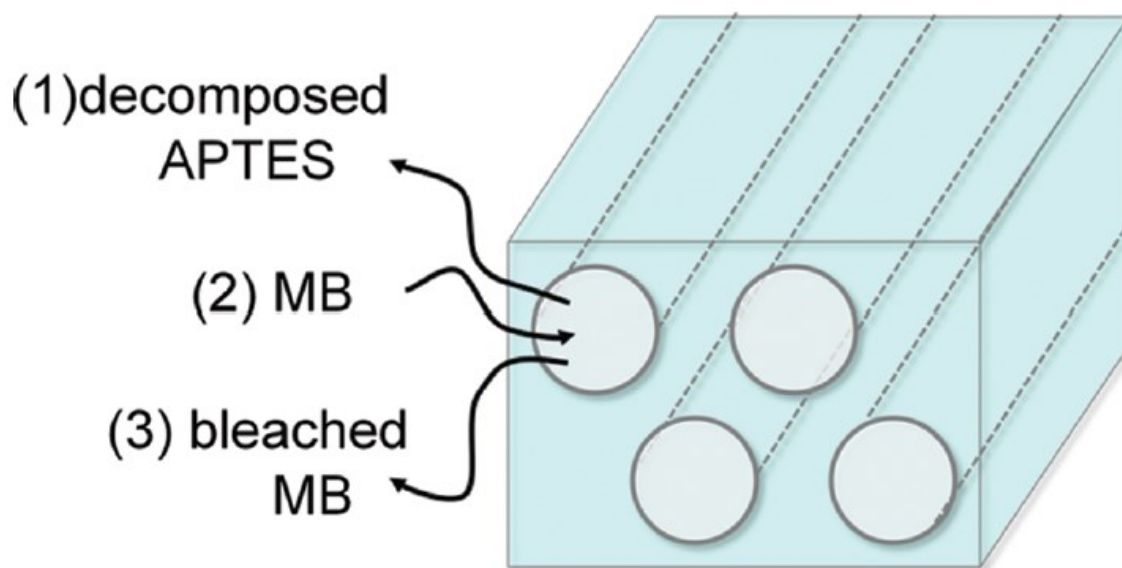
Fig. 3.7. Schematic illustration of phenomenon occurring to the APTES-modified Au-deposited mesoporous $80SiO_2 \cdot 20TiO_2$ sample in MB solution under Vislight irradiation. With Vislight irradiation, (1) APTES starts to be decomposed, and then (2) MB gradually becomes accessible to the sample. (3) The accessed and adsorbed MB on the sample is bleached. Therefore the bleaching rate of MB should be regulated by several factors such as decomposition of APTES, adsorption of MB, bleaching of MB, and also transfer of decomposed APTES and MB in the tubular mesopores of the sample.

3.3.3 Effect of the surface modification on the photocatalysis under Vis light

Since APTES seemed to be an obstacle to adsorption of MB on the sample, heat treatment was carried out for the Au NR-deposited sample prepared with APTES to remove APTES from the sample surface. The TEM image shown in Fig. 3.8 presented that almost all Au NRs were transformed to spherical Au NPs, whereas some short Au NRs were still remained and observed in the TEM image as indicated with white circles. Relatively long Au NRs observed before heat treatment would be preferable to transform because of its high surface energy originated from the morphological anisotropy of NRs. Additionally, the transformation seemed to be associated with a partial collapse of mesoporous framework, which was inferred by the bigger size of spherical Au NPs than the pore size. The DR spectrum shown in Fig. 3.9(a) represented that the sample after heat treatment exhibited a main extinction peak at 528 nm associated with a weak shoulder peaking at 650 nm which was attributed to the longitudinal SPR mode of short Au NRs. The XRD pattern in Fig. 3.9(b) showed no change by heat treatment of the sample. This unveiled that heat treatment did not lead to an increase in size of Au NPs by merging of themselves. Thus, it was concluded that heat treatment could induce only transformation of long Au NRs to spherical Au NPs, resulting in the partial collapse of mesoporous framework. The photocatalytic activity of the sample prepared with APTES was greatly improved by heat treatment, and the exponential photobleaching of MB was observed by Vis light irradiation as shown in Fig. 3.10. Rate constants of the photobleaching were calculated to be 3.78 and 2.47 h^{-1} for the samples prepared without and with APTES, respectively, and the surface areas of

the samples were 384.9 and 275.0 $m^2 \ g^{-1}$. These results suggested that the difference in the rate constants arose mainly from the difference in the surface areas. Besides, the fact that SPR of the short Au NRs at 650 nm was not effectively excited by irradiation of light of 528 nm would also contribute to the relatively low photocatalytic activity. In contrast, because SPR of the sample after heat treatment can be excited by irradiation of light of longer wavelengths compared to the sample prepared without APTES, the higher quantum efficiency of photocatalysis of the heat treated sample is expected under ambient/sun-light irradiation due to the wide wavelength region of their SPR.

Finally, in order to check if the charge separation between Au NPs and TiO_2 was the origin of the Vis light-induced photobleaching of MB, a template deposited with Au NPs by chemical reduction method was prepared for comparison, that is prepared samples in previous chapter. The APTES modification of the template was indispensable for this sample, because if the modification was not carried out, Au NPs formed as colloid NPs in the solution regardless of the presence of the template powder. Au NRs were mainly deposited in the template instead of spherical Au NPs. The location of the deposited Au NRs was supposed to be not on the surface of TiO_2 but on SiO_2 which was the main component of the template. Although some Au NRs would be deposited on TiO_2, a good electronic contact between Au and TiO_2 should not be established. This is because the photodeposition of Au on TiO_2 requires the electron transfer from TiO_2 to Au or Au^{3+} ions, thus much better electronic contact between Au and TiO_2 must have been established compared to the sample prepared by chemical deposition of Au [12]. The sample prepared by the chemical reduction method showed little activity in photocatalysis under Vis light irradiation even after heat treatment was carried out to remove APTES from the sample surface. This result revealed that charge

separation between Au NPs and TiO$_2$ was the origin of the photocatalysis, and that the fabrication of good electronic contact between Au and TiO$_2$ contributed greatly to the high efficiency of photocatalysis under Vis light irradiation as well as the electrostatic attraction between sample surface and the reactant.
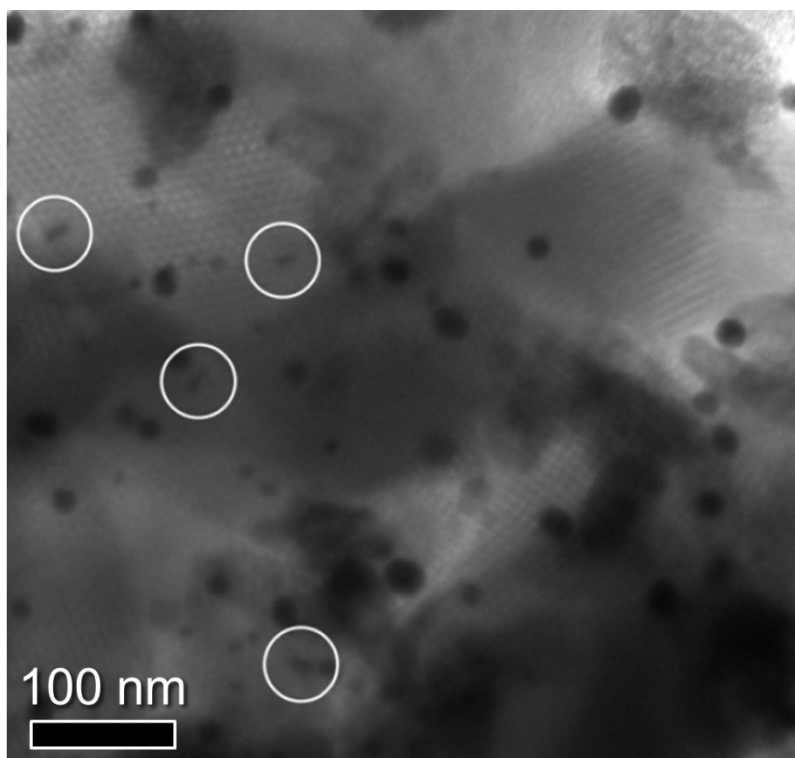
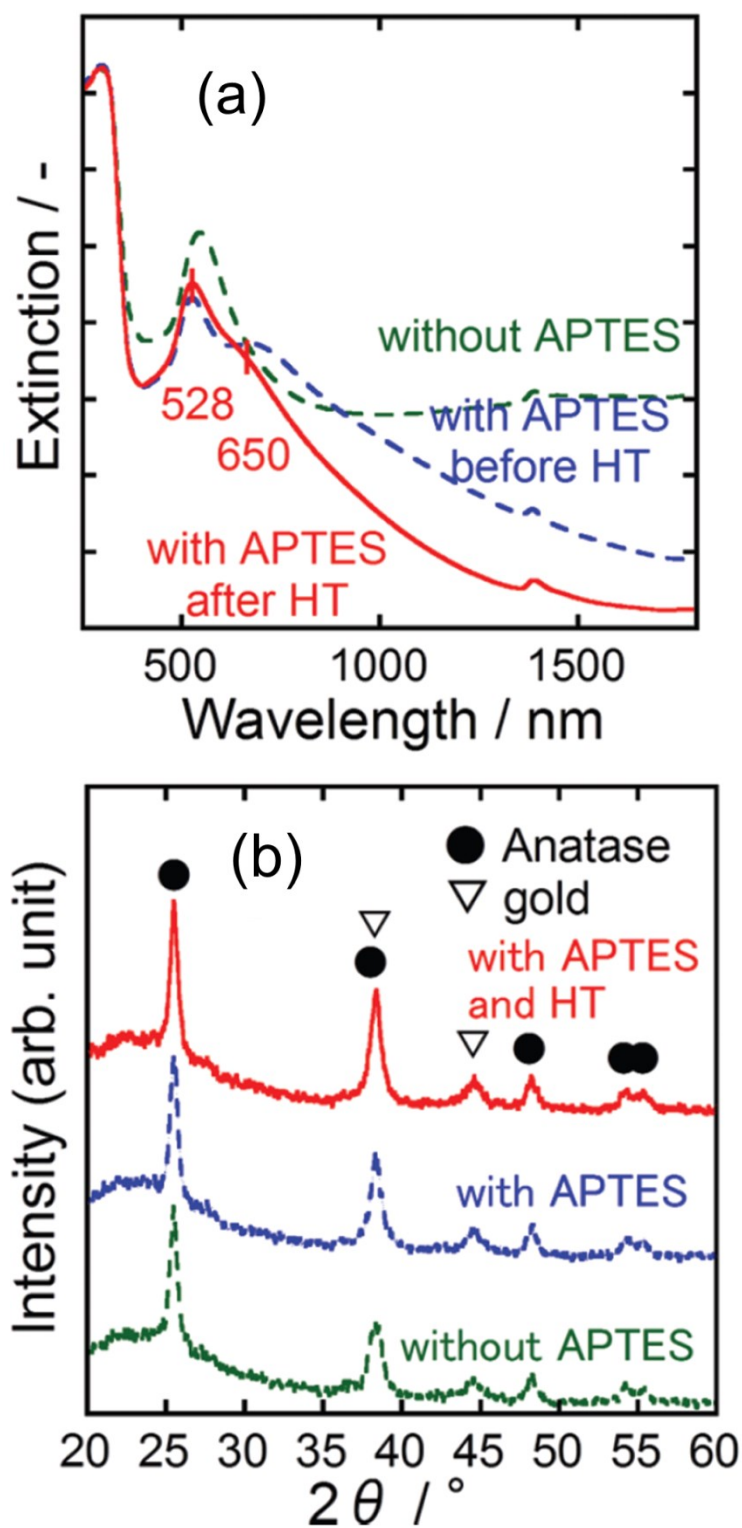Fig. 3.8. TEM image of heat-treated Au-deposited mesoporous $80SiO_2 \cdot 20TiO_2$ sample prepared with APTES.

Fig. 3.9. (a) DR spectra and (b) XRD patterns of heat-treated Au-deposited mesoporous 80SiO$_2$·20TiO$_2$ samples prepared with and without APTES.
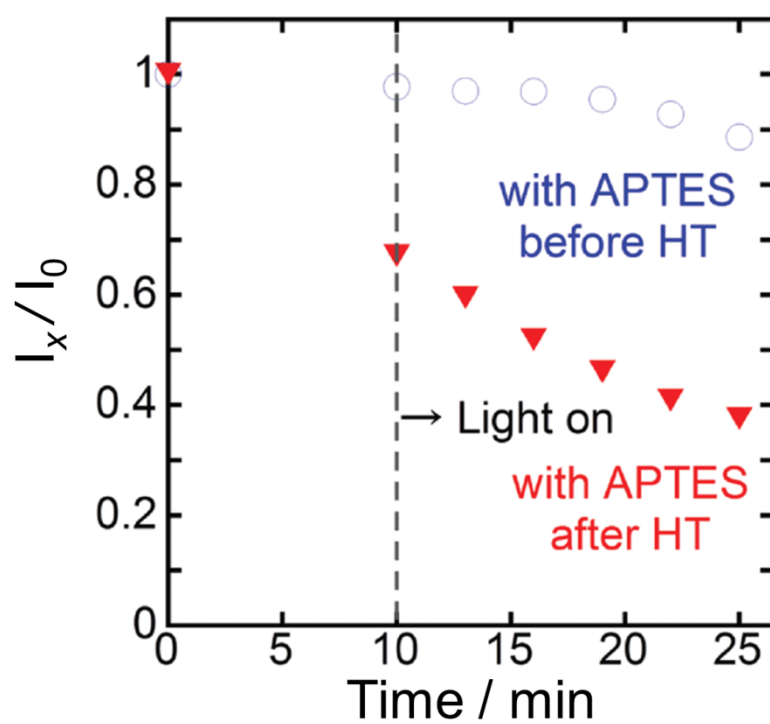
Fig. 3.10. Photobleaching dynamics of MB solution with Au-deposited mesoporous $80SiO_2 \cdot 20TiO_2$ samples prepared with APTES before and after heat treatment. The wavelength of irradiated Vis light is 528 nm.

3.4 Conclusions

Vis light-induced photocatalysis of mesoporous SiO_2–TiO_2 photodeposited with Au NPs was investigated. The sample prepared without APTES worked well as a photocatalyst to bleach MB. However, the sample prepared with APTES showed weak and abnormal photocatalytic activity, showing nonexponential curve in the photobleaching dynamics of MB. Heat treatment to remove APTES from the sample led to the amelioration of the photocatalytic activity. In contrast, the removal of APTES from the sample chemically-deposited with Au NPs resulted in no recovery of the activity. These results indicated that APTES being on the surface of the template suppressed the adsorption of MB onto the sample by electrostatic force, which caused a significant decrease in the photocatalytic activity. Besides, the formation of good electronic contact between Au NPs and TiO_2 was found to be essential to the high Vis light-induced photocatalytic performance. On the other hand, the shape of Au NPs was transformed from sphere to rod by using APTES, which resulted in the expansion of SPR to longer wavelength region. This suggested that the Au NR-deposited samples show photocatalysis upon light irradiation of longer wavelength, which presumably leads to the higher photocatalytic performance of the sample under ambient- and sun-light illuminations that contain various wavelengths.

References

[1] M. Haruta, N. Yamada, Y. Kobayashi, S. Iijima, "Gold catalysts prepared by coprecipitation for low-temperature oxidation of hydrogen and of carbon monoxide", *J. Catal.,* **115**, 301 (1989).

[2] N. Shibata, A. Goto, K. Matsunaga, T. Mizoguchi, S.D. Findlay, T. Yamamoto and Y.

Ikuhara, "Interface Structures of Gold Nanoparticles on TiO$_2$ (110)", *Phys. Rev. Lett.*, **102**, 136105 (2009).

[3] B. Kraeutler and A. J. Bard, "Heterogeneous photocatalytic preparation of supported catalysts. Photodeposition of platinum on titanium dioxide powder and other substrates", *J. Am. Ceram. Soc.*, **100**, 4317 (1978).

[4] Y.-F. Yang, P. Sangeetha and Y.-W. Chen, "Au/TiO$_2$ catalysts prepared by photo-deposition method for selective CO oxidation in H$_2$ stream", *Int. J. Hydrog. Energy*, .**34**, 8912 (2009).

[5] J. Sun, D. Ma, H. Zhang, X. Liu, X. Han, X. Bao, G. Weinberg, N. Pfander and D. Su, "Toward Monodispersed Silver Nanoparticles with Unusual Thermal Stability", *J. Am. Chem. Soc.*, **128**, 15756 (2006).

[6] Z. Li, C. Kubel, VI. Parvulescu and R. Richards, "Size tunable gold nanorods evenly distributed in the channels of mesoporous silica", *ACS Nano*, **2**, 1205 (2008).

[7] I. Romero, J. Aizupurua, G. W. Bryant and F. J. G. Abajo, "Plasmons in nearly touching metallic nanoparticles: singular response in the limit of touching dimers", *Optic. Express*, **14**, 9988 (2006).

[8] G. Kawamura, M. Murakami, T. Okuno, H. Muto and A. Matsuda, "Length control of Ag nanorods in mesoporous SiO$_2$–TiO$_2$ by light irradiation", *RSC Adv.*, **1**, 584 (2011).

[9] Y. Tian and T. Tatsuma, "Plasmon-Induced Photoelectrochemistry at Metal Nanoparticles Supported on Nanoporous TiO$_2$", *Chem. Commun.*, 1810 (2004).

[10] Y. Tian and T. Tatsuma, "Mechanisms and Applications of Plasmon-Induced Charge Separation at TiO$_2$ Films Loaded with Gold Nanoparticles", *J. Am. Chem. Soc.*, **127**, 7632 (2005).

[11] J. T. Carneiro, C. C. Yang, J. A. Moma, J. A. Moulijn and G. Mul, "How gold

deposition affects anatase performance in the photo-catalytic oxidation of cyclohexane", *Catal. Lett.*, **129**, 12 (2007).

[12] E. Kowalska, O. O. P. Mahaney, R. Abe, B. Ohtani, "Visible-light-induced photocatalysis through surface plasmon excitation of gold on titania surfaces", *Phys. Chem. Chem. Phys*., **12**, 2344 (2010) (2010).

Chapter 4 Investigation of photocatalytic activity of Au/SiO$_2$-TiO$_2$ under UV, Vis and NIR light

4.1 Introduction

In the previous chapter, Au NPs and Au NRs were deposited in the template by photodeposition method to form the interface between TiO$_2$ and Au, and Au/SiO$_2$-TiO$_2$ prepared by photodeposition method showed the photocatalysis under Vis light. However, the sample prepared with surface modification of the template showed weak and abnormal photocatalytic activity. Heat treatment to remove surface-modified organic being from the sample led to the amelioration of the photocatalytic activity. In contrast, the removal of organic beings from the sample chemically-deposited with Au NPs resulted in no recovery of the activity. These results indicated that organic being on the surface of the template suppressed the adsorption of MB onto the sample by electrostatic force, which caused a significant decrease in the photocatalytic activity.

In this chapter, Au NPs/SiO$_2$-TiO$_2$ and Au NRs/SiO$_2$-TiO$_2$ were prepared by photodeposition method without surface modification of the template, and detailed investigations of the photocatalytic activities of prepared sample were carried out to achieve the high photocatalytic activity under UV, Vis and NIR light irradiation. First, effects of Au amount in the template on the photocatalytic activity were investigated to optimize the amount of Au. If the amount of Au NPs get too high in the mesopores, their accessibility for the reactants decreases and slight blocking effects hinder oxygen diffusion to the Au NPs and reactivity with the electrons stored on the Au [1,2]. Second, action spectra were measured with prepared samples. The action spectrum represents the quantum yields plotted against wavelength of light. It shows what wavelength of

light is most effectively used for a specific chemical reaction. The effects of the SPR wavelength of Au NPs and Au NRs on the photocatalysis under Vis and NIR light were investigated by measurement of action spectra.

4.2 Experimental

4.2.1 Preparation of $80SiO_2 \cdot 20TiO_2$ mesoporous template via a sol–gel route

$80SiO_2 \cdot 20TiO_2$ was used as the template of Au NPs prepared in chapter 3. For a typical synthesis, 1.74 g of Pluronic P123, 2.92 g of NaCl and 100 ml of 1 mM hydrochloric acid were added to 4.17 g of tetraethoxysilane and stirred at 35°C for 24 h. 1.70 g of titanium tetra-n-butoxide was then added to the solution and stirred for further 6 h. The solution was transferred into an autoclave vessel and kept at 100°C for 4 h. The precipitated powder was collected by suction filtration, then washed with ion-exchanged water [IEW] and ethanol [EtOH], and dried in an ambient environment. The obtained powder was calcined at 550°C for 5 h to remove the residual P123 from the mesopore.

4.2.2 Preparation of mesoporous TiO_2 with controlled particle size

Mesoporous TiO_2 with controlled particle size was synthesized by using surfactants as the structure-directing agent under base conditions. In a typical synthesis process, firstly, 0.5 g hexadecyl trimethyl ammonium bromide and 0.06 g triethanolamine were dissolved completely in 20 ml distilled water at 95°C under different stirring rate for 1 h. Then, 1.5 ml titanium tetra-n-butoxide was added at a speed of 1 ml/min. After continuous stirring for 1 h, the as-synthesized mesoporous TiO_2 were collected by centrifugation at 12,000 rpm for 30 min and then washed with

EtOH to remove the residual reactants. To remove surfactants completely, the as-synthesized mesoporous TiO_2 was dispersed under ultrasound for 20 min and calcined at 550°C.

4.2.3 Deposition of Au NPs by UV radiation

The prepared template (0.574 g) was dispersed in a mixture of 1 mM $HAuCl_4$ aqueous solution (2.4 ml, Kishida, Japan), IEW (11.9 mL) and methanol (14.3 mL, Wako, Japan), and then stirred at 25°C for 1.5 min under UV radiation (USHIO SP-7, 230–440 nm, 93 mW cm^{-2} at 365 nm) to deposit Au NPs. After the suction filtration and washing with IEW, the powder was dried in an ambient environment. The amount of Au deposited on the template was fixed to be 0.6 mol% ($0.6Au/SiO_2$–TiO_2 or Au NPs/SiO_2-TiO_2). 0.3, 1.2 and 1.8 mol% Au-deposited powders were also prepared using the same method. For deposition of Au NRs (0.6 mol% Au), template powder was immersed in a $HAuCl_4$ ethanol solution, and the solution was placed under reduced pressure. Then light intensity and irradiation time were changed to 30 mW cm^{-2} and 15 min.

4.2.4 Characterization of prepared samples

X-ray diffraction [XRD] patterns were recorded on a Rigaku Ultima IV diffractometer (30 kV, 20 mA, Japan) with CuKα radiation (λ = 1.5406 Å). Transmission electron microscope [TEM] images were taken by a JEOL JEM-2100F microscope at an acceleration voltage of 200 kV (Japan). UV–Vis-NIR diffuse reflectance [DR] spectra were measured with a JASCO V-670 UV–Vis-NIR

spectrophotometer (Japan). Surface areas were determined by N_2 adsorption isotherms with the Brunauer–Emmett–Teller [BET] method using a Micromeritics TriStar II 3020 adsorption analyzer (USA). The samples were degassed at 150°C for 2 h in a vacuum prior to the measurement of surface area.

4.2.5 Evaluation of photocatalytic activity

The photocatalytic activities of the prepared mesoporous SiO_2-TiO_2 before and after Au NPs deposition were determined by measuring the generation rate of acetone by photooxidation of 2-propanol and reaction rate of photobleaching of methylene blue [MB] in aqueous solution under a light illumination. When 2-propanol was used for evaluation, the prepared powder (10 mg) was suspended in an aqueous solution containing 5 vol% 2-propanol (20 mL). The photocatalyst powder was stirred magnetically in the dark for 10 min to allow the complete adsorption of 2-propanol on the surface. Then the suspension was photoirradiated with UV (<380 nm, 1.8 mW cm^{-2} at 365 nm) or Vis light (>480 nm, 40 mW cm^{-2}) using an Asahi HAL-320 light source (300 W Xe lamp, Japan) with cut-off filters (Y48, Asahi Techno Glass, Japan) under magnetic stirring. A small amount (1 mL) of the solution was collected after light irradiation for certain periods (20, 40 and 60 min) and centrifuged at 5000 rpm for 5 min to separate the powder sample from the solvent. The amount of generated acetone in the solution was measured by gas chromatography (Shimadzu, GC-2014 equipped with a flame ionization detector, Japan). When MB was used for evaluation, the prepared powder (10 mg) was stirred in an aqueous solution of 1.88×10^{-5} M MB (20 mL) in the dark for 10 min to allow the complete adsorption of MB on the surface of the samples. Then the suspension was photoirradiated with UV or Vis light under magnetic

stirring; 1 mL of the solution was collected after light irradiation for certain periods (5, 10, 15, 20, 25, 30, 35 and 40 min). After the elimination of powder samples from the solution, the concentration of MB in the solution was evaluated by recording the absorbance of MB at 664 nm with a spectrophotometer (JASCO V-560, Japan).

For the measurement of action spectra, a portion of the prepared photocatalyst (10 mg) was suspended in an aqueous solution containing 5 vol% 2-propanol (20 mL) or MB aqueous solution (1.88×10^{-5} M, 20 mL) and irradiated with monochromatic light (365-1020 nm) for 1 h using a 300 W Xe lamp equipped with a monochromer (Asahi CMS-100, full width at half maximum = 40 nm, Japan). The light flux of the incident light was adjusted to 7.0×10^{-8} mol m^{-2} s^{-1} by adjustment of light intensity using Neutral Density (ND) filter at each wavelength. An apparent quantum yield was calculated as the ratio of the rate of electron consumption by the photocatalytic reaction to the flux of incident photons.

4.3 Results and discussion

4.3.1 Characterization of SiO$_2$-TiO$_2$ and Au/SiO$_2$-TiO$_2$

The XRD pattern and TEM images of an SiO$_2$–TiO$_2$ template are shown in Fig. 4.1. Peaks of anatase TiO$_2$ were clearly observed as well as a halo of amorphous SiO$_2$ at ca. 23° in the XRD pattern (Fig. 4.1(a)). The template possessed an ordered tubular mesoporous structure with a pore diameter of ca. 8 nm that was proved by the TEM image (Fig. 4.1(b)). A high-resolution [HR]-TEM image of SiO$_2$–TiO$_2$ template was inserted in Fig. 4.1(b), and the image showed that nanocrystals with a diameter of 2–5 nm were well dispersed in the template. This d spacing of 3.51 Å is consistent with that of the {011} planes of anatase TiO$_2$ [3]. These results show that the mesoporous SiO$_2$–

TiO$_2$ template with ordered tubular pores consists of amorphous SiO$_2$ and well-dispersed anatase TiO$_2$ nanocrystals.

The TEM images and DR spectrum of an Au NPs/SiO$_2$-TiO$_2$ and Au NRs/SiO$_2$–TiO$_2$ composite are shown in Fig. 4.2 and Fig. 4.3. In Au NPs deposited sample, spherical NPs with a diameter of 7–15 nm were observed on the inside and outside of the template (Fig. 4.2(a)). The inset of Fig. 4.2(a) is a HR-TEM image showing that the observed NP is Au NP, because of the d spacing of 2.35 Å [4]. On the other hand, NRs with a diameter of 7 nm and lengths of 20–80 nm were observed in the mesopores of Au NRs-deposited sample (Fig. 4.2(b)). The specific surface areas of SiO$_2$–TiO$_2$, Au NPs/SiO$_2$-TiO$_2$ and Au NRs/SiO$_2$–TiO$_2$ were 518.2, 303.1 and 353.2 m^2 g^{-1}, respectively. The decrease in specific surface area is due to the Au blockage in the tubular mesopores. However, the relatively narrow decrease range indicates that there are interpores in this template like SBA-15 [5]. The specific surface area of Au NPs/SiO$_2$–TiO$_2$ was smaller than that of Au NRs/SiO$_2$–TiO$_2$. This is presumably because the number of Au NPs was larger than Au NRs when the same amount of Au atoms was deposited, resulting in effective blocking of the mesopores. The specific surface area of Au/SiO$_2$–TiO$_2$ decreased with increasing the amount of deposited Au because the Au blockage in the tubular mesopores would occur more often. Au NPs/SiO$_2$–TiO$_2$ showed extinctions at shorter wavelength than 380 nm and at ca. 542 nm. On the other hand, Au NRs/SiO$_2$–TiO$_2$ showed extinction peaks at 525 and 712 nm in the DR spectrum (Fig. 4.3). In comparison with the spectra of mesoporous SiO$_2$ and SiO$_2$–TiO$_2$ templates made by the similar sol–gel method, the extinction below 380 nm was attributed to light absorption by the band gap of anatase TiO$_2$, and the extinction peaks at 542, 525 and 712 nm were defined as the extinction by SPR of the deposited

Au NPs and NRs. The wavelength of SPR was well consistent with the size and shape of the deposited Au [6-8].
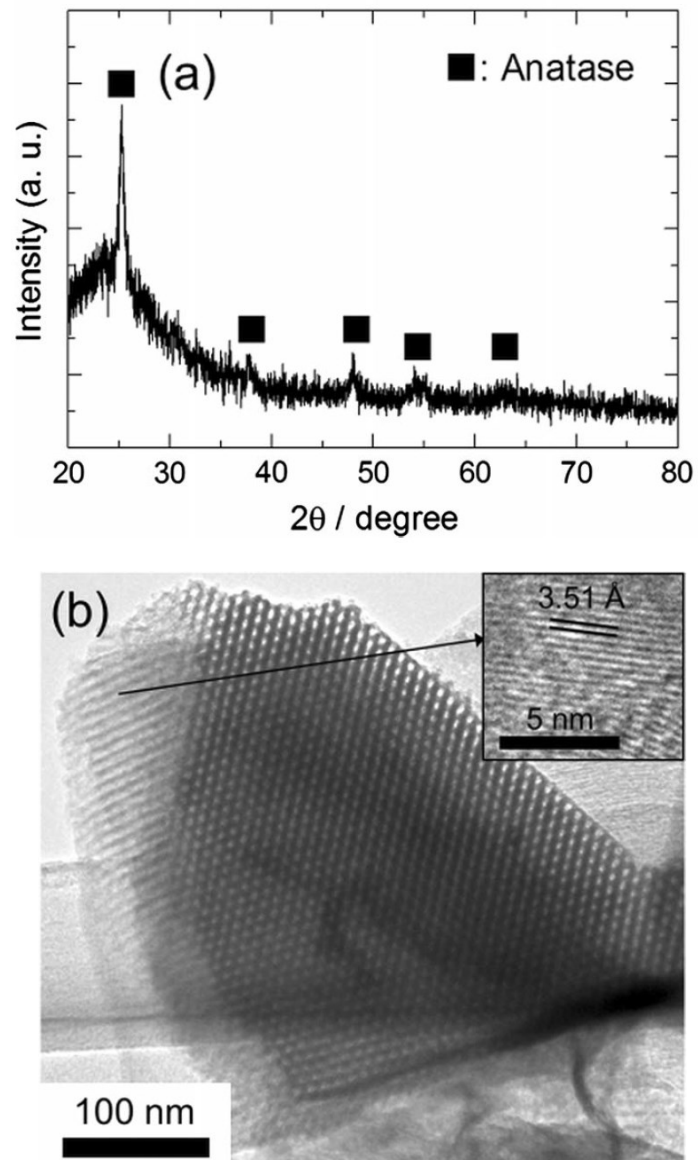
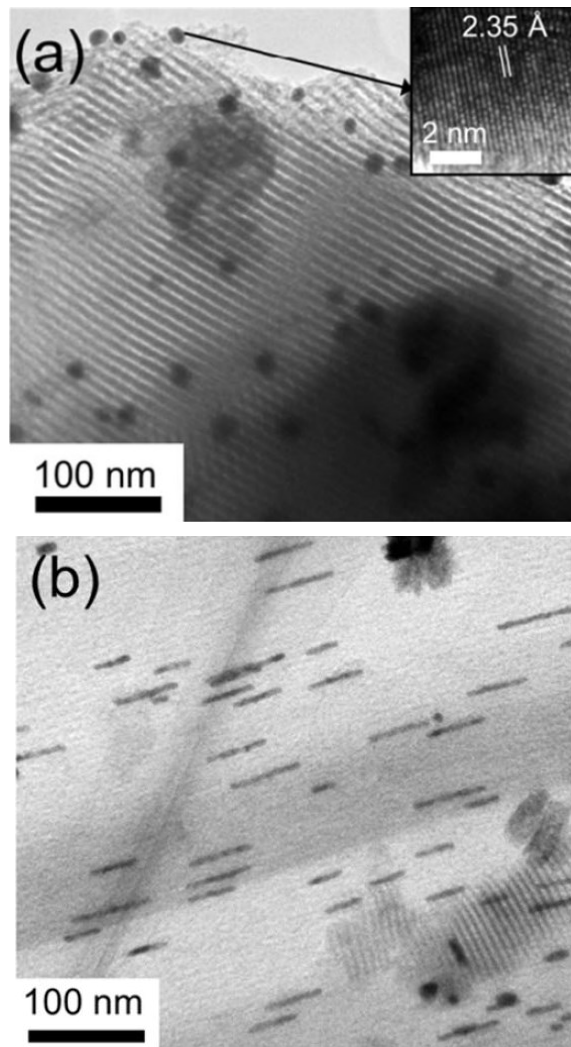Fig. 4.1. (a) XRD pattern and (b) TEM image of mesoporous SiO_2-TiO_2.

Fig. 4.2. TEM images of (a) Au NPs and (b) Au NRs/SiO$_2$–TiO$_2$. The inset of (a) is an
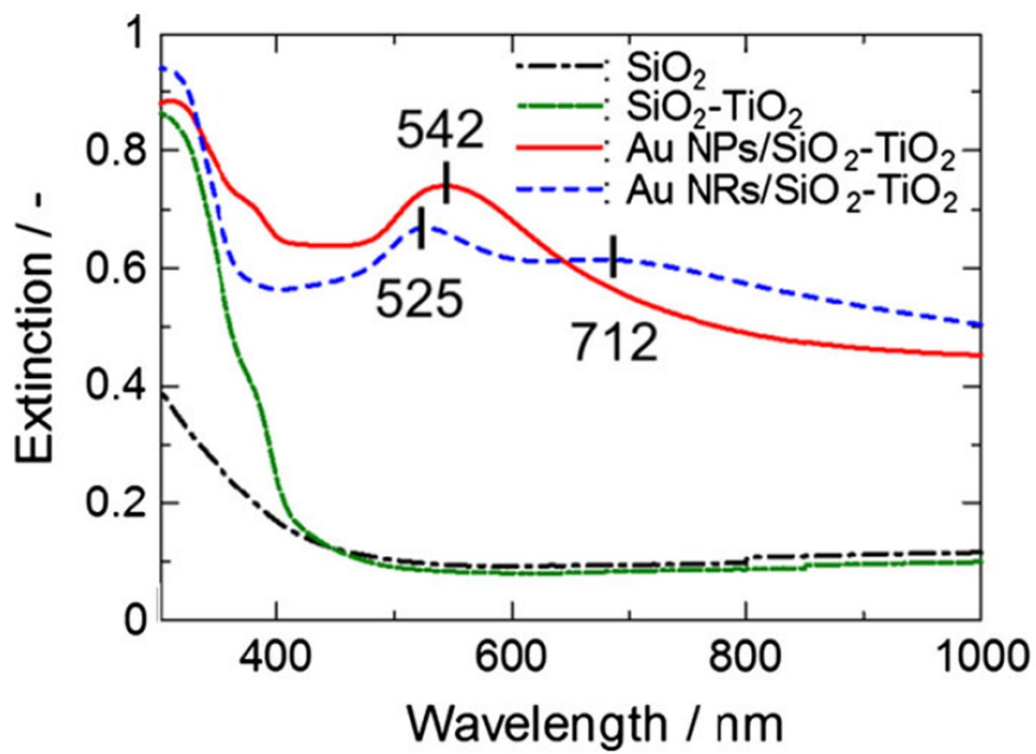
HR-TEM image of observed Au NP.

Fig. 4.3. DR spectra of Au NPs/SiO$_2$-TiO$_2$ and Au NRs/SiO$_2$-TiO$_2$.

4.3.2 Photocatalytic property of prepared samples under UV

The photobleaching dynamics of MB solution and photoxidation dynamics of 2-propanol with samples before and after Au deposition under UV are shown in Fig. 4.4 and Fig. 4.5. For comparative purposes, commercially available Degussa P25 (AEROSIL, Japan) was employed, and the results by P25 are also shown in Fig. 4.5. First, adsorption of MB on the samples was saturated by stirring for 10 min before light irradiation. The y axes in Fig. 4.4(a) and Fig. 4.5(a) denote the absorbance of MB solution after light irradiation for certain time (I_x) divided by the initial absorbance of MB solution after adsorption process (I_0). The absorbance of MB decreased by 60, 40, 20, 15 and 8 % by the adsorption process for 10 min when the SiO_2–TiO_2 and 0.3, 0.6, 1.2 and 1.8Au/SiO_2–TiO_2 powders were used, respectively (Fig. 4.4(a)). 25 % decrement of MB absorbance was confirmed with Au NRs/SiO_2–TiO_2. Meanwhile, the absorbance of MB did not decrease when P25 was used (see the inset of Fig. 4.4(a) and Fig. 4.5(a)). The differences in the amount of adsorption of MB were in good agreement with the specific surface areas of each powder (see Table 4.1 and 4.2). The absorbance of MB solution decreased by further 34 % after UV radiation for 30 min when the SiO_2–TiO_2 powder was used. This value of decrease was almost the same as that of P25. On the other hand, decreases of the absorbance by 75 and 80 % occurred after UV radiation for 30 min when Au NPs/SiO_2–TiO_2 and Au NRs/SiO_2–TiO_2 were used. Decreases of the absorbance by 44, 20 and 14 % occurred after UV radiation when 0.3, 1.2 and 1.8Au/SiO_2-TiO_2 powders were used, respectively. In the case of photooxidation of 2-propanol, about 4.0 μmol acetone was generated under UV radiation for 60 min when SiO_2-TiO_2 and P25 were used. On the other hand, Au NPs/SiO_2-TiO_2 and Au NRs/SiO_2-TiO_2 generated 5.54 and 5.76 μmol acetone under

UV radiation for 60 min, respectively. Also, 4.58, 3.79 and 3.49 μmol acetone were generated under UV radiation for 60 min when 0.3, 1.2 and 1.8Au/SiO$_2$-TiO$_2$ powders were used, respectively. First-order reaction rate constants of MB photobleaching, k_{UV}, and generation rate of acetone by 2-propanol photoxidation, R_{UV}, under UV are also shown in Table 4.1 and Table 4.2. 0.6Au/SiO$_2$–TiO$_2$ showed the highest k_{UV} and R_{UV} among the powders with the difference amount of Au. Au NRs/SiO$_2$–TiO$_2$ showed almost the same k_{UV} and R_{UV} as Au NPs/SiO$_2$–TiO$_2$. It is worth mentioning here that the surface areas of Au NPs/SiO$_2$–TiO$_2$ and Au NRs/SiO$_2$–TiO$_2$ were smaller than that of SiO$_2$–TiO$_2$ (303.1, 353.2 and 518.2 m^2 g^{-1}, respectively). This indicates that the photocatalytic activity of the template per surface area was doubtlessly improved by the deposition of Au. This improvement of the photocatalytic activity by the deposition of Au NPs is presumably due to the fact that the charge separation lifetime is elongated by the formation of a Schottky barrier at the Au–TiO$_2$ interface [1,9-11]. However, 1.2 and 1.8Au/SiO$_2$–TiO$_2$ showed lower value than that of the template. This result is presumably due to the large decrease in specific surface area, leading to blockage of access of MB and 2-propanol to the inside of the powders. To investigate effects of blockage region by deposition of Au NPs to the photocatalytic activity, mesoporous TiO$_2$ with controlled particle size was prepared and used as the template for the deposition of Au. The diameter of prepared mesoporous TiO$_2$ was ca. 50 nm (Fig. 4.6), which is smaller than SiO$_2$-TiO$_2$ template. Therefore, specific surface area of mesoporous TiO$_2$ was larger than that of SiO$_2$-TiO$_2$ (shown in Table 4.3). This specific surface area decreased with increasing the amount of Au. Although the specific surface area of SiO$_2$-TiO$_2$ decreased less than half by the deposition of 1.8 mol% of Au (518.2 m^2 g^{-1} to 221.6 m^2 g^{-1}), the specific surface area of mesoporous TiO$_2$ decreased to 66%

104

when 1.8 mol% Au was deposited in mesoporous TiO_2 (758.1 m^2 g^{-1} to 507.5 m^2 g^{-1}). This difference is presumably due to the decrease of number of Au NPs deposited in a template particle. Since the size of template particles became small, the number of Au NPs deposited in a template particle decreased and then the blockage region by Au NPs decreased. The photobleaching dynamics of MB solution and photoxidation dynamics of 2-propanol with mesorporous TiO_2 and Au/TiO_2 under UV are shown in Fig. 4.7. 0.6Au/TiO_2 showed the highest photocatalytic activity with both photobleaching of MB and phtotooxidation of 2-propanol (7.58×10^{-2} min^{-1} and 9.2 μmol h^{-1}, respectively). When the amount of Au increased over 0.6 mol%, the photocatalytic properties decreased like the case of SiO_2-TiO_2. These results probably indicate that the decrease of the photocatalytic properties with different amount of Au is due to the decrease of specific surface areas by deposition of Au NPs.

On the other hand, higher photocatalytic activity of Au/SiO_2–TiO_2 than that of P25 can also be related to the effect of Si–O–Ti bond formed in the mesoporous SiO_2–TiO_2 template because the existence of Si–O–Ti bonds causes the lowering of both the HOMO and LUMO levels as compared with TiO_2 [12].
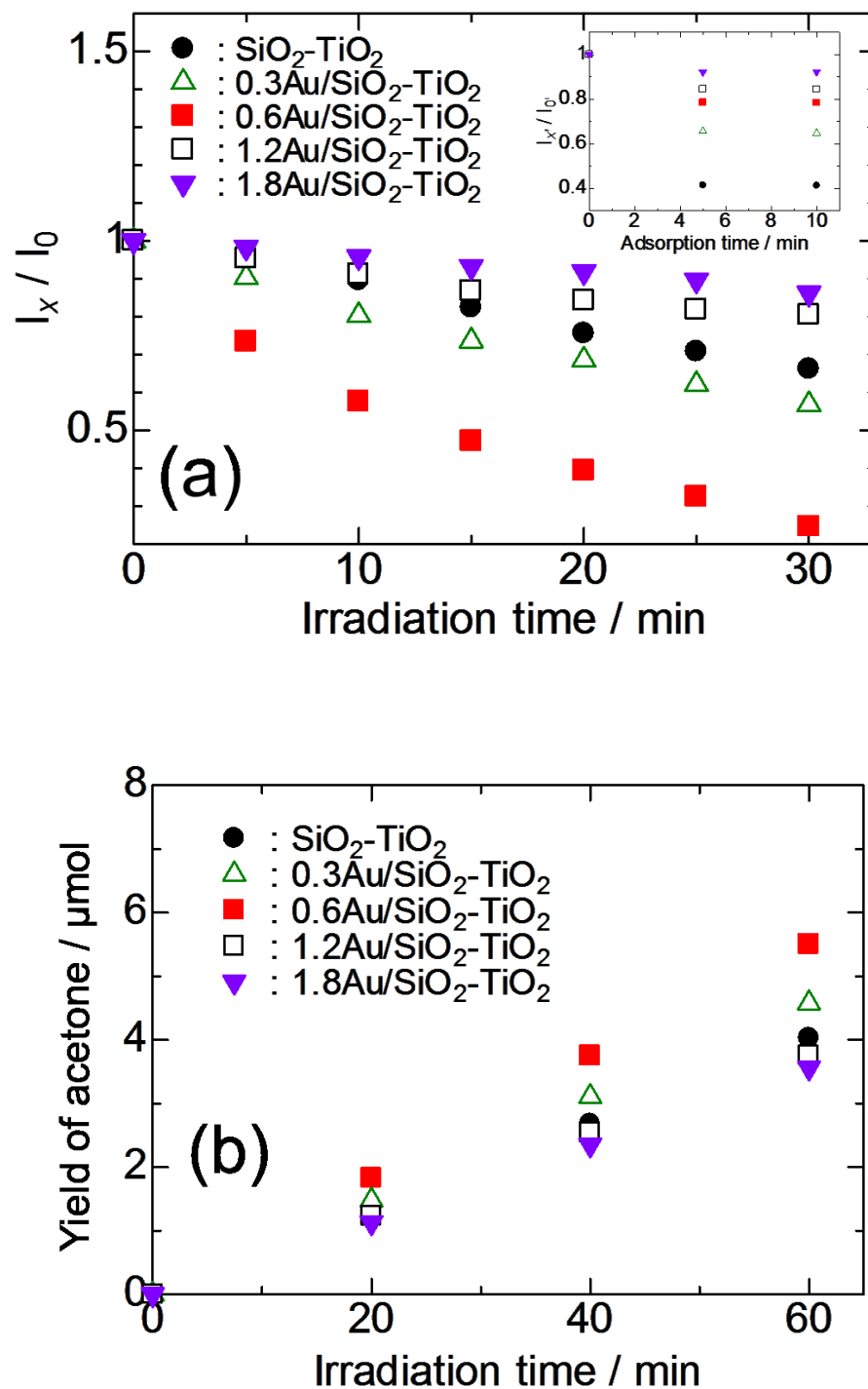
Fig.4.4. (a) Photobleaching dynamics of MB solution and (b) photooxidation dynamics of 2-propanol with Au/SiO$_2$-TiO$_2$ with various amount of Au under UV (<380 nm) radiation. The inset in panel (a) shows the adsorption dynamics for MB on each sample.
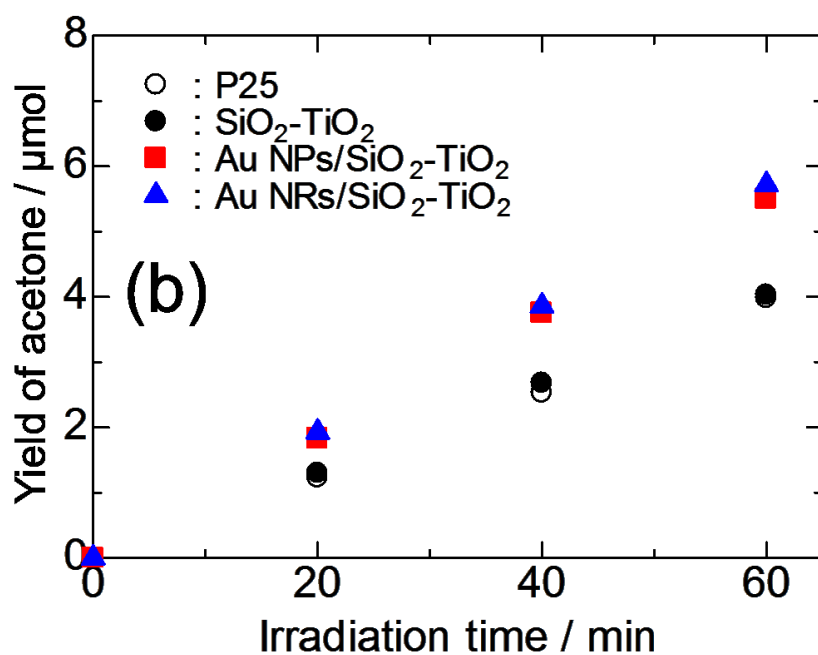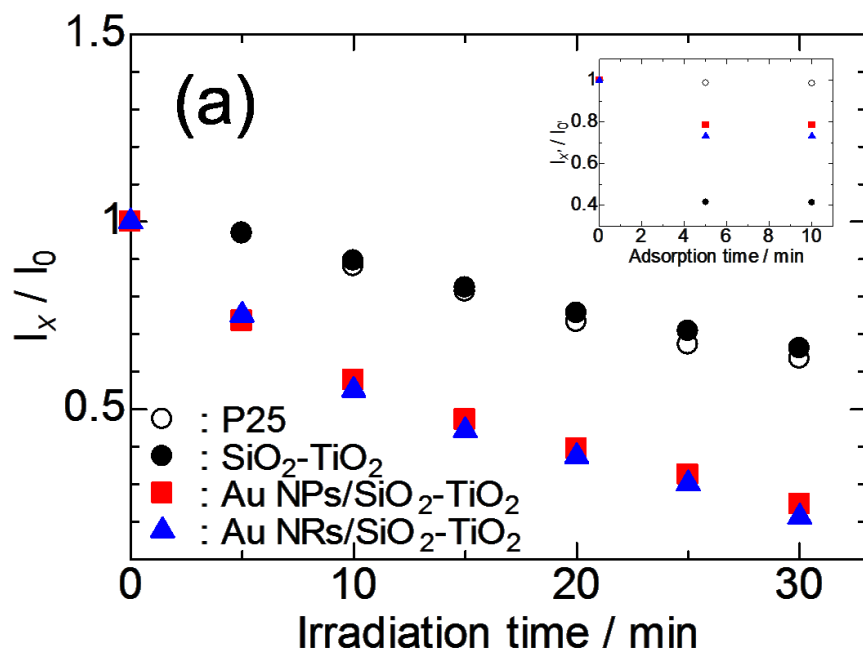
Fig. 4.5. (a) Photobleaching dynamics of MB solution and (b) photooxidation dynamics of

2-propanol with P25, SiO_2-TiO_2 and Au NPs and NRs/SiO_2-TiO_2 under UV (<380 nm) radiation.

The inset in panel (a) shows the adsorption dynamics for MB on each sample.

Table 4.1. Specific surface areas and rate constants of MB photobleaching under UV (k_{UV})

radiation for Au/SiO$_2$-TiO$_2$ with various amount of Au.

Catalyst	Specific surface area [m^2 g^{-1}]	k_{UV} [min^{-1}]	R_{UV} [μmol h^{-1}]
SiO$_2$-TiO$_2$	518.2	1.18×10^{-2}	4.03
0.3Au/SiO$_2$-TiO$_2$	425.1	1.59×10^{-2}	4.58
0.6Au/SiO$_2$-TiO$_2$	303.1	5.22×10^{-2}	5.54
1.2Au/SiO$_2$-TiO$_2$	261.8	1.43×10^{-2}	3.79
1.8Au/SiO$_2$-TiO$_2$	221.6	5.72×10^{-3}	3.49

Table 4.2. Specific surface areas and rate constants of MB photobleaching under UV (k_{UV})

radiation for P25, SiO$_2$-TiO$_2$ and Au NPs and NRs/SiO$_2$-TiO$_2$.

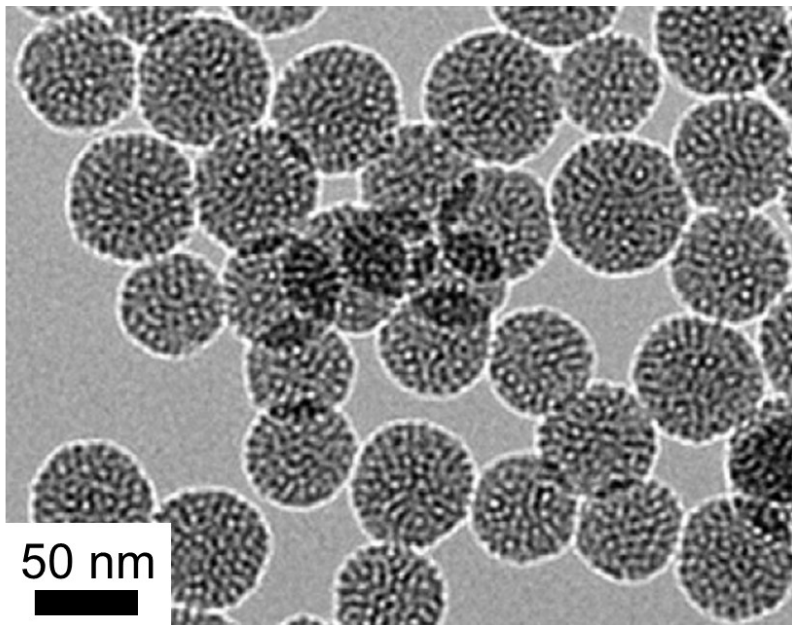| Catalyst	Supecific surface area [m^2 g^{-1}]	k_{UV} [min^{-1}]	R_{UV} [μmol h^{-1}]
P25	52.3	1.29×10^{-2}	3.98
SiO$_2$-TiO$_2$	518.2	1.18×10^{-2}	4.03
Au NPs/SiO$_2$-TiO$_2$	303.1	5.22×10^{-2}	5.54
Au NRs/SiO$_2$-TiO$_2$	353.2	5.34×10^{-2}	5.76

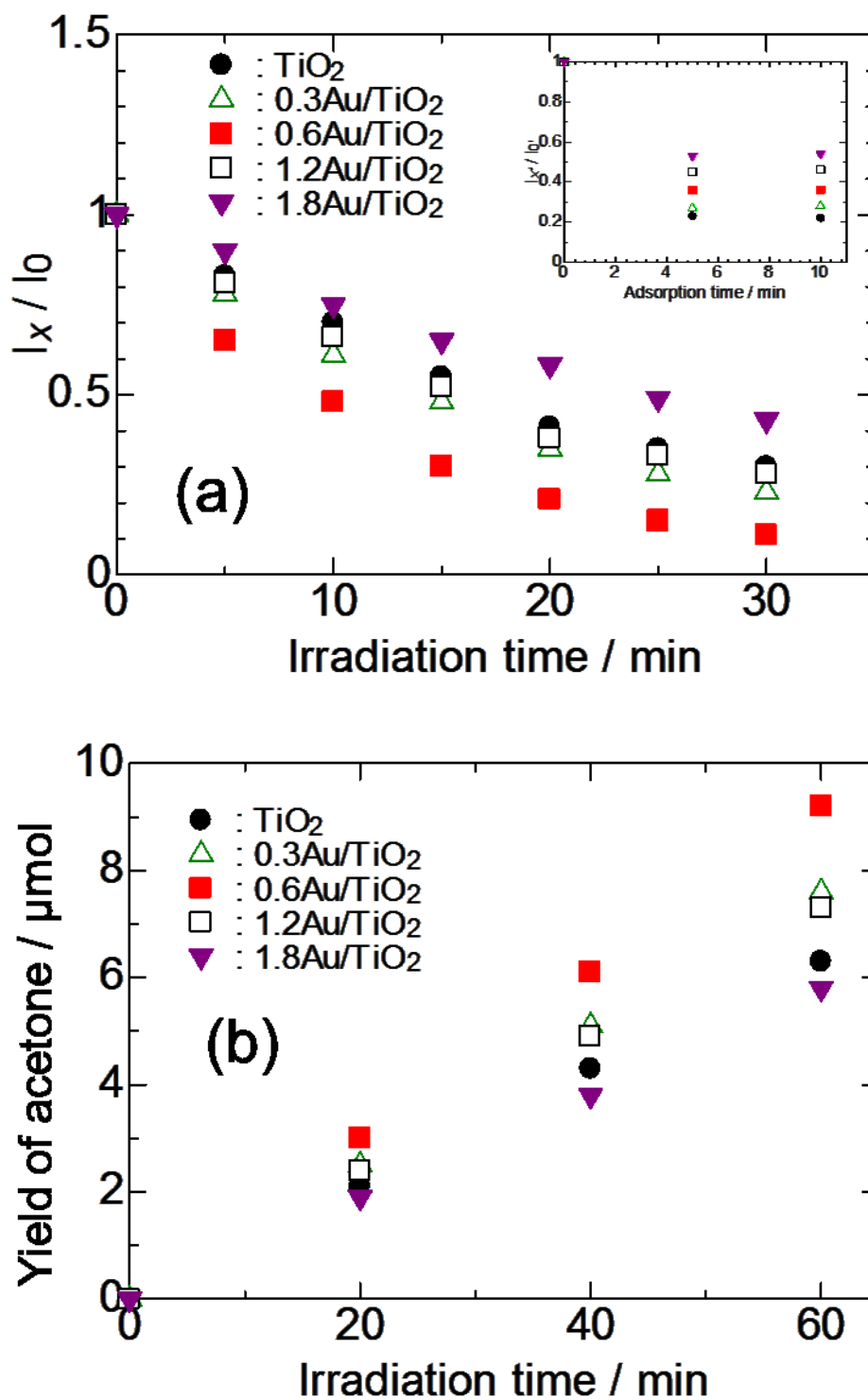Fig. 4.6. TEM image of mesoporous TiO$_2$ with controlled particle size.

Fig. 4.7. (a) Photobleaching dynamics of MB solution and (b) photooxidation dynamics of 2-propanol with mesoporous TiO_2 and Au/TiO_2 with various amount of Au under UV (<380 nm) radiation. The inset in panel (a) shows the adsorption dynamics for MB on each sample.

110

Table 4.3. Specific surface areas and rate constants of MB photobleaching under UV (k_{UV})

radiation for mesoporous TiO_2 and Au/TiO_2 with various amount of Au.

Catalyst	Supecific surface area [m^2 g^{-1}]	k_{UV} [min^{-1}]	R_{UV} [μmol h^{-1}]
Mesoporous TiO_2	758.1	4.12×10^{-2}	6.31
0.3Au/TiO_2	703.5	5.02×10^{-2}	7.62
0.6Au/TiO_2	653.2	7.58×10^{-2}	9.23
1.2Au/TiO_2	551.1	4.41×10^{-2}	7.32
1.8Au/TiO_2	451.5	2.81×10^{-3}	5.87

4.3.3 Photocatalytic property of prepared samples under Vis

SiO$_2$–TiO$_2$ template showed a decrease of the absorbance of MB solution by 13 % after Vis light irradiation for 30 min, whereas P25 showed little photocatalytic activity under Vis light (Fig. 4.8(a)). This tendency was also observed in the case of photoxidation of 2-propanol (Fig. 4.8(b)), SiO$_2$–TiO$_2$ template generated 0.56 μmol acetone after Vis light irradiation for 60 min although P25 did not generated acetone under Vis light. These differences in the photocatalytic activity between two samples under Vis light irradiation could be derived from the structural defects that should be contained in the mesoporous template, and the defects can absorb Vis photons [13]. Au NPs/SiO$_2$–TiO$_2$ composite showed decrease of the absorbance by 25 % and generation of 6.11 μmol acetone after Vis light irradiation. From these results, the first-order reaction rate constants, k_{Vis}, and generation rate, R_{Vis}, under Vis light were calculated, and the values of 1.04×10^{-2} min^{-1} and 6.11 μmol h^{-1} for Au NPs/SiO$_2$–TiO$_2$ were approximately 2 and 12 times higher than those of the SiO$_2$–TiO$_2$, respectively (see Table 4.4). Additionally, the photocatalytic activities of 0.3, 1.2 and 1.8Au/SiO$_2$–TiO$_2$ under Vis light were lower than that of 0.6Au/SiO$_2$–TiO$_2$ (Table 4.5 and Fig. 4.8). A deposition of Au onto TiO$_2$ enables SPR-induced photocatalysis under Vis light [14]; however, too much deposition leads to a decrease in surface area and Au blockage in mesopores. In previous chapter, the Au/SiO$_2$–TiO$_2$ prepared by heat-reduction method exhibited almost no photocatalytic activity because many Au NPs were deposited on SiO$_2$. Conversely, in this work, Au was deposited by a light-reduction method through an excitation of electrons of TiO$_2$, followed by a transfer of the electrons from TiO$_2$ to Au ions. Therefore, Au NPs should be deposited on TiO$_2$, and the interface of Au/TiO$_2$ causes SPR-induced photocatalysis, resulting in the high photocatalytic activity of

Au/SiO$_2$–TiO$_2$ in this work. Furthermore, Au NRs/SiO$_2$–TiO$_2$ composite showed even larger decrease of the absorbance of MB solution (35 %) and generation of agetone (7.54 μmol) than that of Au NPs/SiO$_2$–TiO$_2$. This improvement of photocatalytic activity is probably due to the wider absorption wavelength region of SPR by Au NRs. Au NPs showed extinction at 500–600 nm in Vis region. On the other hand, Au NRs showed extinction at 500–800 nm (shown in Fig. 4.3). In the next section, the action spectra for the samples were measured to investigate the detailed mechanisms of the photocatalysis.

In these experiments, hydrogen production was not observed. Hydrogen production occurs when H$^+$ in aqueous solution reacted with excited electrons in the semiconductor under light irradiation. However, oxygen reacts with the excited electrons in preference to hydrogen generation if oxygen is present in the aqueous solution. Therefore, the property of hydrogen production with a photocatalyst is usually investigated after the removal of the oxygen with an inert gas such as nitrogen and argon [15,16]. Actually, hydrogen production was observed by removal of oxygen in the solution with nitrogen gas under UV and Vis light irradiation in my experiments. About 1.0 and 0.3 ml (about 45 and 13 μmol, respectively) of hydrogen were produced with Au NPs/SiO$_2$-TiO$_2$ for 1 h under UV and Vis light irradiation.
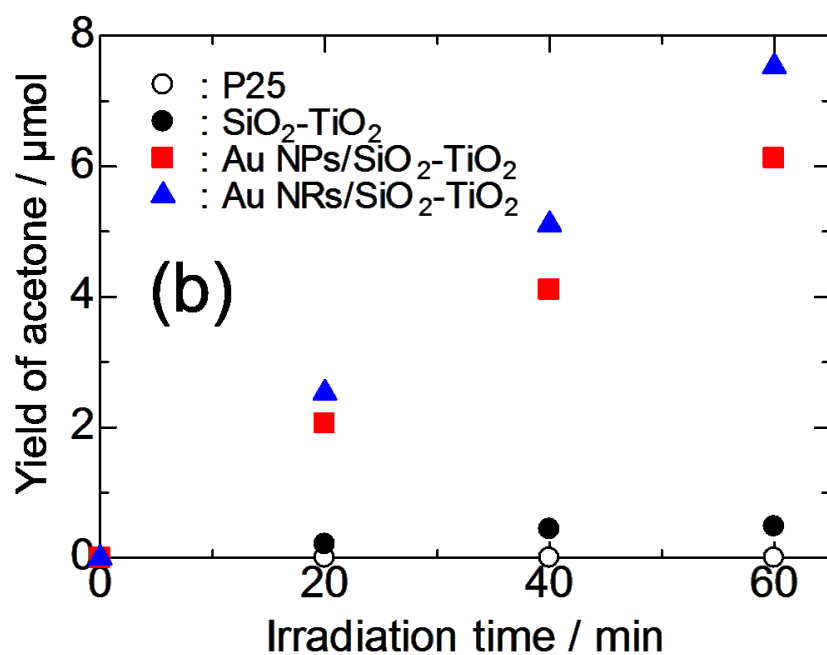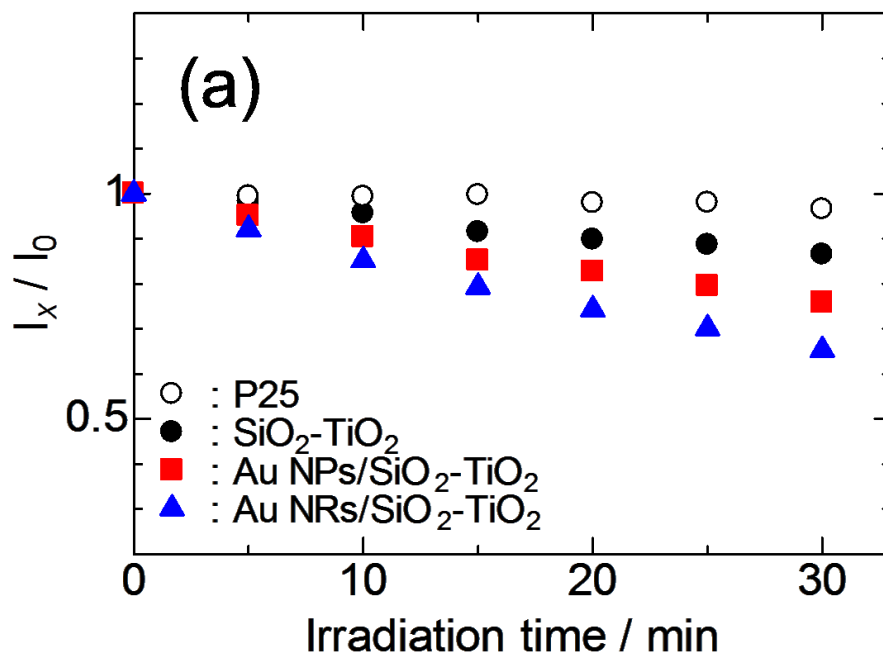
Fig. 4.8. (a) Photobleaching dynamics of MB solution and (b) photooxidation dynamics of 2-propanol with P25, SiO_2-TiO_2 and Au NPs and NRs/SiO_2-TiO_2 Vis (>480 nm) light irradiation.
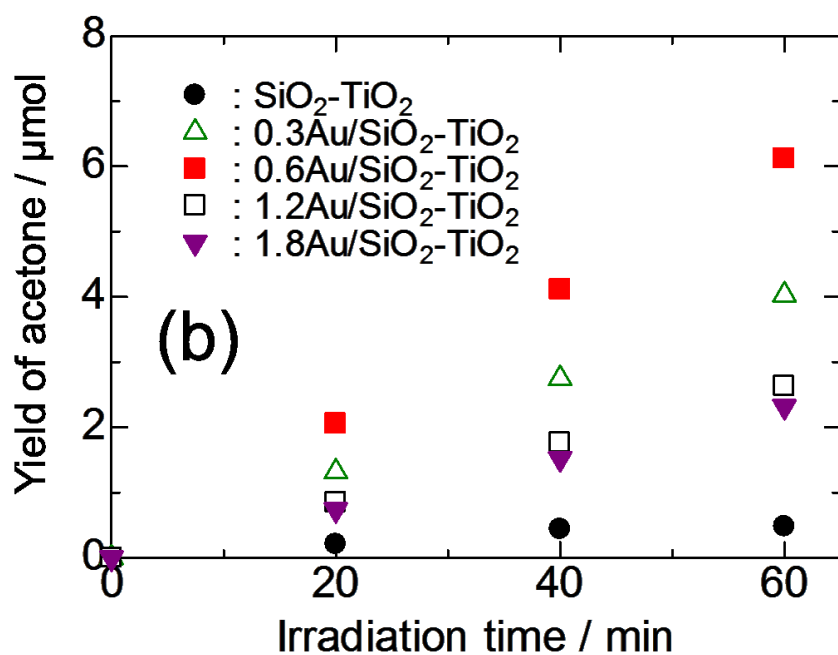
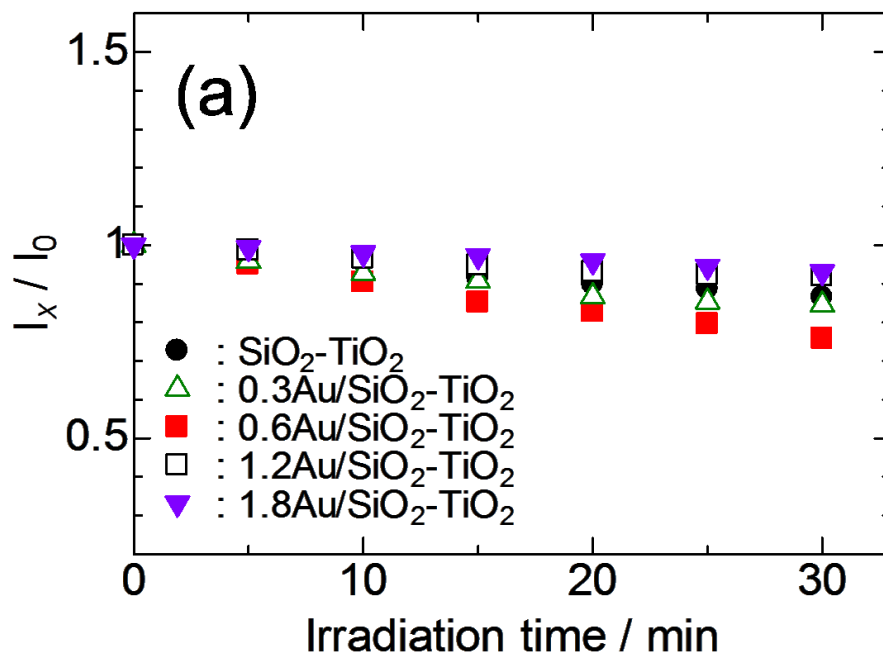Fig. 4.9. (a) Photobleaching dynamics of MB solution and (b) photooxidation dynamics of 2-propanol with Au/SiO$_2$-TiO$_2$ with various amount of Au under Vis (>480 nm) light irradiation.

Table 4.4. Specific surface areas and rate constants of MB photobleaching under Vis (k_{Vis}) light irradiation for P25, SiO_2-TiO_2 and Au NPs and NRs/SiO_2-TiO_2.

Catalyst	Supecific surface area [m^2g^{-1}]	k_{Vis} [min^{-1}]	R_{Vis} [$\mu mol\ h^{-1}$]
P25	52.3	6.31×10^{-4}	0.01
SiO_2-TiO_2	518.2	5.33×10^{-3}	0.56
Au NPs/SiO_2-TiO_2	303.1	1.04×10^{-2}	6.11
Au NRs/SiO_2-TiO_2	353.2	1.83×10^{-2}	7.54

Table 4.5. Specific surface areas and rate constants of MB photobleaching under Vis (k_{Vis}) light irradiation for Au/SiO_2-TiO_2 with various amount of Au.

Catalyst	Supecific surface area [m^2g^{-1}]	k_{Vis} [min^{-1}]	R_{Vis} [$\mu mol\ h^{-1}$]
SiO_2-TiO_2	518.2	5.33×10^{-3}	0.56
0.3Au/SiO_2-TiO_2	425.1	6.72×10^{-3}	4.02
0.6Au/SiO_2-TiO_2	303.1	1.04×10^{-2}	6.11
1.2Au/SiO_2-TiO_2	261.8	3.15×10^{-3}	2.64
1.8Au/SiO_2-TiO_2	221.6	2.23×10^{-3}	2.34

4.3.4 Action spectra of prepared samples

The action spectra of photobleaching of MB with no photocatalyst and mesoporous SiO_2–TiO_2 before and after Au deposition are shown in Fig. 4.10. The DR spectra of Au NPs/SiO_2-TiO_2 and Au NRs/SiO_2–TiO_2 composite and absorption spectrum of MB solution are also shown in the same figure. No photobleaching of MB occurred when MB solution containing no photocatalyst was irradiated with light of any wavelength (open circles). This indicates that light irradiation itself has no direct influence on photobleaching of MB in the solution. In contrast, photobleaching of MB occurred when the solution with SiO_2–TiO_2 was exposed to lights of 365 and 600–700 nm (closed circles). The bleaching occurred presumably because the wavelengths of incident light overlapped with the absorption wavelengths of TiO_2 and MB. Since the photobleaching did not occur when the irradiation of light of 600–700 nm was carried out to the pure MB solution, it was found that the adsorption of MB on the surface of SiO_2–TiO_2 is indispensable to the photobleaching of MB under the Vis light of 600–700 nm, though the structural defects in the mesoporous template would have small contribution to the photobleaching under Vis light irradiation. On the other hand, a peak at 540 nm appeared in the action spectrum of Au NPs/SiO_2–TiO_2 in addition to the peaks at 365 and 600–700 nm (closed squares). This new peak in the action spectrum and the SPR peak of Au NPs/SiO_2–TiO_2 in the DR spectrum have comparable wavelengths. Therefore, a trigger of photobleaching caused by light of 540 nm was attributed to the light absorption by SPR of Au NPs. Au NRs/SiO_2–TiO_2 showed photobleaching of MB when the sample was exposed to lights of 365 and 500–1000 nm (closed triangles). These wavelengths are consistent with the SPR peaks of Au NRs/SiO_2–TiO_2. Thus, SPR of Au NRs was also found to be able to use for

photobleaching of MB.

The action spectra of photooxidation of 2-propanol with prepared samples are shown in Fig. 4.11. From these action spectra, we can see that the almost the same results as that of photobleaching of MB except the absorption wavelength region of MB. 2-propanol solution does not absorb the light. Therefore, peaks by SPR of Au NPs and NRs were clearly observed in action spectra of photooxidation of 2-propanol with Au NPs/SiO_2-TiO_2 and Au NRs/SiO_2-TiO_2. These results concluded that the photocatalysis under Vis light irradiation occurs by the light absorption of SPR of Au NPs and Au NRs and MB adsorbed on samples. Au NPs/SiO_2–TiO_2 can cause Vis light absorption in the range of 500–700 nm and Au NRs/SiO_2–TiO_2 can cause Vis light absorption in the range of 500–1000 nm, leading to the high and the highest photocatalytic activity under Vis light irradiation, respectively.
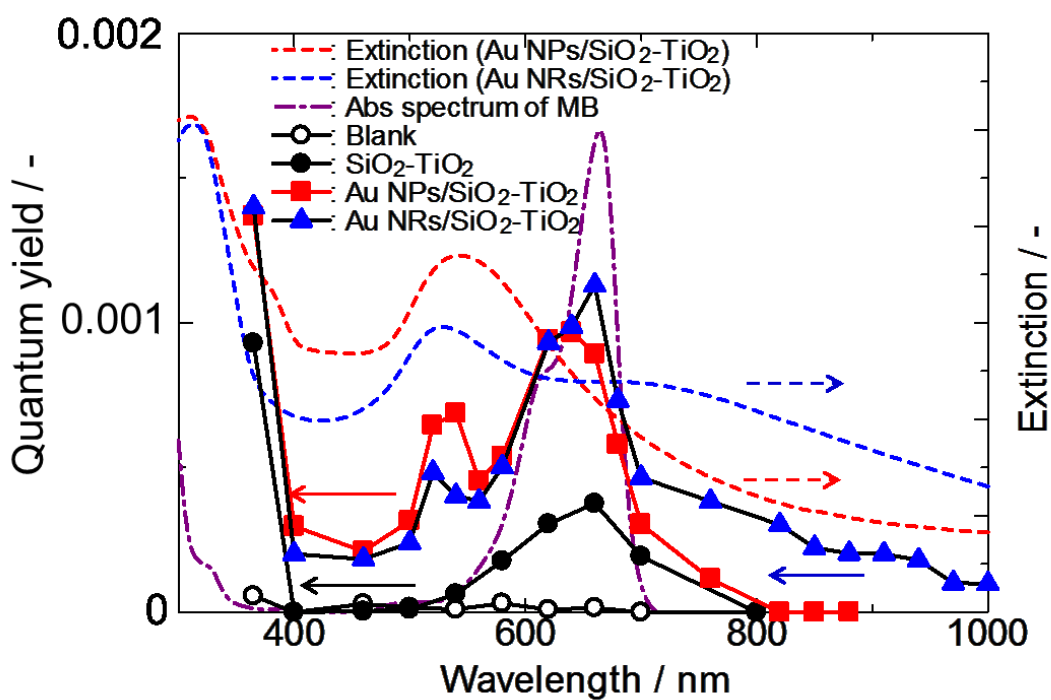
Fig. 4.10. Action spectra of MB bleaching using MB solution with no samples ($\bigcirc$), SiO_2-TiO_2 ($\bullet$), and Au NPs/SiO_2-TiO_2 ($\blacksquare$) and Au NRs/SiO_2-TiO_2 ($\blacktriangle$). DR spectrum of Au NPs and NRs/SiO_2-TiO_2 and absorption supectrum of MB solution are also shown as references.

Fig. 4.11. Action spectra of photooxidation of 2-propanol with SiO_2-TiO_2 (●), and Au NPs/SiO_2-TiO_2 (■) and Au NRs/SiO_2-TiO_2 (▲). DR spectrum of Au NPs and NRs/SiO_2-TiO_2 and absorption supectrum of MB solution are also shown as references.
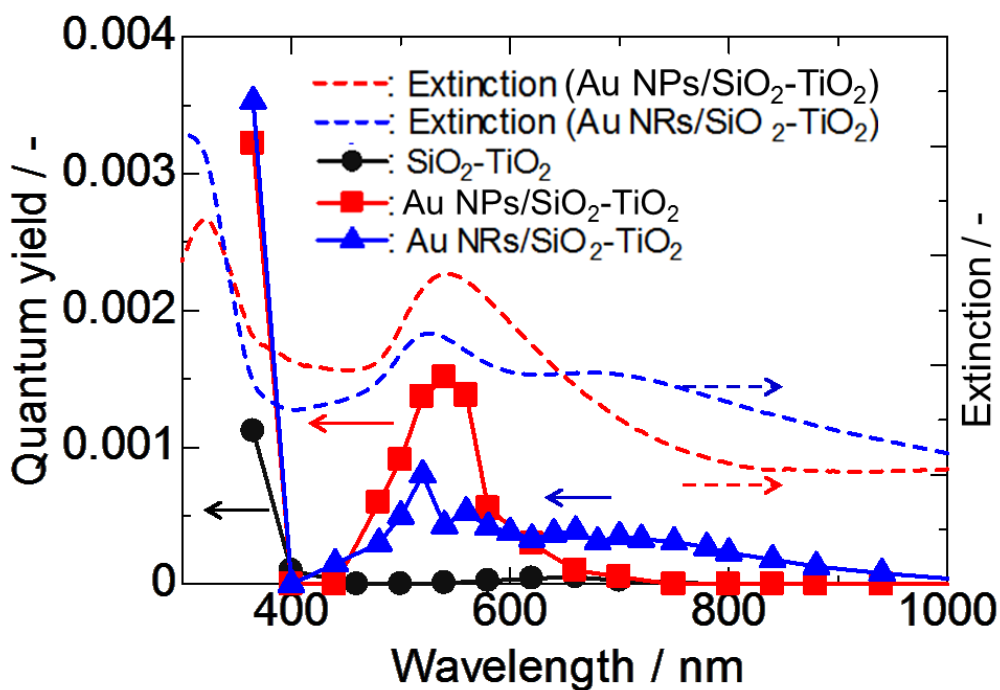
4.3.5 Photocatalytic activity under simultaneous irradiation of UV and Vis

The electrons excited in TiO_2 transfer to Au NPs from CB of TiO_2 and react with reactants on the surface of Au NPs when Au-TiO_2 photocatalyst was illuminated by UV [11,17]. On the other hand, the electrons excited in Au NPs transfer to CB of TiO_2 when Vis light was irradiated [18,19]. Therefore, it was expected that photocatalytic activity under simultaneous irradiation of UV and Vis light decreased because generated holes remain in TiO_2 or Au and electrons transferred from the other, thus the recombination of charges could occur. The photooxidation dynamics of 2-propanol and photobleaching dynamics of MB using SiO_2-TiO_2, Au NPs/SiO_2-TiO_2 and Au NRs/SiO_2-TiO_2 under individual and simultaneous irradiation of UV and Vis light is shown in Fig. 4.12 and Fig. 4.13, and the generation rates of acetone (R_{UV+Vis}) and first-order reaction rate constant (k_{UV+Vis}) are summarized in Table 4.6 and Table 4.7. The photobleaching reaction of MB is a reduction reaction in contrast to the case of acetone generation from 2-propanol, which is an oxidation reaction. Therefore, we can discuss the behavior of both negative and positive charges generated by light irradiation. Since the rate of photocatalytic reactions depends on the number of photons of the incident light, the flux of photons was adjusted to be the same (7.0×10^{-8} mol m^{-2}s^{-1}). Thus, the simultaneous irradiation of UV and Vis light possesses the photon flux of 1.4×10^{-7} mol m^{-2}s^{-1}. In the case of photoxidation of 2-propanol, 4.38 μmol of acetone was generated under simultaneous irradiation when SiO_2-TiO_2 was used, and this amount was almost the same as that obtained under UV radiation. On the other hand, the photocatalytic activity of Au NPs/SiO_2-TiO_2 and Au NRs/SiO_2-TiO_2 was clearly improved by simultaneous Vis light irradiation with UV radiation. Moreover, the improved generation rate

(R_{UV+Vis}) was almost the same as the summed rates of R_{UV} and R_{Vis} (R_{UV+Vis}), which were obtained under independent UV and Vis light irradiation. This result indicates that both reactions under independent UV and Vis light irradiation occurred in parallel when Au/SiO$_2$-TiO$_2$ photocatalyst was illuminated UV and Vis light simultaneously. Even in the case of the photobleaching of MB, similar tendency was confirmed, that is the improvement of photocatalytic activity under simultaneous irradiation was not confirmed when SiO$_2$-TiO$_2$ was used, and the photocatalytic activity of Au NPs/SiO$_2$-TiO$_2$ and Au NRs/SiO$_2$-TiO$_2$ was clearly improved by simultaneous irradiation. The first-order reaction rate constants under the irradiation were calculated from these results and are shown in Table 4.7. The rate constants of SiO$_2$-TiO$_2$ under UV or simultaneous irradiation were almost the same, but the rate constants of Au NPs/SiO$_2$-TiO$_2$ and Au NRs/SiO$_2$-TiO$_2$ under simultaneous irradiation were clearly higher than those obtained under UV and Vis light irradiation. The rate constant under simultaneous irradiation was almost the same as summed rate constants obtained under independent UV and Vis light irradiation. This result is analog of the case of 2-propanol experiments. For comparative purposes, Au/SiO$_2$ and stand-alone Au NPs were prepared and used as photocatalysts. Fig. 4.14 shows the dynamics of acetone generation from 2-propanol and MB photobleaching with the photocatalysts. Obviously, photooxidation of 2-propanol and photoreduction of MB did not occur when Au/SiO$_2$ and Au NPs were used. This indicates that the increase of photocatalytic activity under simultaneous irradiation of UV and Vis light occurs only when both TiO$_2$ and Au NPs exist. Schematic image of the mechanism for the improvement under simultaneous UV and Vis light irradiation is shown in Fig. 4.15. Under the irradiation of UV and Vis light, electrons and holes are generated in TiO$_2$ and Au. The generated electrons transfer to

the other side from TiO_2 or Au NPs, and the holes remain in TiO_2 and Au NPs. The generated charges do not suffer with recombination but are used for photocatalyses effectively.
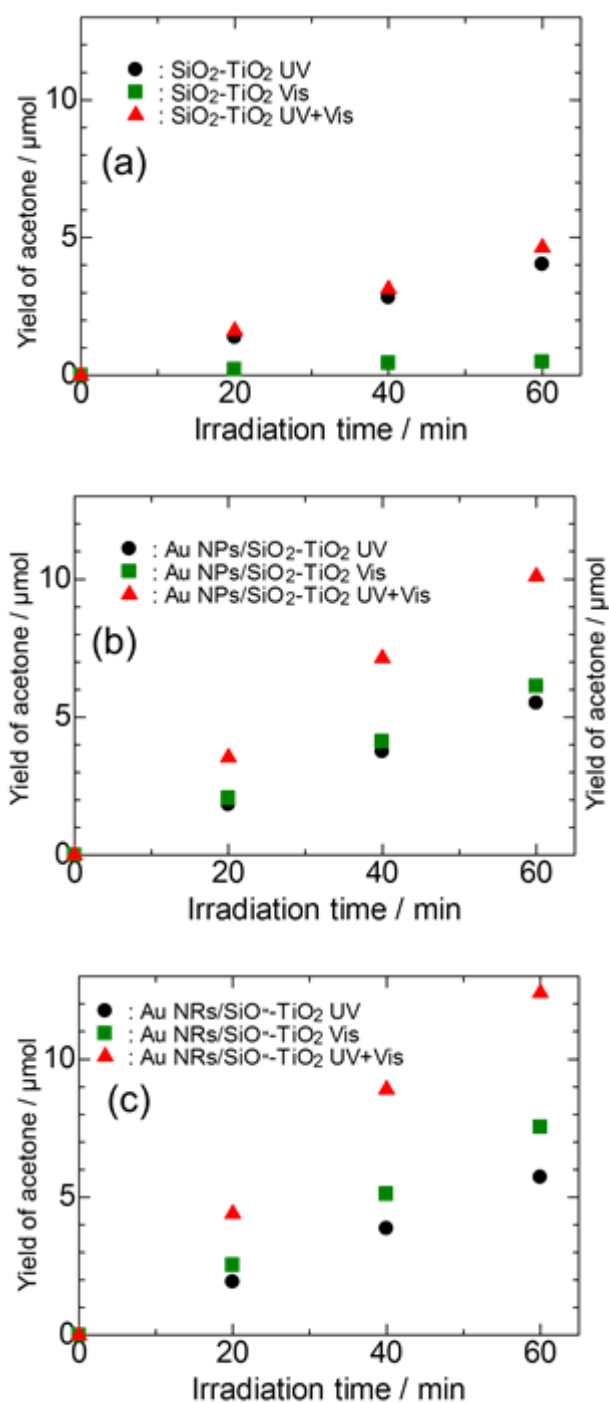
Fig. 4.12. Photooxidation dynamics of 2-propanol with (a) SiO_2-TiO_2, (b) Au NPs/SiO_2-TiO_2 and (c) Au NRs/SiO_2-TiO_2, under individual and simultaneous irradiation of UV and Vis light.

Fig. 4.13. Photobleaching dynamics of MB with(a) SiO_2-TiO_2, (b) Au NPs/SiO_2-TiO_2 and (c) Au NRs/SiO_2-TiO_2, under individual and simultaneous irradiation of UV and Vis light.

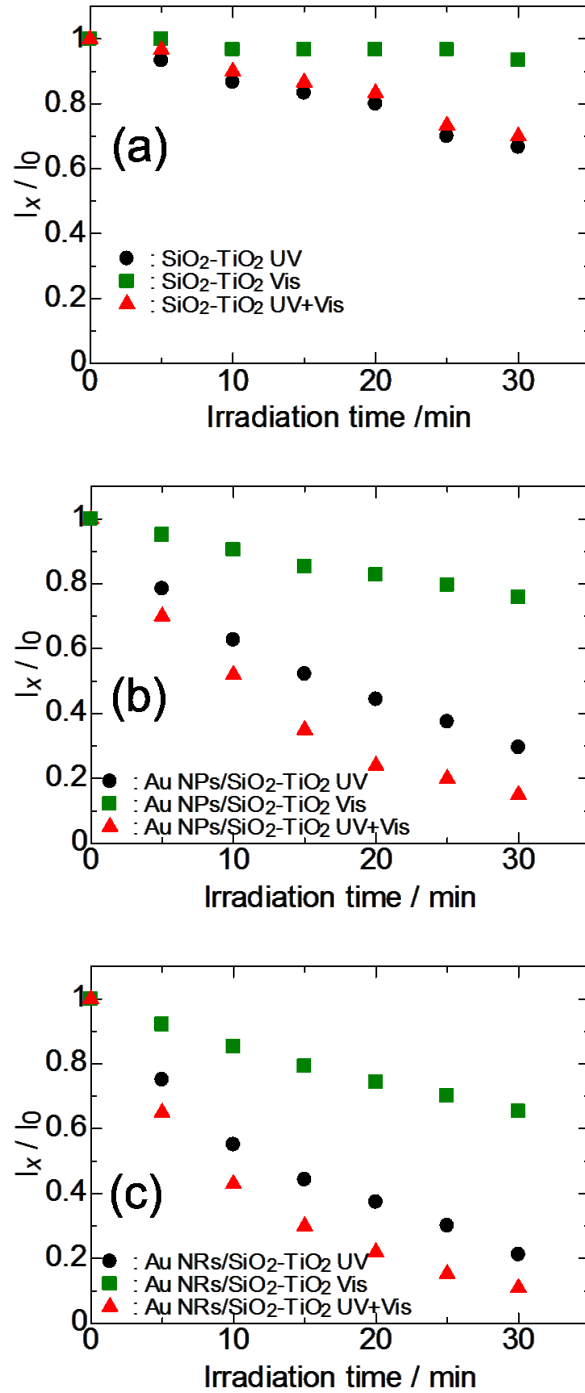Table 4.6. Generation rate of acetone by photooxidation of 2-propanol with SiO_2-TiO_2 and Au NPs/SiO_2-TiO_2 and Au NRs/SiO_2-TiO_2 under UV (R_{UV}), Vis (R_{Vis}) and simultaneous irradiation (R_{UV+Vis}).

	R_{UV}[μmol h^{-1}]	R_{Vis}[μmol h^{-1}]	R_{UV+Vis}[μmol h^{-1}]
SiO_2-TiO_2	4.03	0.56	4.38
Au NPs/SiO_2-TiO_2	5.56	6.12	10.1
Au NRs/SiO_2-TiO_2	5.72	7.53	12.4

Table 4.7. First-order reaction rate constant (k) of MB photobleaching with SiO_2-TiO_2 and Au NPs/SiO_2-TiO_2 and Au NRs/SiO_2-TiO_2 under UV (k_{UV}), Vis (k_{Vis}) and simultaneous irradiation (k_{UV+Vis}).

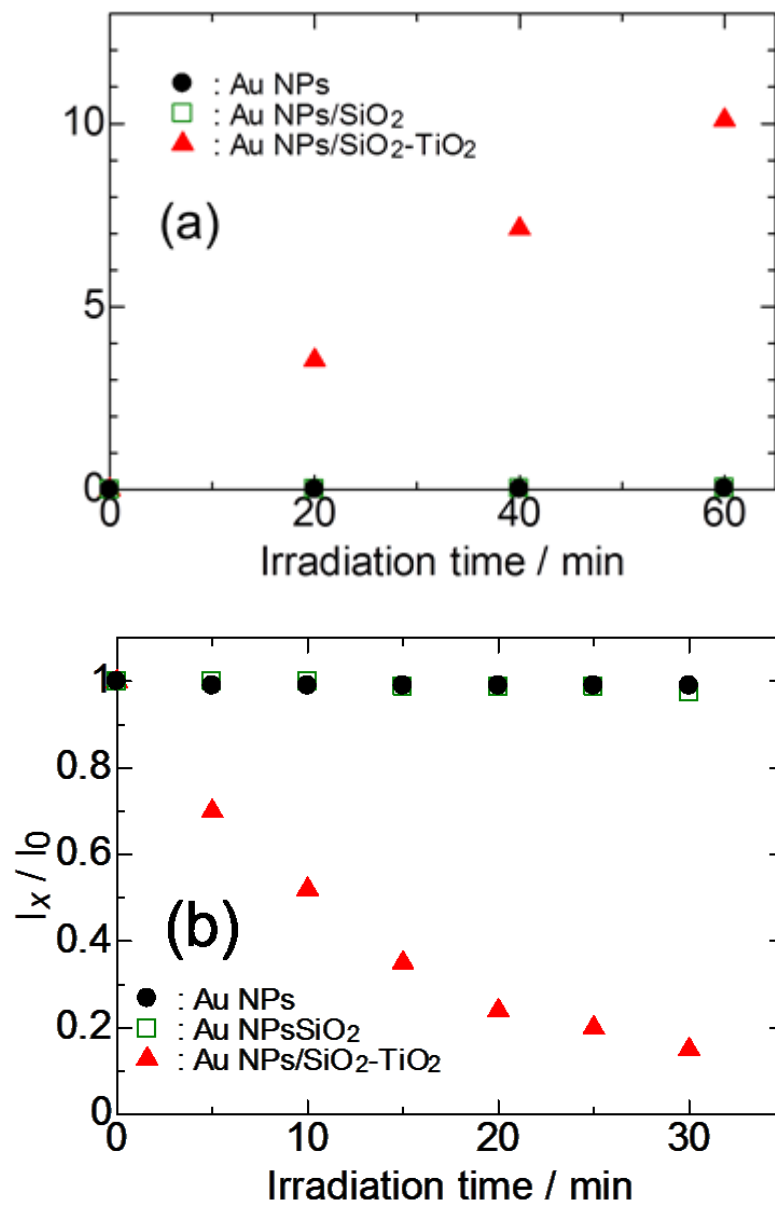|	k_{UV} [min^{-1}]	k_{Vis} [min^{-1}]	k_{UV+Vis} [min^{-1}]
SiO_2-TiO_2	1.32×10^{-2}	2.01×10^{-3}	1.12×10^{-2}
Au NPs/SiO_2-TiO_2	5.22×10^{-2}	1.04×10^{-2}	6.58×10^{-2}
Au NRs/SiO_2-TiO_2	5.34×10^{-2}	1.83×10^{-2}	7.56×10^{-2}

Fig. 4.14. Photoreaction dynamics of (a) 2-propanol and (b) MB with Au NPs/SiO$_2$-TiO$_2$, Au/SiO$_2$ and Au NPs under simultaneous irradiation of UV and Vis light.
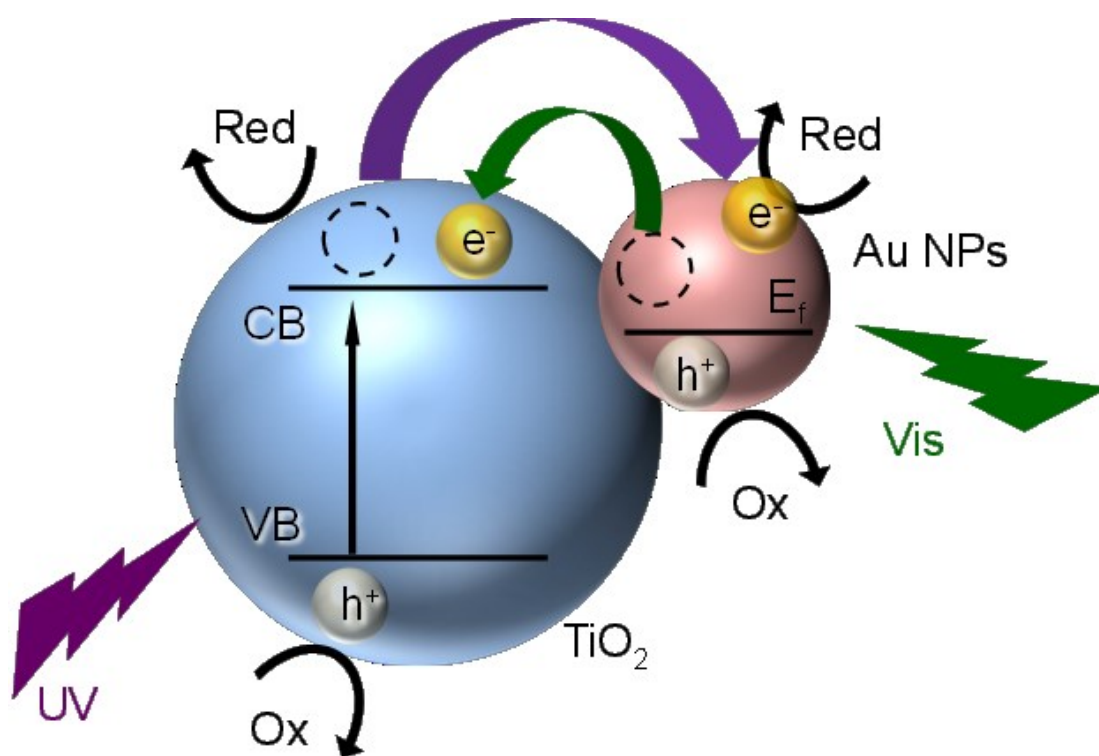
Fig. 4.15. Schematic illustration of possible charge behavior in Au/SiO$_2$-TiO$_2$ under simultaneous irradiation of UV and Vis light.

4.4 Conclusions

Mesoporous SiO_2–TiO_2 was synthesized by the sol–gel method and then Au NPs and NRs were deposited in the tubular mesopores by photodeposition method. The photocatalytic properties of them under UV and Vis light irradiation were separately measured and compared to that of the commercially available photocatalyst, P25. Au NRs/SiO_2–TiO_2 showed the highest photocatalytic activity among the samples under both UV and Vis light irradiation. The reasons of the high photocatalytic activity of Au/SiO_2–TiO_2 were investigated by measuring the action spectra and were considered to be the high specific surface area (353.2 m^2g^{-1}), the formation of Schottky barrier between Au NPs and TiO_2, and the light absorption by SPR of Au NRs. Au NRs/SiO_2–TiO_2 also showed the highest photocatalytic activity among the samples under both simultaneous light irradiation. The generation rate of acetone with Au NRs/SiO_2-TiO_2 under individual irradiation of UV and Vis light were 5.72 and 7.53 h^{-1}, and the rate constants of MB were $5.34×10^{-2}$ and $1.83×10^{-2}$ min^{-1}, respectively. The photocatalytic activity under simultaneous irradiation was clearly higher than those under independent light irradiation (12.4 h^{-1} and $7.56×10^{-2}$ min^{-1}, respectively). This phenomenon was not observed when SiO_2-TiO_2, Au/SiO_2 and stand-alone Au NPs were used as photocatalyst instead of Au NPs/SiO_2-TiO_2. Therefore, the increase of photocatalytic activity under simultaneous irradiation of UV and Vis light occurs only when both TiO_2 and Au NPs exist. Furthermore, the generation rate of acetone and rate constant of MB achieved by simultaneous irradiation were almost the same values as summed activities under independent UV and Vis light irradiation. This result indicates that the charges derived from UV absorption of TiO_2 and Vis absorption of SPR of Au NPs are efficiently used for photocatalysis without recombination even under simultaneous irradiation of UV

and Vis light.

References

[1] I. Bannat, K. Wessels, T. Oekermann, J. Rathousky, D. Bahnemann and M. Wark, "Improving the Photocatalytic Performance of Mesoporous Titania Films by Modification with Gold Nanostructures", *Chem. Mater.*, **21**, 1645 (2009).

[2] A. Orlov, D. A. Jefferson, M. Tikhov and R.M. Lambert, "Enhancement of MTBE photocatalytic degradation by modification of TiO_2", *Catal. Commun.*, **8**, 821 (2007).

[3] PDF Card #00-001-0562 PCPDFWIN, Version 2, JCPDS-ICDD, 2009.

[4] PDF Card #00-001-0172 PCPDFWIN,Version 2, JCPDS-ICDD, 2009.

[5] D. Zhao, J. Feng, Q. Huo, N. Melosh, G. H. Fredrickson, B. F. Chmelka and G. D. Stucky, "Triblock copolymer syntheses of mesoporous silica with periodic 50 to 300 angstrom pores", *Science*, **279**, 548 (1998).

[6] X.Huang, S. Neretina and M. A. El-Sayed, "Gold Nanorods: From Synthesis and Properties to Biological and Biomedical Applications", *Adv. Mater.*, **21**, 4880 (2009).

[7] J. Perez-Juste, I. Pastoriza-Santos, L. M. Liz-Marzan and P. Mulvaney, "Gold nanorods: synthesis, characterization and applications", *Chem. Rev.*, **249**, 1870 (2005).

[8] B. J. Wiley, Y. Sun and Y. Xia, "Synthesis of Silver Nanostructures with Controlled Shapes and Properties", *Acc. Chem. Res.*, **40**, 1067 (2007).

[9] V. Iliev, D. Tomova, L. Bilyarska and G. Tyuliev, "Influence of the size of gold nanoparticles deposited on TiO_2 upon the photocatalytic destruction of oxalic acid", *J. Mol. Catal. A: Chem.*, **263**, 32 (2007).

[10] K. Yu, Y. Tian and T. Tatsuma, "Size Effects of Gold Nanaoparticles on Plasmon-Induced Photocurrents of Gold-TiO_2 Nanocomposites", *Phys. Chem. Chem.*

Phys., **8**, 5417 (2006).

[11] S. Sakthivel, M. V. Shankar, M. Palanichamy, B. Arabindoo, D. W. Bahnemann and V. Murugesan, "Enhancement of photocatalytic activity by metal deposition: characterisation and photonic efficiency of Pt, Au and Pd deposited on TiO_2 catalyst.", *Water. Res.*, **38**, 3001 (2004).

[12] M. Fujishima, H. Takatori and H. Tada, "Interfacial chemical bonding effect on the photocatalytic activity of TiO_2-SiO_2 nanocoupling systems", *J. Colloid Interface Sci.*, **361**, 628 (2011).

[13] D. Li, N. Ohashi, S. Hishita, T. Kolodiazhny and H. Haneda, "Origin of visible-light-driven photocatalysis: a comparative study on N/F-doped and N–F-codoped TiO_2 powders by means of experimental", *J. Solid State Chem.*, **178**, 3293 (2005).

[14] E. Kowalska, O. O, P. Mahaney, R. Abe, B. Ohtani, "Visible-light-induced photocatalysis through surface plasmon excitation of gold on titania surfaces", *Phys. Chem. Chem. Phys*., **12**, 2344 (2010).

[15] M. Bowker, C. Morton J. Kennedy, H. Bahruji, J. Greves, W. Jones, P.R. Davies, C. Brookes, P. P. Wells and N. Dimitratos, "Hydrogen production by photoreforming of biofuels using Au, Pd and Au–Pd/TiO_2 photocatalysts", *J. Catal.*, **310**, 10 (2014).

[16] H. Yuzawa, T. Yoshida and H. Yoshida, "Gold nanoparticles on titanium oxide effective for photocatalytic hydrogen formation under visible light", *Appl. Catal. B Environ.*, **115**, 294 (2012).

[17] T. Sreethawong and S. Yoshikawa, "Comparative investigation on photocatalytic hydrogen evolution over Cu-, Pd-, and Au-loaded mesoporous TiO_2 photocatalysts", *Catal. Commun.*, **6**, 661 (2005).

[18] Y. Tian and T. Tatsuma, "Mechanisms and Applications of Plasmon-Induced Charge Separation at TiO$_2$ Films Loaded with Gold Nanoparticles", *J. Am. Chem. Soc.*, **127**, 7632 (2005).

[19] A. Furube, L. Du, K. Hara, R. Katoh and M. Tachiya, "Ultrafast Plasmon-Induced Electron Transfer from Gold Nanodots into TiO$_2$ Nanoparticles", *J. Am. Chem. Soc.,* **129**, 14852 (2007).

General conclusions

In this thesis, Au NPs and Au NRs were deposited on the photoactive mesoporous SiO$_2$-TiO$_2$ template and the photocatalysis using SPR of Au NPs and Au NRs deposited in the template was investigated. The effects of TiO$_2$-Au interface, surface modification of the template and SPR wavelength of Au NPs and Au NRs on the photocatalysis under Vis and NIR light irradiation were discussed.

The results and discussion in each chapter are summarized as follow:

In chapter 2, TiO$_2$ nanocrystal-containing mesoporous SiO$_2$ templates were fabricated by sol-gel method and Au NPs or Au NRs were deposited in the as-formed tubular mesopores by thermal reduction method. A morphology change of the Au NPs was then investigated when the content of TiO$_2$ in the template was varied. Au NRs with a length of 10 to 400 nm were obtained in the template containing 20 mol% TiO$_2$ and the length of Au NRs was shortened with increasing in TiO$_2$ content because thermoexcited conduction electrons are generated from TiO$_2$ and these generated electrons transfer to the Au ions to accelerate their reduction. Also Au NPs in the template containing 20 mol% TiO$_2$ were deposited by UV radiation to the sample during heat treatment. UV radiation during Au deposition in the TiO$_2$-containing template produced electrons photocatalytically and accelerated the Au deposition rate, leading to the dominant formation of Au NPs. The rate constant per unit area for photobleaching of MB upon UV radiation by SiO$_2$-TiO$_2$, v and Au NRs/SiO$_2$-TiO$_2$ containing 20 mol% TiO$_2$ was evaluated. Bare SiO$_2$-TiO$_2$ showed 3.24×10^{-2} min^{-1}m^{-2} of rate constant per unit area, the Au NPs- and Au NRs-deposited SiO$_2$-TiO$_2$ composites possessed rate constants that were two and three times larger than that of the bare template. Vis irradiation of the prepared samples had no significant effect on their photocatalytic properties because the

electronic contact between TiO_2 and Au was not formed by thermal reduction method.

In chapter 3, Au NPs and Au NRs were deposited in the SiO_2-TiO_2 by photodeposition method with/without surface modification of the template by 3-aminopropyltriethoxysilane [APTES] and Vis light-induced photocatalysis of prepared samples was investigated. Without APTES, spherical Au NPs with a diameter of < 15 nm formed dominantly at the outside of the mesoporous structure and showed the extinction at 542 nm. The surface modification of the template with APTES prior to the deposition of Au resulted in the formation of Au NRs with a diameter of ca. 5 nm and a length of 10–15 nm in the tubular mesopores of the template and this sample showed two extinction peaks at 528 and 700 nm. Au NPs-deposited sample worked well as a photocatalyst to bleach MB under Vis light irradiation. Au NRs-deposited sample showed weak and abnormal photocatalytic activity, showing nonexponential curve in the photobleaching dynamics of MB because APTES being on the surface of the template suppressed the adsorption of MB onto the sample. Heat treatment to remove APTES from the sample led to the amelioration of the photocatalytic activity. The formation of good electronic contact between Au NPs and TiO_2 was found to be essential to the high Vis light-induced photocatalytic performance.

In chapter 4, comparison of the photocatalytic activities of Au NPs/SiO_2-TiO_2 with different amounts of Au (0.3, 0.6, 1.2 and 1.8 mol% Au) and Au NRs/SiO_2-TiO_2 was carried out under UV, Vis and NIR light irradiation. Au NPs/SiO_2-TiO_2 with an amount of 0.6 mol% Au showed the highest photocatalytic activity among the samples with different amount of Au NPs under both UV and Vis light irradiation. The specific surface area of Au/SiO_2–TiO_2 decreased with increasing the amount of deposited Au NPs, resulting in the decrease of the photocatalytic activity of 1.2 and 1.8Au/SiO_2-TiO_2.

Au NRs/SiO$_2$–TiO$_2$ showed higher photocatalytic activity than Au NPs/SiO$_2$-TiO$_2$ with 0.6 mol% Au under both UV and Vis light irradiation. The reasons of the high photocatalytic activity of Au/SiO$_2$–TiO$_2$ were investigated by measuring the action spectra and were considered to be the high specific surface area (353.2 m^{2}g^{-1}), the formation of Schottky barrier between Au NPs and TiO$_2$, and the wider light absorption by SPR of Au NRs. In order to investigate the detailed mechanism of the photocatalysis, photocatalytic activity of Au/SiO$_2$-TiO$_2$ under simultaneous irradiation of UV and Vis was investigated. Au/SiO$_2$-TiO$_2$ showed higher photocatalytic activity under simultaneous irradiation than those under independent light irradiation. This improvement of the photocatalytic activity was observed only when both TiO$_2$ and Au NPs exist. The generation rate of acetone and rate constant of MB obtained under simultaneous irradiation were almost the same values as summed activities under independent UV and Vis light irradiation. This result indicates that the charges derived from UV absorption of TiO$_2$ and Vis absorption of SPR of Au NPs are efficiently used for photocatalysis without recombination even under simultaneous irradiation of UV and Vis light.

Au NRs/SiO$_2$-TiO$_2$ prepared in this thesis achieved high photocatalytic activity under light irradiation with wide wavelength region from UV to NIR. In particular, the use of NIR light for the photocatalysis is large advantage of this photocatalyst because the lights in NIR region (over 800 nm) were hardly used for the photocatalysis under sunlight due to low energy of NIR light. Therefore this Au NRs/SiO$_2$-TiO$_2$ photocatalyst promises the use as novel photocatalyst acting under NIR light.

Acknowledgements

List of publications

[1] G. Kawamura, T. Okuno, H. Muto and A. Matsuda, "Selective preparation of zero- and one-dimensional gold nanostructures in a TiO_2 nanocrystal-containing photoactive mesoporous template", *Nanoscale Research Letters*, **7**, 27 (8 pages) (2012).

(Chapter 2)

[2] T. Okuno, G. Kawamura, H. Muto and A. Matsuda, "Fabrication of Shape-Controlled Au Nanoparticles in a TiO_2-Containing Mesoporous Template Using UV Irradiation and Their Shape-Dependent Photocatalysis", *Journal of Materials Science & Technology*, **30** (1), 8-12 (2014).

(Chapter 2)

[3] G. Kawamura, T. Okuno, H. Muto and A. Matsuda, "Visible-Light-Induced Photocatalysis of 2D-Hexagonal Mesoporous SiO_2-TiO_2 Deposited with Au Nanoparticles", *Journal of Nanoscience and Nanotechnology*, **14**, 2225-2230 (2014).

(Chapter 3)

[4] T. Okuno, G. Kawamura, H. Muto and A. Matsuda, "Three modes of high-efficient photocatalysis using composites of TiO_2-nanocrystallite-containing mesoporous SiO_2 and Au nanoparticles", *Journal of Sol-Gel Science and Technology*, **74**, 748-755 (2015).

(Chapter 4)

[5] T. Okuno, G. Kawamura, H. Muto and A. Matsuda, "Photocatalytic Properties of

Au-Deposited Mesoporous SiO_2-TiO_2 Photocatalyst Under Simultaneous Irradiation of UV and Visible Light", *Journal of Solid State Chemistry*, **235**, 132-138 (2016).

(Chapter 4)

Achievements

1. **Publications (6, including 3 first-author papers)**

1) <u>Teruhisa Okuno</u>, Go Kawamura, Hiroyuki Muto and Atsunori Matsuda, "Photocatalytic Properties of Au-Deposited Mesoporous SiO_2-TiO_2 Photocatalyst Under Simultaneous Irradiation of UV and Visible Light", *Journal of Solid State Chemistry*, **235**, 132-138 (2016).

2) <u>Teruhisa Okuno</u>, Go Kawamura, Hiroyuki Muto and Atsunori Matsuda, "Three modes of high-efficient photocatalysis using composites of TiO_2-nanocrystallite-containing mesoporous SiO_2 and Au nanoaprticles", *Journal of Sol-Gel Science and Technology*, **74**, 748-755 (2015).

3) Go Kawamura, <u>Teruhisa Okuno</u>, Hiroyuki Muto and Atsunori Matsuda, "Visible-Light-Induced Photocatalysis of 2D-Hexagonal Mesoporous SiO_2-TiO_2 Deposited with Au Nanoparticles", *Journal of Nanoscience and Nanotechnology*, **14**, 2225-2230 (2014).

4) <u>Teruhisa Okuno</u>, Go Kawamura, Hiroyuki Muto and Atsunori Matsuda, "Fabrication of Shape-Controlled Au Nanoparticles in a TiO_2-Containing Mesoporous Template using UV Irradiation and Their Shape-Dependent Photocatalysis", *Journal of Materials Science and Technology*, **30**(1), 8-12 (2014).

5) Go Kawamura, <u>Teruhisa Okuno</u>, Hiroyuki Muto and Atsunori Matsuda, "Selective Preparation of Zero and One-Dimensional Gold Nanostructures in a TiO_2 Nanocrystal-Containing Photoactive Mesoporous Template", *Nanoscale Research*

Letters, **7**, 27 (8 pages) (2012).

6) Go Kawamura, Mai Murakami, <u>Teruhisa Okuno</u>, Hiroyuki Muto and Atsunori Matsuda, "Length Control of Ag Nanorods in Mesoporous SiO_2-TiO_2 by Light Irradiation", *RSC Advances*, **1**, 584-587 (2011).

2. International Conference (10, including 7 first-author presentations)

1) <u>Teruhisa Okuno</u>, Go Kawamura, Hiroyuki Muto and Atsunori Matsuda, "Photocatalysis of Au Nanorod-Deposited Mesoporous SiO_2-TiO_2 under Ultraviolet to Near Infrared Light", *The 9th International Conference on the Science and Technology for Advanced Ceramics (STAC-9)*, 2PS-46, Ibaraki, Japan (2015.10).

2) <u>Teruhisa Okuno</u>, Go Kawamura, Hiroyuki Muto and Atsunori Matsuda, "Au nanoparticles-mesoporous SiO_2-TiO_2 composite for highly efficient photocatalyses", *Sol-Gel 2015*, P-Th-13-14, Kyoto, Japan (2015.9).

3) <u>Teruhisa Okuno</u>, Go Kawamura, Hiroyuki Muto and Atsunori Matsuda, "Photooxidation of 2-Propanol Using Surface Plasmon Resonance of Au Nanoparticles Deposited on Mesoporous SiO_2-TiO_2", *The 3rd International Conference on The Advancement of Materials and Nanotechnology 2013*, Poster A8, Penang, Malaysia (2013.11).

4) <u>Teruhisa Okuno</u>, Go Kawamura, Hiroyuki Muto and Atsunori Matsuda, "Visible-light-induced Photocatalysis Using Mesoporous Oxide-Au Nanoparticle Composite", *8th International Mesostructured Materials Symposium*, P-1-032, Hyogo, Japan (2013.5).

5) Go Kawamura, <u>Teruhisa Okuno</u>, Hiroyuki Muto and Atsunori Matsuda, "Metal Nanorods with Controlled Structures in Mesoporous Oxide Templates", *International Symposium Functional Materials Based on Silicon-Oxygen Systems*、

P-06、Tokyo, Japan (2012.9).

6) <u>Teruhisa Okuno</u>, Go Kawamura, Hiroyuki Muto and Atsunori Matsuda, "Shape Control of Au Nanoparticles in a Photoactive Mesoporous Template and the Photocatalytic Properties", *Challenges in Inorganic and Materials Chemistry*, P95, Toronto, Canada (2012.7).

7) Go Kawamura, Ikuo Hayashi, Mai Murakami, <u>Teruhisa Okuno</u>, Hiroyuki Muto and Atsunori Matsuda, "Orientation- and Length-Controlled Metal Nanorods in Mesoporous Oxide Templates", *Challenges in Inorganic and Materials Chemistry*, P10, Toronto, Canada (2012.7).

8) Go Kawamura, Mitsuru Torigoe, <u>Teruhisa Okuno</u>, Hiroyuki Muto and Atsunori Matsuda, "Preparation of Shape-Controlled Silver Nanoparticle-Doped Mesoporous Titania", *8th Asian Meeting on Electroceramics*, P036_2d02, Penang, Malaysia (2012.7).

9) <u>Teruhisa Okuno</u>, Go Kawamura, Hiroyuki Muto and Atsunori Matsuda, "Fabrication of Shape-Controlled Au Nanoparticles Using Photocatalysis in Mesoporous Oxide", T*he Asia-Pacific Interdisciplinary Research Conference*, 18PP-28, Aichi, Japan (2011.11).

10) <u>Teruhisa Okuno</u>, Go Kawamura, Hiroyuki Muto and Atsunori Matsuda, "Fabrication of Mesoporous (100-x)SiO$_2$-xTiO$_2$ Matrix Loaded with Shape-Controlled Au Nanoparticles", *3rd International Congress on Ceramics*, S2C-P020, Osaka, Japan (2010.11).

3. National Conference (30, including 26 first-author presentations)

1) <u>奥野照久</u>、河村剛、武藤浩行、松田厚範、"Au/SiO$_2$-TiO$_2$ 光触媒における紫

外光・可視光同時照射時の光触媒特性”、日本ゾル-ゲル学会第 13 回討論会、35、北海道 (2015.11).

2) 奥野照久、河村剛、武藤浩行、松田厚範、”Multi-Wavelength Light Responsive Photocatalysts Using Surface Plasmon Resonance of Au Nanoparticles” (International session)、第 56 回ガラス及びフォトニクス材料討論会、EB-02、愛知 (2015.11).

3) 奥野照久、河村剛、武藤浩行、松田厚範、”金ナノロッド含有メソポーラス SiO_2-TiO_2 粉末のマルチ波長応答型光触媒特性”、日本セラミックス協会第 28 回秋季シンポジウム、1L07、富山 (2015.9).

4) 奥野照久、河村剛、武藤浩行、松田厚範、” Au-TiO_2 系光触媒におけるプラズモン誘起光触媒反応の波長依存性”、第 47 回ガラス部会夏季若手セミナー、岡山 (2015.8).

5) 奥野照久、河村剛、武藤浩行、松田厚範、” 紫外光・可視光同時照射下における Au/SiO_2-TiO_2 光触媒のキャリア挙動”、日本化学会第 95 回春季年会、1F7-40、千葉 (2015.3).

6) 奥野照久、河村剛、武藤浩行、松田厚範、”Carrier behavior in Au deposited-mesoporous SiO_2-TiO_2 photocatalyst under UV and Vis light” (International session)、日本セラミックス協会第 53 回セラミックス基礎科学討論会、2B05、京都 (2015.1).

7) 奥野照久、河村剛、武藤浩行、松田厚範、” Au-TiO_2 系光触媒における紫外光・可視光同時照射下での光触媒特性”、日本セラミックス協会第 27 回秋季シンポジウム、1PE05、鹿児島 (2014.9).

8) 奥野照久、河村剛、武藤浩行、松田厚範、”金ナノ粒子析出メソポーラスシリカ-チタニアの作製と光電気化学デバイスへの応用”、第 46 回ガラス部会夏

季若手セミナー、宮城 (2014.8).

9) 河村剛、<u>奥野照久</u>、武藤浩行、松田厚範、"チタニア－金ナノ粒子複合材料の波長依存光触媒特性"、第 25 回東海地区光電気化学研究会、愛知 (2014.8).

10) <u>奥野照久</u>、河村剛、武藤浩行、松田厚範、"Photocatalysis of Mesorporous SiO$_2$-TiO$_2$-Au Nanoparticle Composite under UV and Visible Light"、日本化学会第 94 回春季年会、3H4-24、愛知 (2014.3).

11) <u>奥野照久</u>、河村剛、武藤浩行、松田厚範、"チタニア-シリカ系メソ細孔内への金ナノ粒子析出と電気化学デバイス"、平成 26 年甲南大学合同セミナー、21、兵庫 (2014.1).

12) <u>奥野照久</u>、河村剛、武藤浩行、松田厚範、"Visible-Light-Induced Photocatalysis using Mesoporous Oxides Deposited with Shape-Controlled Au Nanoparticles" (International session)、第 52 回セラミックス基礎科学討論会、2G14、愛知 (2014.1).

13) <u>奥野照久</u>、河村剛、武藤浩行、松田厚範、"金ナノ粒子含有メソポーラス SiO$_2$-TiO$_2$ 触媒を用いた 2-プロパノールの光酸化"、日本セラミックス協会第 26 回秋季シンポジウム、1PB08、長野 (2013.9).

14) 鳥越充、<u>奥野照久</u>、河村剛、武藤浩行、松田厚範、"メソポーラスシリカ-チタニア薄膜細孔内における銀ナノ粒子の形態制御と光特性"、日本セラミックス協会第 26 回秋季シンポジウム、2B23、長野 (2013.9).

15) <u>奥野照久</u>、河村剛、武藤浩行、松田厚範、"金ナノ粒子-メソポーラス酸化物複合体の可視光誘起光触媒特性"、日本ゾル-ゲル学会第 11 回討論会、50、広島 (2013.8).

16) <u>奥野照久</u>、河村剛、武藤浩行、松田厚範、"メソポーラス酸化物を利用した貴金属ナノ粒子の形状制御"、第 46 回東海若手セラミスト懇話会 2013 夏期

セミナー、P15-(C)、愛知(2013.6).

17) 鳥越充、<u>奥野照久</u>、河村剛、武藤浩行、松田厚範、"メソポーラスチタニア薄膜を鋳型とした銀ナノ粒子の形態制御と光特性"、日本セラミックス協会2013年年会、1F21、東京（2013.3).

18) <u>奥野照久</u>、河村剛、武藤浩行、松田厚範、"Visible-Light-Induced Photocatalysis using Mesoporous Oxide Deposited with Au Nanoparticles" (International session)、第51回セラミックス基礎科学討論会、1H21、宮城 (2013.1).

19) <u>奥野照久</u>、河村剛、武藤浩行、松田厚範、"メソポーラス酸化物‐金ナノ粒子ナノコンポジットの作製とその可視光光触媒特性"、日本セラミックス協会第25回秋季シンポジウム、1PK06、愛知 (2012.9).

20) <u>奥野照久</u>、河村剛、武藤浩行、松田厚範、"メソ構造を有した金ナノ粒子‐無機酸化物複合体の作製とメチレンブルーの光消色特性"、日本ゾル‐ゲル学会 第10回討論会、50、神奈川 (2012.7).

21) <u>奥野照久</u>、河村剛、武藤浩行、松田厚範、"金ナノ粒子含有メソポーラス酸化物の光触媒特性"、日本セラミックス協会東海支部第44回 東海若手セラミスト懇話会2012年 夏期セミナー、P24-(C)、静岡 (2012.6).

22) 鳥越充、<u>奥野照久</u>、河村剛、武藤浩行、松田厚範、"チタニア薄膜細孔内への銀ナノ粒子の光析出と表面プラズモン特性"、日本セラミックス協会東海支部第44回 東海若手セラミスト懇話会2012年 夏期セミナー、P28-(A)、静岡 (2012.6).

23) <u>奥野照久</u>、河村剛、武藤浩行、松田厚範、"光触媒能を有するメソポーラス酸化物鋳型による金ナノ粒子の形状制御とその光触媒特性"、日本化学会第92春季年会、1F4-05、神奈川 (2012.3).

24) 河村剛、村上舞、<u>奥野照久</u>、武藤浩行、松田厚範、"表面プラズモン誘起電

荷分離に基づく筒状メソ孔内での銀ナノ粒子の形状制御"、 日本化学会第 92 春季年会, 1F4-08、神奈川 (2012.3).

25) 河村剛、<u>奥野照久</u>、武藤浩行、松田厚範、"メソポーラスシリカ-チタニアにおけるメソ細孔と光触媒能を利用した金ナノ粒子の形態制御と有機物の分解"、 セラミックス基礎討論会第 50 回記念大会、1P15、東京 (2012.1).

26) <u>奥野照久</u>、河村剛、武藤浩行、松田厚範、"メソポーラスシリカ-チタニアを鋳型とした形状制御金ナノ粒子の析出と光触媒特性"、日本セラミックス協会第 24 回秋季シンポジウム、2L06、北海道 (2011.9).

27) <u>奥野照久</u>、河村剛、武藤浩行、松田厚範、"形状制御金ナノ粒子含有メソポーラスシリカ-チタニアの作製"、 日本ゾル-ゲル学会第 9 回討論会、56、大阪 (2011.7).

28) <u>奥野照久</u>、河村剛、武藤浩行、松田厚範、"チタニア含有メソポーラスシリカの光触媒作用を利用した金ナノ粒子の形状制御"、日本化学会年会第 91 回春季年会、1PB-037、神奈川 (2011.3).

29) <u>奥野照久</u>、河村剛、武藤浩行、松田厚範、"メソポーラスシリカ-チタニアを鋳型とした近ナノ粒子の析出及びその形状制御"、平成 22 年度日本セラミックス協会東海支部学術研究発表会、D6、愛知 (2010.12).

30) <u>奥野照久</u>、河村剛、武藤浩行、松田厚範、"メソポーラスシリカ-チタニア内での金ナノ粒子の形状制御"、第 40 回東海若手セラミスと懇話会 2010 年夏季セミナー、P42-(C)、愛知 (2010.7).

4. Awards and Prizes (7)

1) 日本ゾル-ゲル学会第 13 回討論会、ベストポスター賞 (2015.11).

2) The 9th International Conference on the Science and Technology for Advanced

Ceramics (STAC-9), Silver Poster Award (2015.10).

3) 第 47 回ガラス部会夏季若手セミナー、Excellent Presentation Award (2015.8).

4) 第 27 回秋季シンポジウム、 若手優秀ポスター発表賞 (2014.9).

5) 3rd International Conference on the Advancement of Materials and Nanotechnology, Best Poster Award (2013.11).

6) 第 25 回秋季シンポジウム, 優秀ポスター発表賞 (2012.9).

7) 平成 24 年度　卓越した技術化学者養成プログラム　成績優秀者　表彰